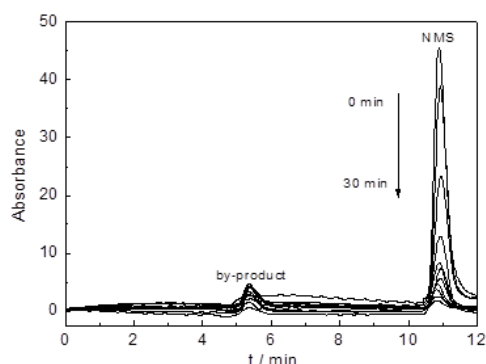
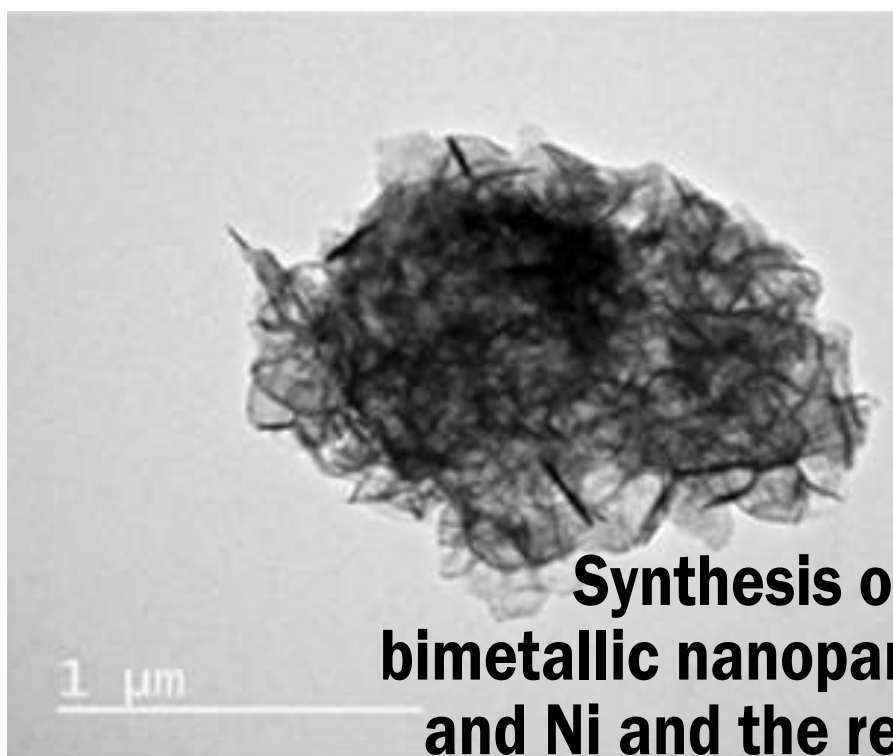


Eclética Química Journal

Volume 43 • number 1 • year 2018



Synthesis of chitosan-stabilised bimetallic nanoparticles containing Fe and Ni and the reductive degradation

Ceramic

Photocatalytic degradation of methylene blue using TiO₂ supported in ceramic material

Piperamides

Antifungal piperamides from *Piper mollicomum* Kunth (Piperaceae)

Catalysis

Advantages of the use of heterogeneous catalyst for Huisgen cycloaddition reaction: synthesis and application of new metalorganic material capable of regeneration and reuse

Adsorption

Removal of textile dye by adsorption on the cake as solid waste from the press-extraction of the macaúba (*Acrocomia aculeata*) kernel oil

Acids

Complexations of Divalent Metallic Ions with Fulvic Acids

Thermal analysis

Study of the thermal behavior in solid state of Mn(II)-Diclofenac Complex

unesp 

UNIVERSIDADE ESTADUAL PAULISTA
"JÚLIO DE MESQUITA FILHO"



Instituto de Química
UNESP
Araraquara

ISSN 1678-4618



UNIVERSIDADE ESTADUAL PAULISTA

Reitor

Sandro Roberto Valentini

Vice-reitor

Sergio Roberto Nobre

Pró-reitor de Planejamento Estratégico e Gestão

Leonardo Theodoro Büll

Pró-reitora de Graduação

Gladis Massini-Cagliari

Pró-reitor de Pós-Graduação

João Lima Sant'Anna Neto

Pró-reitora de Extensão Universitária

Cleopatra da Silva Planeta

Pró-reitor de Pesquisa

Carlos Frederico de Oliveira Graeff



INSTITUTO DE QUÍMICA

Diretor

Eduardo Maffud Cilli

Vice-Diretora

Dulce Helena Siqueira Silva

Editorial Team

Editors

Prof. Assis Vicente Benedetti, Institute of Chemistry Unesp Araraquara, Brazil (Editor-in-Chief)

Prof. Arnaldo Alves Cardoso, Institute of Chemistry Unesp Araraquara, Brazil

Prof. Antonio Eduardo Mauro, Institute of Chemistry Unesp Araraquara, Brazil

Prof. Maysa Furlan, Institute of Chemistry Unesp Araraquara, Brazil

Prof. Maria Célia Bertolini, Institute of Chemistry Unesp Araraquara, Brazil

Prof. Paulo Clairmont Feitosa de Lima Gomes, Institute of Chemistry, Unesp Araraquara, Brazil

Editorial Board

Prof. Jairton Dupont, Instituto de Química, Universidade Federal do Rio Grande do Sul, UFRGS, RS, Brazil

Prof. Enric Brillas, Facultat de Química, Universitat de Barcelona, Spain

Prof. Verónica Cortés de Zea Bermudez, Escola de Ciências da Vida e do Ambiente, Universidade de Trás-os-Montes e Alto Douro, Vila Real, Portugal

Prof. Lauro Kubota, Instituto de Química, Universidade Estadual de Campinas, Unicamp, SP, Brazil

Prof. Ivano Gerardt Rolf Gutz, Instituto de Química, Universidade de São Paulo, USP, SP, Brazil

Prof. Massuo Jorge Kato, Instituto de Química, Universidade de São Paulo, USP, SP, Brazil

Prof. Francisco de Assis Leone, Faculdade de Filosofia, Ciências e Letras, Universidade de São Paulo, Ribeirão Preto, USP-RP, SP, Brazil

Prof. Roberto Santana da Silva, Faculdade de Ciências Farmacêuticas, Universidade de São Paulo, Ribeirão Preto, USP-RP, SP, Brazil

Prof. José Antônio Maia Rodrigues, Faculdade de Ciências, Universidade do Porto, Portugal

Prof. Bayardo Baptista Torres, Instituto de Química, Universidade de São Paulo, USP, SP, Brazil

Technical Staff

Gustavo Marcelino de Souza
Lucas Henrique de Carvalho Machado

Editorial

The launch of this first issue of the EQJ of 2018 reflects a significant step of this new phase of the journal, by publishing seven original articles to the scientific community. As the readers can see, the papers cover several areas of Chemistry, in line with the editorial profile of the EQJ, such as: synthesis of bimetallic nanoparticles applied in medicine degradation studies, dye photocatalytic degradation using TiO₂, chemical constituents of *Piperaceae* and their antifungal activities, heterogeneous catalyst applied on cycloaddition reactions, removal of textile dye using particles prepared from macaúba kernel cake, complexation of metallic ions with fulvic acids, and thermal analysis of Mn(II)-diclofenac complex.

From now on, it is expected that the visibility of the articles will reach a new level due to a sequence of procedures developed by the Editors and staff, which culminated in the indexing of the EQJ in several international databases, such as Scopus and other Elsevier products. It is unquestionable the high significance of this fact that may catalyze the interest of the community in submitting new articles to the EQJ.

The Editor and his team would like to recognize authors and reviewers for their expressive collaboration.

Eclética Química Journal specially thanks the Director of the Institute of Chemistry of UNESP for the significant support provided in the successful accomplishment of this new phase of the journal.

Assis Vicente Benedetti
Editor-in-Chief of EQJ

Instructions for Authors

Preparation of manuscripts

• **Only manuscripts in English will be accepted.** British or American usage is acceptable but they should not be mixed.

• **The corresponding author should submit the manuscript online:**

<http://revista.iq.unesp.br/ojs/index.php/eclética/author>

• **Manuscripts must be sent in editable files as *.doc, *.docx or *.odt.** The text must be typed using font style Times New Roman and size 11. Space between lines should be 1.5 mm and paper size A4.

• **The manuscript should be organized in sections as follows:** Introduction, Experimental, Results and Discussion, Conclusions, and References. Sections titles must be written in bold and numbered sequentially; only the first letter should be in uppercase letter. Subsections should be written in normal and italic lowercase letters. For example: **1. Introduction;** *1.1 History;* **2. Experimental;** *2.1 Surface characterization;* *2.1.1 Morphological analysis*

• **The cover letter should include:** the authors' full names, e-mail addresses, ORCID code and affiliations, and remarks about the novelty and relevance of the work. The cover letter should also contain the suggestion of 3 (three) suitable reviewers (please, provide full name, affiliation, and e-mail).

• **The first page of the manuscript** should contain the title, abstract and keywords. *Please, do not give authors names and affiliation, and acknowledgements since a double-blind reviewer system is used. Acknowledgements should be added to the proof only.*

• **All contributions should include** an Abstract (200 words maximum), three to five Keywords and a Graphical Abstract (8 cm wide and 4 cm high) with an explicative text (2 lines maximum).

• **References should be numbered** sequentially in superscript throughout the text and compiled in brackets at the end of the manuscript as follows:

Journal:

[1] Adorno, A. T. V., Benedetti, A. V., Silva, R. A. G. da, Blanco, M., Influence of the Al content on the phase transformations in Cu-Al-Ag Alloys, *Eclét. Quim.* 28 (1) (2003) 33-38. <https://doi.org/10.1590/S0100-46702003000100004>.

Book:

[2] Wendlant, W. W., *Thermal Analysis*, Wiley-Interscience, New York, 3rd ed., 1986, ch1.

Chapter in a book:

[3] Ferreira, A. A. P., Uliana, C. V., Souza Castilho, M. de, Canaverolo Pesquero, N., Foguel, N. V., Pilon dos Santos, G., Fugivara, C. S., Benedetti, A. V., Yamanaka, H., Amperometric Biosensor for Diagnosis of Disease, In: *State of the Art in Biosensors - Environmental and Medical Applications*, Rincken, T., ed., InTech: Rijeka, Croatia, 2013, Ch. 12.

Material in process of publication:

[4] Valente Jr., M. A. G., Teixeira, D. A., Lima Azevedo, D., Feliciano, G. T., Benedetti, A. V., Fugivara, C. S., Caprylate Salts Based on Amines as Volatile Corrosion Inhibitors for Metallic Zinc: Theoretical and Experimental Studies, *Frontiers in Chemistry*. <https://doi.org/10.3389/fchem.2017.00032>.

- Figures, Schemes, and Tables should be numbered sequentially and presented at the end of the manuscript.
- Nomenclature, abbreviations, and symbols should follow IUPAC recommendations.
- Figures, schemes, and photos already published by the same or different authors in other publications may be reproduced in manuscripts of **Eclet. Quim. J.** only with permission from the editor house that holds the copyright.
- Graphical Abstract (GA) should be a high-resolution figure (900 dpi) summarizing the manuscript in an interesting way to catch the attention of the readers and accompanied by a short explicative text (2 lines maximum). GA must be submitted as *.jpg, *.jpeg or *.tif.
- **Communications** should cover relevant scientific results and are limited to 1,500 words or three pages of the Journal, not including the title, authors' names, figures, tables and references. However, Communications suggesting fragmentation of complete contributions are strongly discouraged by Editors.
- **Review articles** should present state-of-the-art overviews in a coherent and concise form covering the most relevant aspects of the topic that is being revised and indicate the likely future directions of the field. Therefore, before beginning the preparation of a Review manuscript, send a letter (1 page maximum) to the Editor with the subject of interest and the main topics that would be covered in Review manuscript. The Editor will communicate his decision in two weeks. Receiving this type of manuscript does not imply acceptance to be published in **Eclet. Quím. J.** It will be peer-reviewed.
- **Short reviews** should present an overview of the state-of-the-art in a specific topic within the scope of the Journal and limited to 5,000 words. Consider a table or image as corresponding to 100 words. Before beginning the preparation of a Short Review manuscript, send a letter (1 page maximum) to the Editor with the subject of interest and the main topics that would be covered in the Short Review manuscript.
- **Technical Notes:** descriptions of methods, techniques, equipment or accessories developed in the authors' laboratory, as long as they present chemical content of interest. They should follow the usual form of presentation, according to the peculiarities of each work. They should have a maximum of 15 pages, including figures, tables, diagrams, etc.
- **Articles in Education in Chemistry and chemistry-correlated areas:** research manuscript related to undergraduate teaching in Chemistry and innovative experiences in undergraduate and graduate education. They should have a maximum of 15 pages, including figures, tables, diagrams, and other elements.
- **Special issues** with complete articles dedicated to Symposia and Congresses can be published by **Eclet. Quim. J.** under the condition that a previous agreement with Editors is established. All the guides of the journal must be followed by the authors.
- **Eclet. Quim. J.** Ethical Guides and Publication Copyright:

Before beginning the submission process, please be sure that all ethical aspects mentioned below were followed. Violation of these ethical aspects may prevent authors from submitting and/or publishing articles in **Eclet. Quim. J.**

- The corresponding author is responsible for listing as authors only researchers who have really taken part in the work, and for informing them about the entire manuscript content and for obtaining their permission for submitting and publishing.
- Authors are responsible for carefully searching for all the scientific work relevant to their reasoning irrespective of whether they agree or not with the presented information.
- Authors are responsible for correctly citing and crediting all data used from works of researchers other than the ones who are authors of the manuscript that is being submitted to **Eclet. Quim. J.**
- Citations of Master's Degree Dissertations and PhD Theses are not accepted; instead, the publications resulting from them must be cited.

- Explicit permission of a non-author who has collaborated with personal communication or discussion to the manuscript being submitted to **Eclét. Quím. J.** must be obtained before being cited.
- Simultaneous submission of the same manuscript to more than one journal is considered an ethical deviation and is conflicted to the declaration has been done below by the authors.
- Plagiarism, self-plagiarism, and the suggestion of novelty when the material was already published are unaccepted by **Eclét. Quím. J.**
- The word-for-word reproduction of data or sentences as long as placed between quotation marks and correctly cited is not considered ethical deviation when indispensable for the discussion of a specific set of data or a hypothesis.
- Before reviewing a manuscript, the *turnitin* anti-plagiarism software will be used to detect any ethical deviation.
- The corresponding author transfers the copyright of the submitted manuscript and all its versions to **Eclét. Quím. J.**, after having the consent of all authors, which ceases if the manuscript is rejected or withdrawn during the review process.
- Before submitting manuscripts involving human beings, materials from human or animals, the authors need to confirm that the procedures established, respectively, by the institutional committee on human experimentation and Helsinki's declaration, and the recommendations of the animal care institutional committee were followed. Editors may request complementary information on ethical aspects.
- When a published manuscript in EQJ is also published in other Journal, it will be immediately withdrawn from EQJ and the authors informed of the Editor decision.
- **Manuscript Submission**

For the first evaluation: the manuscripts should be submitted in three files: the cover letter as mentioned above, the graphical abstract and the entire manuscript.

The entire manuscript should be submitted as *.doc, *.docx or *.odt files.

The Graphical Abstract (GA) 900 dpi resolution is mandatory for this Journal and should be submitted as *.jpg, *.jpeg or *.tif files as supplementary file.

The cover letter should contain the title of the manuscript, the authors' names and affiliations, and the relevant aspects of the manuscript (no more than 5 lines), and the suggestion of 3 (three) names of experts in the subject: complete name, affiliation, and e-mail).

- **Resubmission** (manuscripts "rejected in the present form" or subjected to "revision"): a letter with the responses to the comments/criticism and suggestions of reviewers/editors should accompany the revised manuscript. All modifications made to the original manuscript must be highlighted.

- **Editor's requirements**

Authors who have a manuscript accepted in **Eclética Química Journal** may be invited to act as reviewers.

Only the authors are responsible for the correctness of all information, data and content of the manuscript submitted to **Eclética Química Journal**. Thus, the Editors and the Editorial Board cannot accept responsibility for the correctness of the material published in **Eclética Química Journal**.

- **Proofs**

After accepting the manuscript, **Eclét. Quím. J.** technical assistants will contact you regarding your manuscript page proofs to correct printing errors only, i.e., other corrections or content improvement are not permitted. The proofs shall be returned in 3 working days (72 h) via e-mail.

- **Authors Declaration**

The corresponding author declares, on behalf of the other authors, that the article being submitted is original and has been written by the stated authors who are all aware of its content and approve its submission. Declaration should also state that the article has not been published previously and is not under consideration for publication elsewhere, that no conflict of interest exists and if accepted, the article will not be published elsewhere in the same form, in any language, without the written consent of the publisher.

• **Appeal**

Authors may only appeal once about the decision regarding a manuscript. To appeal against the Editorial decision on your manuscript, the corresponding author can send a rebuttal letter to the editor, including a detailed response to any comments made by the reviewers/editor. The editor will consider the rebuttal letter, and if deemed appropriate, the manuscript will be sent to a new reviewer. The Editor decision is final.

• **Contact**

Gustavo Marcelino de Souza (ecletica@iq.unesp.br)

Copyright Notice

The corresponding author transfers the copyright of the submitted manuscript and all its versions to Eclét. Quim. J., after having the consent of all authors, which ceases if the manuscript is rejected or withdrawn during the review process.

The articles published by **Eclética Química Journal** are licensed under the Creative Commons Attribution 4.0 International License.

SUMMARY

EDITORIAL BOARD.....	3
EDITORIAL.....	4
INSTRUCTIONS FOR AUTHORS.....	5

ORIGINAL ARTICLES

Synthesis of chitosan-stabilized bimetallic nanoparticles containing Fe and Ni and the reductive degradation of nimesulide.....	10
<i>Andressa Aparecida Gonçalves, Annelise França Araújo, Manoel José Mendes Pires, Rodrigo Moreira Verly, Débora Vilela Franco, Leonardo Morais da Silva</i>	
Photocatalytic degradation of methylene blue using TiO ₂ supported in ceramic material.....	26
<i>Raul Fernando de Mello Peters, Pâmela Andréa Mantey dos Santos, Tiele Caprioli Machado, Diosnel Antonio Rodriguez Lopez, Ênio Leandro Machado, Adriane de Assis Lawisch Rodriguez</i>	
Antifungal piperamides from Piper <i>mollicomum</i> Kunth (Piperaceae).....	33
<i>Herlle Aparecido da Silva, Lydia Fumiko Yamaguchi, Maria Cláudia Marx Young, Clécio Souza Ramos, André Márcio Araújo Amorim, Massuo Jorge Kato, Ronan Batista</i>	
Advantages of the use of heterogeneous catalyst for Huisgen cycloaddition reaction: synthesis and application of new metalorganic material capable of regeneration and reuse.....	39
<i>Mônica Freire Belian, Moara Targino da Silva, Aline de Andrade Alves, Ronaldo Nascimento de Oliveira, Wagner Eduardo da Silva</i>	
Removal of textile dye by adsorption on the cake as solid waste from the press-extraction of the macaúba (<i>Acrocomia aculeata</i>) kernel oil.....	48
<i>Alice Santos Caldeira, José Domingos Fabris, David Lee Nelson, Sandra Matias Damasceno</i>	
Complexations of Divalent Metallic Ions with Fulvic Acids.....	54
<i>Denise de Oliveira Vaz, Andreia N. Fernandes, Bruno Szpoganicz</i>	
Study of the thermal behavior in solid state of Mn(II)-Diclofenac Complex.....	59
<i>Marcelo Kobelnik, Valdecir Ângelo Quarcioni, Adélia Emília de Almeida, Clóvis Augusto Ribeiro, Marisa Spirandeli Crespi</i>	

Synthesis of chitosan-stabilised iron and nickel nanoparticles and the application in the reductive degradation of nimesulide

Andressa Aparecida Gonçalves¹, Annelise França Araújo¹, Manoel José Mendes Pires², Rodrigo Moreira Verly¹, Débora Vilela Franco², Leonardo Morais da Silva¹⁺

¹ Federal University of Vales do Jequitinhonha e Mucuri (UFVJM), Department of Chemistry, 5000 MGT 367 Hwy, km 583, 39100-000 Diamantina, Minas Gerais, Brazil

² Federal University of Vales do Jequitinhonha e Mucuri (UFVJM), Institute of Science and Technology - Faculty of Chemical Engineering, 5000 MGT 367 Hwy, km 583, 39100-000 Diamantina, Minas Gerais, Brazil

+ Corresponding author: Leonardo Morais da Silva, phone: +55 38 3532 6000, e-mail address: lsilvamorais@hotmail.com

ARTICLE INFO

Article history:

Received: January 21, 2018

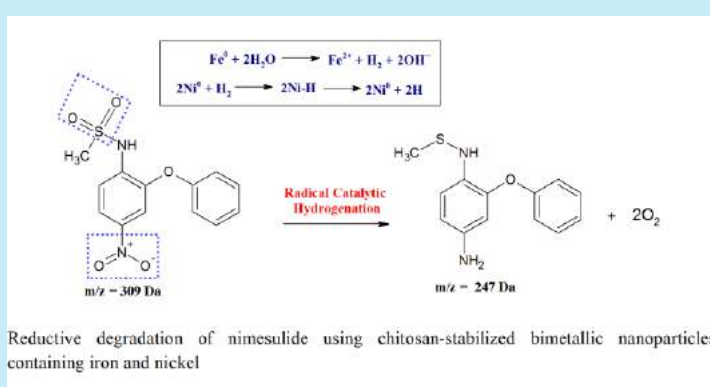
Accepted: May 9, 2018

Published: May 29, 2018

Keywords:

1. iron-nickel nanoparticles
2. emerging pollutants
3. stabilisation of nanoparticles
4. chitosan

ABSTRACT: Chitosan (CHI)-stabilised Ni-Fe bimetallic nanoparticles (bNP/CHI) were synthesised varying the content of nickel and denoted as 2-bNP/CHI, 17-bNP/CHI, and 27-bNP/CHI. The nanoparticles were characterised using several techniques and used in the removal of nimesulide. XRD and Mössbauer analyses confirmed the formation of an amorphous structure containing Fe⁰ and Fe₂O₃ while the FT-IR analysis confirmed the presence of chitosan in the nanoparticles. A very high removal of nimesulide was obtained after only 15 min of treatment with the 17-bNP/CHI system. The by-product obtained after the reductive treatment was identified using the chromatography analysis coupled to the mass spectrometry technique.



1. Introduction

Several organic substances used by the modern society are important pollutants which cause deleterious effects on the environment. In addition, several organic substances are classified as “emerging contaminants” and their occurrence in the environment is caused by the anthropic activities. Several studies have demonstrated the presence of different organic pollutants in rivers and wastewaters (e.g., drugs, pesticides, herbicides, hormones, etc.)¹⁻³.

The evaluation of the toxicological impacts on the environment of these classes of pollutants is not a facile task. Despite the fact that the pollution

burden is commonly found at low levels in the environment (e.g., in water bodies, in parts per billion or parts per trillion)¹⁻³, it is verified the simultaneous occurrence of several different anthropic substances for a given contaminated sample. Therefore, the complications arising from the combined toxicological effects comprise an environmental concern of extreme relevance. In addition, it is a fact that the emerging pollutants are not efficiently removed from contaminated waters and effluents using the traditional technologies based on physical and biological processes³.

From these considerations, the use of more efficient water and wastewater alternative treatment technologies is desirable to ensure that

the emerging contaminants can be effectively removed from the environment^{2, 3}. In principle, these contaminants can be removed using advanced reductive and/or oxidative chemical processes, which can permit the conversion of the toxic dissolved organic matter into less harmful substances⁴⁻⁶.

Regarding the occurrence of drugs in the environment, it was verified that the drug nimesulide (NMS) can be considered an emerging contaminant since its occurrence was already verified in different samples^{2, 3}. For instance, Papageorgiou *et al.*³ verified a high concentration of nimesulide in contaminated waters.

Nimesulide is a nitroaromatic substance/compound (e.g., NAC) widely used by the population due to its strong anti-inflammatory properties. In fact, nimesulide commonly exhibits better results for patients in comparison to other similar drugs (e.g., ibuprofen and diclofenac)⁷. The molecular structure of nimesulide (C₁₃H₁₂N₂O₅S) is shown in Figure 1. As can be seen, the molecular structure is characterised by an aromatic ring containing the phenyl and nitrophenyl groups interconnected to the other aromatic ring by an oxygen atom⁸.

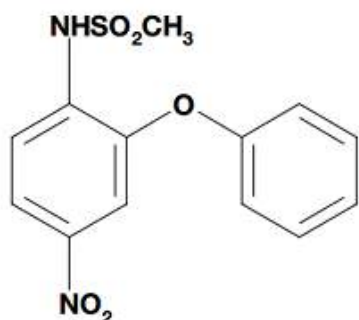


Figure 1. Chemical structure of nimesulide (NMS).

It is important to emphasise that the major deleterious effects on the environment caused by NACs are due to the nitroaromatic moiety present in these substances⁹⁻¹⁰. It is worth mentioning that NACs and the organochlorine substances are well-known contaminants that can be found in the environment. Fortunately, the negative impacts on the environment caused by NACs can be circumvented by removal of the functional nitro group in a redox reaction involving the use of different iron-containing particles (e.g., microparticles or nanoparticles). In this case, the parental substance (e.g., nimesulide) can be converted into less harmful substances (by-

products) that are naturally degraded in the environment⁹⁻¹⁰.

The modification of the zero-valent iron (ZVIn) system with incorporation of other metal can result in modifications in the reductive properties of the metallic system for heterogeneous redox reactions, as is the case of the reductive degradation of NACs. In fact, the use of a dissimilar metal, such as cobalt, nickel, and palladium, in conjunction with iron can permit to synthesise bimetallic systems highly active for the reductive degradation of different organic pollutants⁴⁻⁶. This type of bimetallic nanoparticle system (e.g., bNPs) was used with success in the reductive degradation of several organics¹⁰⁻¹³.

The magnetic properties of ZVIn and Fe-based bNPs cause the phenomenon of agglomeration, which in turn decrease the performance of the redox process (heterogeneous reaction) for the degradation of different organic pollutants. Thus, to avoid this undesirable phenomenon, these ferromagnetic nanoparticles are commonly stabilised/encapsulated using carboxymethyl cellulose (CMC) or chitosan (CHI). In addition, some studies reported the stabilisation of ferromagnetic nanoparticles by means of supporting them on silica microparticles^{11-12, 14-16}. It is worth mentioning that CHI is an important polymeric material used in the field of environmental nanotechnology due its interesting properties such as good biodegradability, biocompatibility, and low immunogenicity^{17, 18}.

The aims of the present work are: (i) the fabrication and characterisation of bimetallic nanoparticles composed of Fe and Ni stabilised with chitosan (CHI), denoted as bNP/CHI, and (ii) the study of the removal/transformation of nimesulide (NMS) in contaminated water during the redox reaction with the bNP/CHI system. The by-product obtained after the reductive treatment was identified using the chromatography analysis coupled to the mass spectrometry technique. A high degree of dispersibility was verified for the stabilised nanoparticles. As a result, a rapid removal of nimesulide was obtained using the bNP/CHI system.

2. Materials and methods

2.1 Materials

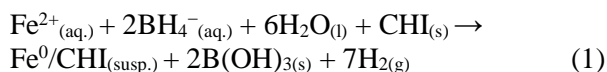
All chemicals used in this work (e.g., nimesulide, chitosan, FeSO₄·7H₂O, C₂H₄O₂, C₃H₆O, C₂H₅OH, NaBH₄, Ni(NO₃)₂·6H₂O, NaOH,

C₂H₃N, CH₃OH, and C₂HF₃O₂) were “Purum p.a.” products purchased from Sigma–Aldrich, Synth, and Fluka. High-quality chitosan from Sigma–Aldrich (product reference: C3646-100G) obtained from shrimp shells (*Pandalus borealis*) with a deacetylation degree $\geq 75\%$ was used throughout in this work.

Solutions were prepared using ultra-pure water obtained from a PURELAB (Brazil) purification system (model Classic Di-MK2).

2.2 Synthesis of the bNP/CHI system containing Ni and Fe

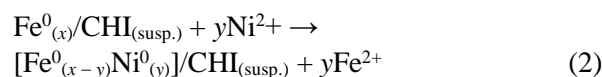
Firstly, the suspension containing the chitosan-stabilized zero-valent iron nanoparticles (Fe⁰/CHI_(susp.)) denoted as ZVIn/CHI_(susp.) was synthesised through chemical reduction of the Fe²⁺ ions using borohydride. In this case, 0.1 g of CHI_(s) was dissolved in 30 mL of a 5 % (v/v) acetic acid solution, while 2.0 g of FeSO₄·7H₂O was dissolved in 40 mL of water. These two solutions were mixed in an Erlenmeyer flask (e.g., reaction flask) resulting in a total volume of 70 mL. The mixture was agitated (250 rpm and 30 min) using an orbital shaker (IKA, model KS 260). After that, the pH was adjusted to 6.8 with the addition of some drops of a NaOH solution (5.0 M). After the previous immersion of the reaction flask in an ultrasonic bath (5 min), the reduction of Fe²⁺ was carried out by dropwise addition in the reaction flask of 6.90 mL of a NaBH₄ solution (2.3 M) under strong agitation (250 rpm and 5 min). The reduction of iron ions (Fe²⁺) resulted in the hydrogen evolution and a black suspension composed of the stabilised nanoparticles (Fe⁰/CHI_(susp.)) was obtained as represented by Equation 1:



In comparison with the non-stabilised Fe⁰-nanoparticles, it was verified that the use of CHI indeed increased the dispersibility of the Fe⁰-nanoparticles resulting in a stable black suspension (e.g., Fe⁰/CHI_(susp.)) that is not prone to agglomeration^{11, 18}.

In the second step of the synthesis, the suspension containing the stabilised bimetallic nanoparticles (Fe⁰–Ni⁰/CHI_(susp.), denoted as bNP/CHI_(susp.)) was obtained from the as-prepared Fe⁰/CHI_(susp.) nanoparticles through chemical

reduction of the Ni²⁺ ions. In this case, the chitosan-stabilised bimetallic nanoparticles containing Ni⁰ and Fe⁰ was obtained by adding 0.2615, 0.5230, and 1.046 g of Ni(NO₃)₂·6H₂O in the suspensions already containing the Fe⁰/CHI_(susp.) nanoparticles (250 rpm and 20 min). Therefore, the nominal (theoretical) Ni:Fe molar ratios considered in the present work were 0.125:1.0, 0.25:1.0, and 0.5:1.0, respectively. Each flask containing the as-prepared nickel solution (Ni²⁺_(aq.)) was covered using Parafilm[®]. In all cases, these flasks were immersed in an ultrasonic bath for 5 min. The suspension containing the stabilised nanoparticles was filtered (0.45- μm pore size) using a vacuum. Afterward, the suspension was rinsed using ethanol and acetone. As a result, the previously stabilised iron nanoparticles (Fe⁰/CHI_(susp.)) were partially covered with nickel as described by Equation 2:



As indicated in Equation 2, a fraction of the less noble metal (Fe) present in the Fe⁰/CHI_(susp.) nanoparticles was oxidized (Fe⁰ \rightarrow Fe²⁺_(aq.) + 2e⁻) in the presence of the Ni²⁺ ions with the concomitant reduction of the latter (Ni²⁺_(aq.) + 2e⁻ \rightarrow Ni⁰).

The energy dispersive X-ray spectrometry (EDS) technique was used to determine the real composition of the freshly prepared bimetallic nanoparticles (e.g., expressed in weight percentage, wt.%). It was obtained the following Ni:Fe weight ratios: 0.02:0.98, 0.17:0.83, and 0.27:0.73 (see further discussion). The nanoparticles were described as 2-bNP/CHI_(susp.), 17-bNP/CHI_(susp.), and 27-bNP/CHI_(susp.), respectively. The non-stabilised Ni–Fe bimetallic nanoparticles described as “bNP” were prepared using the aforementioned method in the absence of CHI.

2.3 Physicochemical characterisation of the bNP/CHI system

The composition of the nanoparticles was determined using the EDS technique (Oxford Instruments) with the aid of a scanning electron microscope from TESCAN. High-resolution images were obtained using a transmission electron microscope from FEI Tecnai (G2-20 SuperTwin at 200 kV). The structural analysis of the

nanoparticles was accomplished with the XRD technique (XRD-6000 diffractometer from Shimadzu) using standard conditions (Cu–K α radiation: $\lambda = 0.15406$ nm, 40 kV, 30 mA, and $0.2^\circ \text{ min}^{-1}$). Fourier transform infrared (FT-IR) analyses were accomplished using a spectrometer from Varian (model 640-IR FT-IR). All samples were prepared using the standard KBr pellet method. ^{57}Fe Mössbauer analyses were conducted at 24°C under constant acceleration mode. The spectrometer was composed of Wissel and EG&G-Ortec modules using a $^{57}\text{Co/Rh}$ radiation source. The calibration procedure was done using a standard $\alpha\text{-Fe}$ foil. BET and BJH methods were used for evaluation of the specific surface area (SSA) ($\text{m}^2 \text{ g}^{-1}$) and the pore size distribution (PSD), respectively. Experiments were carried out using a Quantachrome equipment (Autosorb-1).

2.4 Degradation of NMS with the bNP/CHI system

The degradation/transformation of nimesulide with the bNP/CHI_(susp.) system in water phase was accomplished at $24 \pm 3^\circ \text{C}$. The reactor flask (Erlenmeyer, $V = 100$ mL) was closed with Parafilm[®] to minimise the undesirable reaction (oxidation) of the as-prepared nanoparticles with the oxygen present in the air. The reaction medium (e.g., NMS and the nanoparticle suspension) was strongly agitated at different agitation frequencies using a model KS 260 orbital shaker from IKA.

The degradation of NMS (conditions: $[\text{NMS}]_0 = 40 \text{ mg L}^{-1}$ and $f = 250 \text{ rpm}$) with the bNP/CHI_(susp.) system was firstly accomplished as a function of the Ni⁰-percentage. Afterward, the particular composition of the bNP/CHI_(susp.) system that exhibited the best performance for the reductive degradation of NMS was used in the additional studies carried out as a function of the NMS and bNP/CHI_(susp.) concentrations. The agitation frequency was also varied in these studies (e.g., 0, 100, and 250 rpm). It is worth mentioning that no further changes were verified in the rate of the degradation process for agitation frequencies higher than 250 rpm.

For each experimental run, a new nimesulide solution ($V = 100$ mL and pH 11.7) was used for the reaction with the as-prepared bNP/CHI_(susp.) nanoparticles. Aliquots ($V = 5$ mL) were obtained at regular intervals of the reaction and then filtered ($0.45\text{-}\mu\text{m}$ pore size) for further chemical analyses.

2.5 Characterisation of the NMS solutions treated with the bNP/CHI_(susp.) system

All samples were analysed using the UV-Vis technique (Cary 50 from Varian). In addition, further experiments were conducted using the reverse-phase high-performance liquid chromatography (RP-HPLC) technique following the method reported in the literature¹⁹. A chromatograph from Varian (Pro Star 315) using an UV-detector was used throughout. Experimental conditions: $V = 20 \mu\text{L}$; $\lambda = 393 \text{ nm}$; $Q = 0.8 \text{ mL min}^{-1}$; C_{18} column (Nucleosil-Nucleodur: particle size = $3 \mu\text{m}$, $l = 125 \text{ mm}$, and $\varnothing = 4.6 \text{ mm}$). The isocratic elution was accomplished using a solution composed of acetonitrile/0.8% TFA and water/0.1% TFA (60:40 (v/v)).

2.6 Identification of the by-product formed after the reductive degradation of nimesulide

The by-product formed after the degradation/transformation of nimesulide during the redox reaction with the bNP/CHI_(susp.) system was obtained at an elution time of 5.3 min. This by-product was identified with the liquid chromatography-electrospray ionization-mass spectrometry (LC-ESI-MS) technique using a model LCMS-2020 system from SHIMADZU.

3. Results and discussion

3.1 Composition of the bimetallic system and the reductive degradation of nimesulide

The influence of nickel present in the bimetallic system (bNP/CHI_(susp.)) on the reductive degradation/transformation of nimesulide was investigated with the aid of the UV-Vis technique. Figure 2 shows the degradation of nimesulide as a function of the composition (e.g., nickel content) of the bimetallic system stabilised with chitosan.

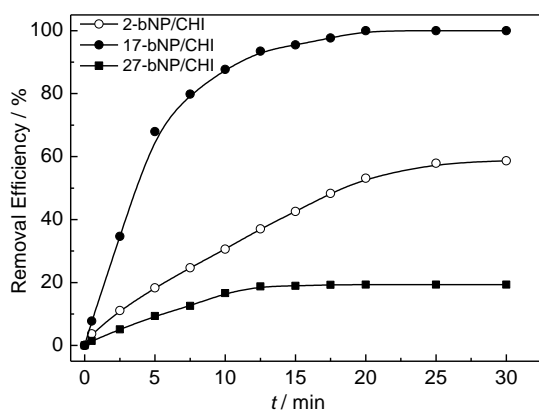


Figure 2. Dependence of the removal of NMS as a function of the nanoparticle composition. Conditions: $[NMS]_0 = 40 \text{ mg L}^{-1}$; $[bNP/CHI]_0 = 0.8 \text{ g L}^{-1}$; $f = 250 \text{ rpm}$; $T = 24 \pm 3 \text{ }^\circ\text{C}$.

As can be seen, removal efficiencies of 58 %, 100 %, and 20 % were achieved after 30 min of the redox reaction using the 2-bNP/CHI_(susp.), 17-bNP/CHI_(susp.), and 27-bNP/CHI_(susp.) systems, respectively. In addition, the degradation of nimesulide obeys a pseudo first-order kinetic model ($r^2 > 0.996$). In this sense, according to the experimental findings shown in Figure 2, the apparent rate constant (k_{ap}) depends on the Ni⁰-content with a maximum of 0.214 min^{-1} (17-bNP/CHI_(susp.)). Accordingly, k_{ap} -values of 0.0289 and 0.0177 min^{-1} were obtained for the 2-bNP/CHI_(susp.) and 27-bNP/CHI_(susp.) systems, respectively. According to the literature^{5, 20}, a possible explanation for this behaviour is a decrease in the surface concentration of the redox sites containing Fe⁰ promoted by a surface excess of the metallic centres containing the Ni⁰ species.

The best catalyst for the degradation of nimesulide was the 17-bNP/CHI_(susp.) system due to a trade-off between the surface concentrations of the active surface sites containing Fe⁰ (less noble metal) and the catalyst (e.g., Ni⁰), which in turn promotes the hydrogenation of NMS (see further discussion). Therefore, the 17-bNP/CHI_(susp.) system was then characterised with different ex-situ techniques (e.g., EDS, XRD, TEM, BET, FT-IR, and Mössbauer). In addition, this system was used on the degradation/conversion of nimesulide under different experimental conditions.

3.2 The composition of the nanoparticles and the degradation of nimesulide

The degradation of nimesulide as a function of the type of nanomaterial is shown in Figure 3.

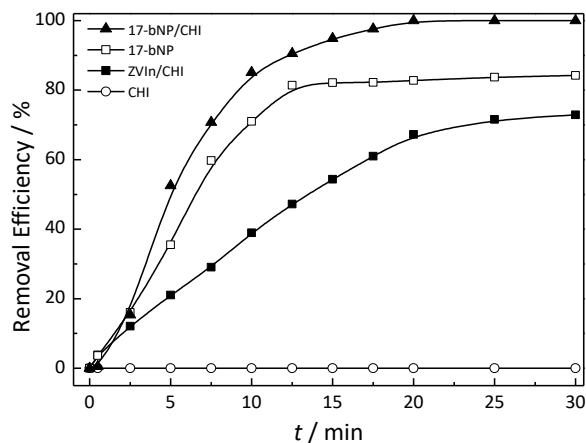


Figure 3. Influence of the composition of nanomaterial and chitosan on the removal of NMS. Conditions: $[NMS]_0 = 40 \text{ mg L}^{-1}$; $[\text{nanomaterial}]_0 = 0.8 \text{ g L}^{-1}$; $f = 250 \text{ rpm}$; $T = 24 \pm 3 \text{ }^\circ\text{C}$.

Figure 3 clearly shows that the degradation/removal of nimesulide depends on the composition of the nanomaterial. As can be seen, the best findings were obtained with the 17-bNP/CHI system. Removal percentages of 72 %, 84 %, and 100 % were obtained for nimesulide using the ZVIn/CHI, 17-bNP (e.g., non-stabilised), and 17-bNP/CHI systems, respectively. As expected, there was no removal of NMS using only the stabilising agent (CHI_(s)).

According to these results, a high dispersability of the stabilised nanoparticles in the aqueous medium has promoted the formation of a high active surface area for the redox reaction thus leading to an accentuated degradation rate of nimesulide. Also, due to its catalytic properties for the hydrogenation reaction²¹⁻²³, the Ni⁰-particles promoted the occurrence of the reductive degradation reaction (see further discussion). As can be seen, the other nanomaterials were less effective for the degradation of nimesulide. In principle, this behaviour can be correlated with the formation of a passive oxide layer which partially hinders the electron transfer in the active surface sites^{22, 23}. In addition, in this case, the formation of the H[•]-radicals is not catalysed causing a decrease in the rate for the overall redox reaction involving NMS.

3.3 The influence of the hydrodynamic conditions on the degradation reaction

The degradation rate of nimesulide can be affected by the hydrodynamic conditions (e.g., agitation frequency) since the redox reaction involving the Fe^0 -centres is a heterogeneous process with a possible influence of the mass-transport of the active species. In this sense, Figure 4 shows the influence of the agitation frequency on the degradation/removal of nimesulide using the bNP/CHI system.

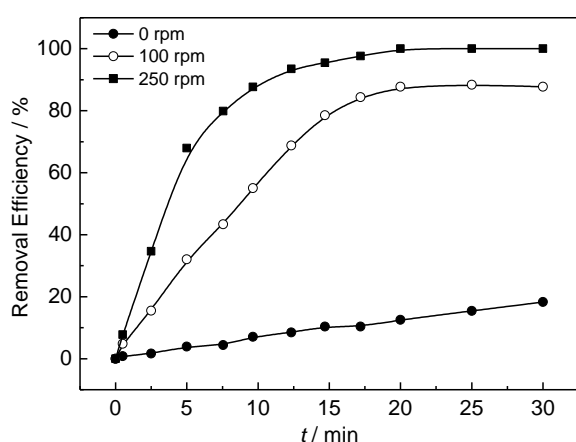


Figure 4. Influence of the agitation frequency (f) on the removal efficiency. Conditions: $[\text{NMS}]_0 = 40 \text{ mg L}^{-1}$; $[\text{17-bNP/CHI}]_0 = 0.8 \text{ g L}^{-1}$; $T = 24 \pm 3 \text{ }^\circ\text{C}$.

As seen, the removal of NMS depends on the hydrodynamic conditions as a consequence of the influence of mass-transport on the overall redox kinetics. It was verified a complete removal (100 %) of nimesulide after 20 min of reaction for an agitation frequency of 250 rpm. On the contrary, in the case of the other hydrodynamic conditions the removal was less than 83 %. Similar results were previously reported²⁴. The removal of NMS was not affected by agitation frequencies higher than 250 rpm. Therefore, it is assumed under this condition that the removal of nimesulide is under kinetic control and, therefore, the mass-transport no longer affects the heterogeneous redox reaction. All further studies in the present work were conducted at 250 rpm.

3.4 Physicochemical characterisation of the 17-bNP/CHI_(susp.) system

Figure 5 shows the TEM images obtained for the 17-bNP/CHI_(susp.) system.

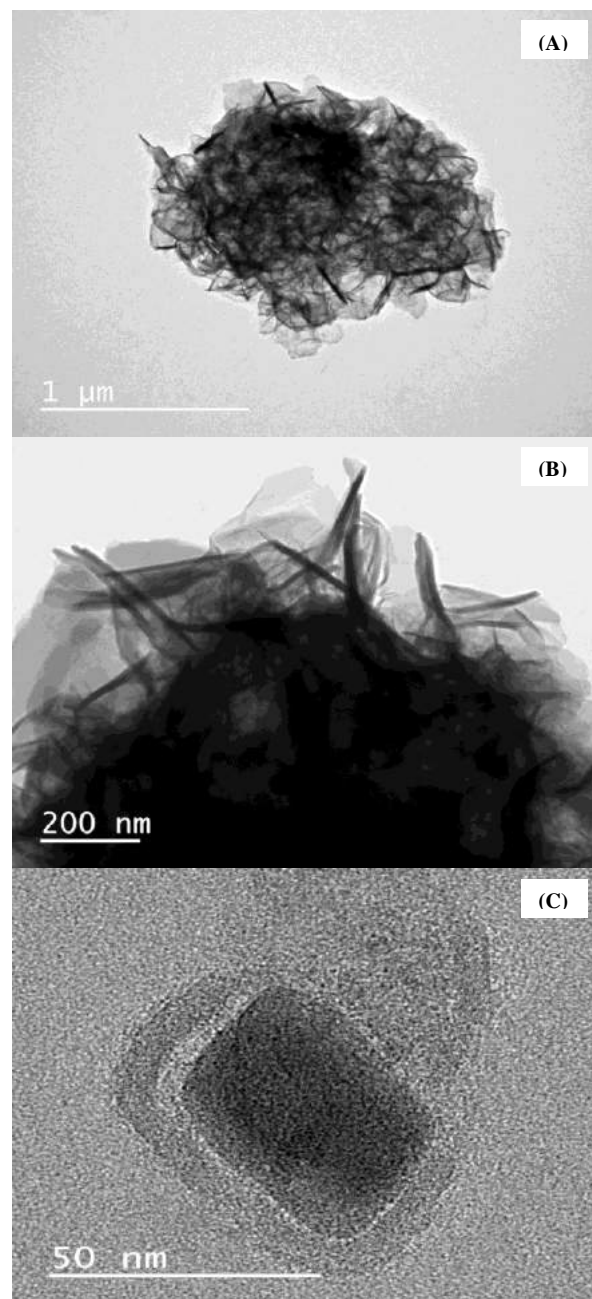


Figure 5. TEM images obtained for 17-bNP/CHI.

As can be seen, the individual clusters composed of bimetallic nanoparticles stabilised with chitosan (17-bNP/CHI_(susp.)) exhibit a rectangular morphology (Figure 5C) with a size of $\approx 50 \text{ nm}$. These findings are in agreement with the literature¹¹. In addition, according to the literature²², the bimetallic nanoparticles can be partially covered with a passive layer (e.g., Fe_3O_4 and/or Fe_2O_3) since the freshly synthesised

nanoparticles were in contact with the atmospheric air.

The EDS technique was used to obtain the composition of the metallic nanoparticles

expressed in weight percentage (wt.%) (see the Table 1).

Table 1. Elemental composition of the different nanoparticle systems expressed in wt.%

Element	ZVIn/CHI	17-bNP	2-bNP/CHI	17-bNP/CHI	27-bNP/CHI
C	20.7	-	26.2	22.2	26.5
Fe	19.0	48.8	9.5	13.8	7.4
Ni	-	1.2	1.2	2.8	2.8
O	60.3	50.0	63.1	61.2	63.2

As expected, the presence of Fe and Ni was verified for the bNP/CHI_(susp.) systems. The presence of carbon was also verified for the different samples. The occurrence of oxygen in the samples is due to the presence of chitosan and iron oxides/hydroxides. This study conducted using the EDS technique revealed the following Ni:Fe weight ratios: 0.02:0.98, 0.17:0.83, and 0.27:0.73. Thus, the different metallic nanoparticles were described in the present study as 2-bNP/CHI_(susp.), 17-bNP/CHI_(susp.), and 27-bNP/CHI_(susp.), respectively.

The XRD data are presented in Figure 6. The first aspect to be noted is the predominant amorphous character of the diffractograms, showing broad background signals.

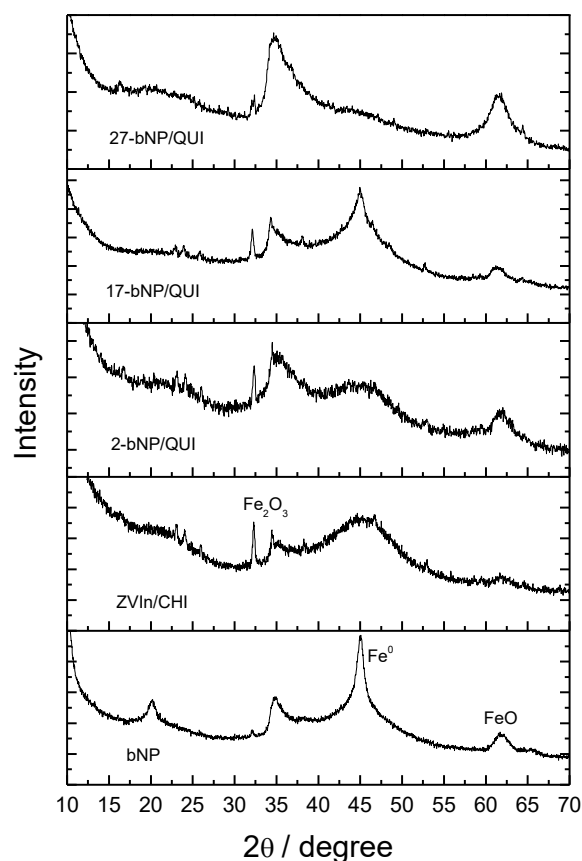


Figure 6. Diffractograms obtained for the different metallic systems composed of nanoparticles.

With the exception of the 27-bNP/CHI_(susp.) system, the diffractograms showed a band centred at $\sim 45^\circ$. Similar findings were recently reported by Weng *et al.*²³ and by Kuang *et al.*²⁵. In fact, the most intense peak of Fe⁰ is expected at 44.7° (ICSD 631728). On the whole, these findings are consistent with the presence of Fe⁰ as small clusters with poor crystallinity.

Additional interesting findings were verified in the diffractograms for the 30–40° and 60–65° intervals, where the XRD bands can be attributed to the presence of $\text{Na}_3\text{Fe}_5\text{O}_9$ and non-stoichiometric Fe^{3+} oxide-hydroxide, as well as FeO . It is worth mentioning that the presence of anhydrous or hydrated iron oxide-hydroxide for as-synthesised metallic nanoparticles was recently reported by different authors^{22, 26, 27}.

The specific surface area (SSA) and pore size distribution (PSD) were obtained for the 17-bNP/CHI_(susp.) system from the BET and BJH analyses, respectively (see [Supplementary Material, Fig. S1](#)). An SSA value of 769 $\text{m}^2 \text{g}^{-1}$ was verified for the 17-bNP/CHI_(susp.) system. On the contrary, an SSA value of only 33 $\text{m}^2 \text{g}^{-1}$ was verified for the 17-bNP system (see [Supplementary Material, Fig. S1](#)). Lin *et al.*²⁸ reported an SSA value of 15 $\text{m}^2 \text{g}^{-1}$ for the non-stabilised Fe^0 - Ni^0 nanoparticles. In addition, Weng *et al.*²³ reported an SSA value of 85.6 $\text{m}^2 \text{g}^{-1}$ for the chitosan-stabilised nanoparticles containing Fe^0 and Ni^0 . A comparison of these findings with those obtained in the present work highlights the higher SSA-value obtained for the 17-bNP/CHI_(susp.) system.

The high specific surface area obtained for 17-bNP/CHI_(susp.) can be ascribed to a good dispersion of the Fe^0 - Ni^0 nanoparticles propitiated by the stabilising agent (e.g., CHI) since the latter strongly inhibits the agglomeration phenomenon. It is worth mentioning that the high SSA-value obtained for the 17-bNP/CHI_(susp.) system can improve the removal rate of NMS. Also, it was verified a narrow interval for the PSD (e.g., 17–21 nm) for this particular system, characterising the existence of mesopores.

The 17-bNP/CHI_(susp.) system was also characterised using the Mössbauer technique (see [Supplementary Material, Fig. S2](#)). The experimental findings were simulated using a distribution function associated with super-paramagnetic particles containing Fe. The band (e.g., doublet distribution) was characterised by isomeric shifts in the range of 0.137 to 0.146 mm s^{-1} . Also, it was verified a quadrupole splitting in the range of 0.0 to 2.0 mm s^{-1} . However, the most probable value is 0.7 mm s^{-1} . In the Mössbauer spectrum, the super-paramagnetic behaviour appears as doublet signals. This relatively broad distribution of quadrupole confirms the presence of iron phases exhibiting a poor degree of crystallinity (e.g., oxide-hydroxides and $\alpha\text{-Fe}_2\text{O}_3$), as was

previously verified in the XRD study. These findings are in good agreement with the literature^{29–33}.

3.5 Nimesulide removal with the 17-bNP/CHI system

UV-Vis spectra obtained as a function of the reductive degradation reaction are presented in [Figure 7](#).

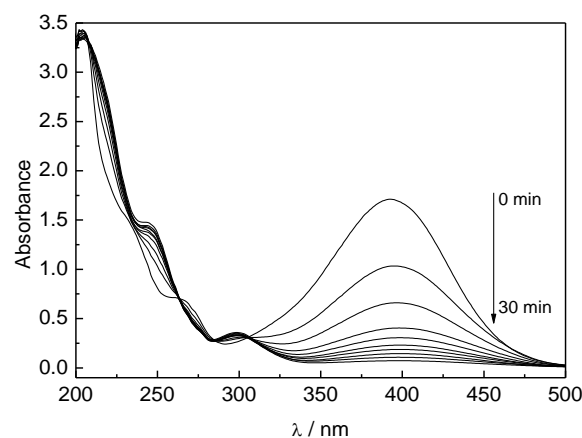


Figure 7. UV-Vis spectra of the dissolved organic matter obtained as a function of the reaction time. Conditions: $[\text{NMS}]_0 = 40 \text{ mg L}^{-1}$; $[\text{17-bNP/CHI}]_0 = 0.8 \text{ g L}^{-1}$; $T = 24 \pm 3 \text{ }^\circ\text{C}$.

It is clearly verified that the UV-band centred at 393 nm ($t = 0$) strongly decreased exhibiting a small bathochromic shift as the reductive degradation reaction proceeds. In principle, these findings are related to the reduction of the nitroaromatic moiety present in the molecular structure of NMS⁹. In addition, the appearance of a new band in the 230–330 nm interval of the spectrum can be attributed to the formation of an aromatic by-product. According to the literature⁵, the initial step in the redox reaction involving the NACs and Fe^0 -based nanoparticles is the hydrogenation of the N–O bond resulting in the appearance of nitroso compounds which can be then hydrogenated with the formation of hydroxylamine compounds. Finally, these compounds can be converted in other substances (e.g., NH_4^+ and/or N_2).

According to the literature³⁴, the agglomerates containing the bimetallic nanoparticles partially covered by an insulating oxide layer may result in the water splitting with the generation of hydroxyl radicals. As a result, the organic substance (NMS)

might also be degraded by an advanced oxidation process. However, this possibility was not considered in this study since the total organic carbon (TOC) did not change over the course of the redox reaction with NMS.

The chromatography analysis (HPLC) was carried out for different reaction times (see [Supplementary Material, Fig. S3](#)). It was verified a strong reduction of the peak exhibited by NMS (e.g., elution at ~ 11 min). In addition, the occurrence of a less intense peak observed at an elution time of 5.3 min can be ascribed to the formation of an aromatic substance. These findings are in good agreement with the UV-Vis study (see [Figure 7](#) and the discussion thereof).

3.6 Influence of the nanoparticle concentration on the reductive degradation of NMS

[Figure 8](#) shows the degradation of NMS in terms of the removal efficiency as a function of the nanoparticle concentration using the 17-bNP/CHI_(susp.) system. [Table 2](#) gathers the values of the apparent heterogeneous rate constant (k_{ap}) obtained for the reductive degradation of NMS.

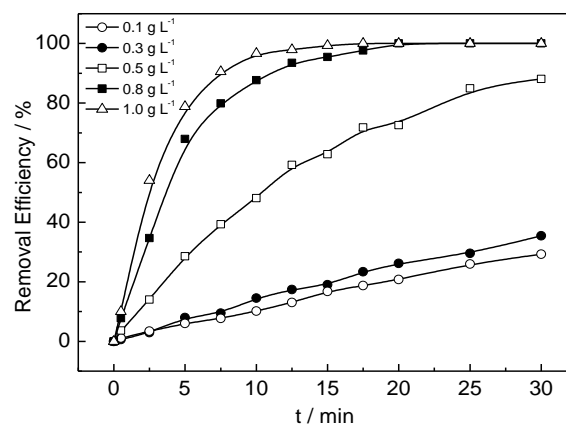


Figure 8. Removal efficiency as a function of the 17-bNP/CHI concentration. Conditions: $[NMS]_0 = 40 \text{ mg L}^{-1}$, $f = 250 \text{ rpm}$; $T = 24 \pm 3 \text{ }^\circ\text{C}$.

As can be seen, for an increase in the concentration of nanoparticles from 0.1 to 1.0 g L^{-1} the degradation increased from 18% to 100% ($\Delta t = 15 \text{ min}$), respectively. As a result, k_{ap} -values (see [Table 2](#)) increased from 1.17×10^{-2} to $3.29 \times 10^{-2} \text{ min}^{-1}$, respectively.

Table 2. The kinetic parameter (k_{ap}) obtained for the different concentrations of the bimetallic nanoparticles

$[17\text{-bNP/CHI}]_0$ (g L^{-1})	k_{ap} (min^{-1})	r^2
0.1	1.17×10^{-2}	0.995
0.3	1.45×10^{-2}	0.996
0.5	7.20×10^{-2}	0.992
0.8	2.14×10^{-2}	0.997
1.0	3.29×10^{-2}	0.996

Conditions: $[NMS]_0 = 40 \text{ mg L}^{-1}$; $T = 24 \pm 3 \text{ }^\circ\text{C}$ and $f = 250 \text{ rpm}$.

3.7 The reuse of the bimetallic nanoparticles in different experimental runs

It was verified after the first application of the nanoparticles in the reductive treatment that their reuse and stability (dispersability) strongly depend on $[NMS]_0$. In fact, it was verified that when $[NMS]_0 < 30 \text{ mg L}^{-1}$ and $[17\text{-bNP/CHI}_{(susp.)}]_0 = 1.0 \text{ g L}^{-1}$ the bimetallic nanoparticles might be only reused twice with a loss in efficacy, i.e., the use of the non-fresh nanoparticles in a second experimental run resulted in a decreased removal of about $30\text{--}50 \%$. In addition, it was confirmed that when $[NMS]_0 > 30 \text{ mg L}^{-1}$ and $[17\text{-bNP/CHI}_{(susp.)}]_0 = 1.0 \text{ g L}^{-1}$ the bimetallic

nanoparticles can no longer be used for promoting the degradation of NMS in a second experimental run. In fact, during a second experiment using the same bimetallic nanoparticles, these species were completely oxidised with the formation of a brownish precipitate that exhibited characteristics of the hydrated iron oxide. In this sense, the brownish precipitate was dried under vacuum and then subjected to the EDS analysis where the presence of iron, oxygen, and a low content of carbon were confirmed.

Grieger *et al.*³⁵ conducted a study on the environmental benefits and risks involving the use of Fe^0 -based nanoparticles in remediation processes. It was verified by these authors that

there are no significant risks to the environment in these cases. In fact, the solid product (e.g., mostly oxides) obtained after the reductive degradation of organic substances is not soluble in water and its presence in the environment does not pose any hazard.

3.8 Dependence of the heterogeneous rate constant on the initial concentration of nimesulide

Table 3 shows the k_{ap} -values obtained for the different concentrations of nimesulide.

Table 3. The kinetic parameter (k_{ap}) obtained for the different concentrations of nimesulide

[NMS] ₀ (mg L ⁻¹)	k_{ap} (min ⁻¹)	r^2
10	1.85	0.991
20	1.74×10^{-1}	0.996
30	3.11×10^{-1}	0.996
40	2.14×10^{-1}	0.997
50	9.57×10^{-2}	0.997

Conditions: [17-bNP/CHI]₀ = 0.8 g L⁻¹; $T = 24 \pm 3$ °C and $f = 250$ rpm

As can be seen, k_{ap} -values strongly decreased from 1.85 min⁻¹ to 9.57×10^{-2} min⁻¹ for an increase in the concentration of nimesulide from 10 to 50 mg L⁻¹, respectively. This behaviour indicates the occurrence of a surface heterogeneous redox reaction where there is a competition between the adsorbates (e.g., NMS) for the active Fe⁰-sites and, therefore, the overall concentration of the active surface sites available for the reductive degradation reaction can considerably decrease with an increase of the nimesulide concentration.

For the special case when [NMS]₀ = 10 mg L⁻¹, it was verified a removal percentage of 100 % for NMS after 2.5 min of reaction. Nonetheless, in the case of higher [NMS]₀-values a removal percentage higher than 75 % was only obtained after 15 min of reaction. These findings are in agreement with the literature²².

3.9 FT-IR analysis of the 17-bNP/CHI system

The FT-IR study was carried out under different experimental conditions for CHI_(s) and 17-bNP/CHI_(susp.) (see [Supplementary Material, Figure S4](#)). First, it was observed that the major absorption bands exhibited by CHI were also verified for the 17-bNP/CHI_(susp.) system, before and after the reductive reaction, thus confirming the presence of

CHI in the bimetallic nanoparticle system. The strong absorption band located at 3268 cm⁻¹, observed for the stabilised nanoparticles, can be ascribed to the presence of water, as well as to the symmetric stretching of the N–H bond of the amide groups of CHI^{23, 36}. The band observed at 1643 cm⁻¹ can be ascribed to the symmetric stretching of the N–H bond. The other bands observed at 1373 and 1052 cm⁻¹ are related to bending of the C–CH₃ bond and the symmetric stretching of the C–O bond, respectively^{23, 36}. On the whole, the FT-IR findings indicate that the chemical properties of CHI are almost unaffected by the reductive degradation reaction.

3.10 Identification of the by-product formed during the reductive degradation of nimesulide

The LC-ESI-MS analysis was accomplished for the by-product obtained at the elution time of 5.3 min. [Figure 9](#) shows the spectra obtained for the NMS (A) and by-product (B) after the redox reaction with the 17-bNP/CHI_(susp.) system. As can be seen, the nimesulide is identified by the positive ion [M + H]⁺ exhibiting an m/z ratio of 309 Da, while the by-product obtained from the catalytic hydrogenation of NMS is identified by an m/z ratio of 247 Da.

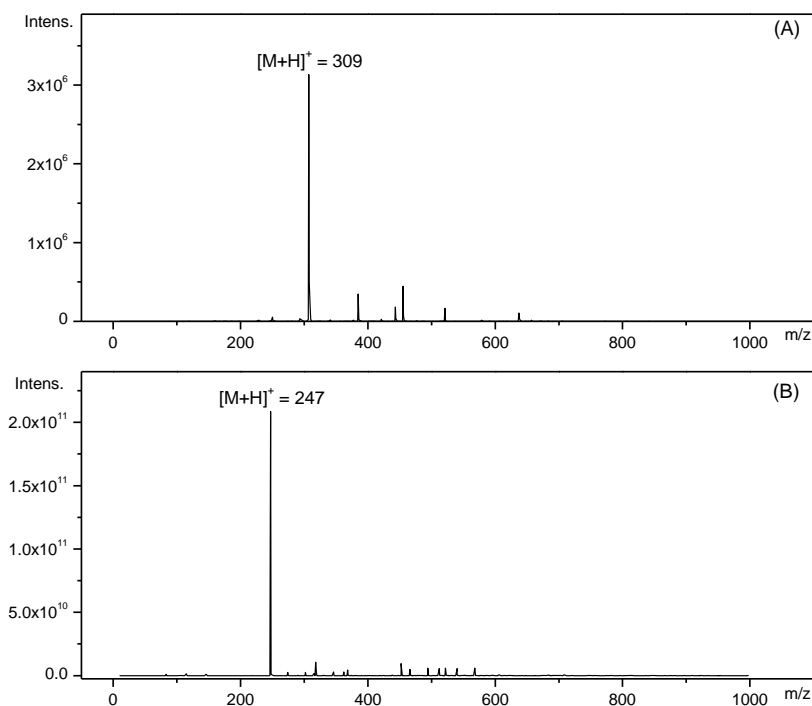


Figure 9. ESI-MS spectra obtained before (A) and after (B) the reductive reaction of NMS with 17-bNP/CHI. Conditions: $[\text{NMS}]_0 = 40 \text{ mg L}^{-1}$ and $[\text{17-bNP/CHI}]_0 = 0.8 \text{ g L}^{-1}$.

Taking into account the literature⁶, it was proposed in the present study that the bimetallic nanoparticles composed of 17-bNP/CHI_(susp.) resulted in the formation of adsorbed H[•]-radicals due to the catalytic action of the Ni⁰-centres.

Afterward, these radicals were incorporated in the molecular structure of NMS resulting in the reductive degradation/conversion of the parental substance. The overall redox process is shown in Figure 10.

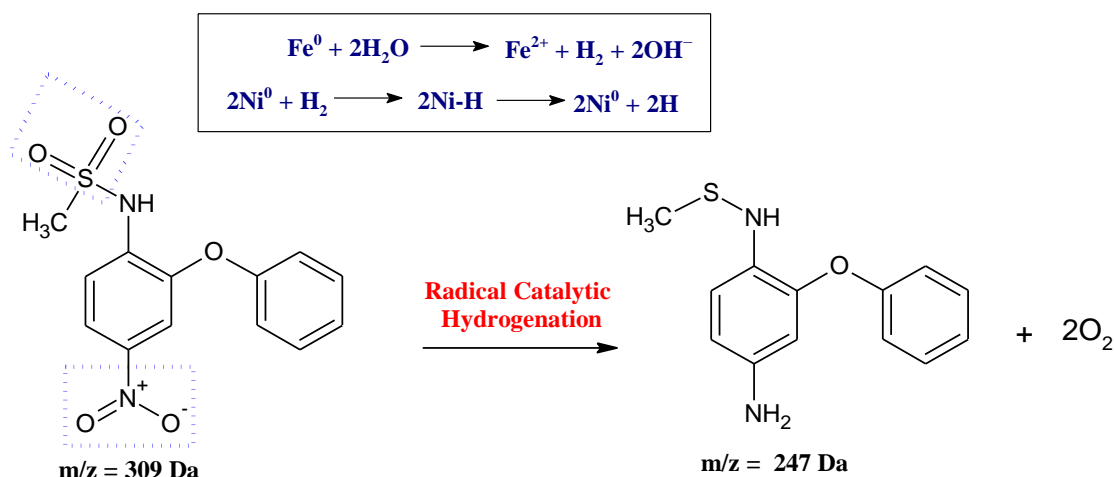


Figure 10. Representation of the reductive transformation of the parental substance (NMS) during the redox reaction with the bimetallic nanoparticles composed of 17-bNP/CHI.

As can be seen, the redox process is characterised by the formation of hydrogen from the water splitting in conjunction with the

oxidation of the Fe⁰-sites. Afterward, the hydrogen molecule is converted into hydrogen radicals due to the catalytic action of Ni⁰. As a result, the

degradation/transformation of NMS is propitiated by its reaction with the hydrogen radicals with the concomitant release of two oxygen molecules. In this sense, the removal of the nitro and sulphonyl groups during the redox process resulted in the formation of an amine and thioester by-product characterised by an m/z ratio of 247 Da.

From the above considerations, it can be expected the formation of less-harmful organic substances after the reductive treatment since the functional groups present in the structure of NMS were removed/converted during the redox reaction⁹. Therefore, the use of bimetallic nanoparticles containing Fe and Ni stabilised with chitosan in reductive treatment processes aiming for the degradation of NACs, as is the case of nimesulide, may be quite interesting from the environmental viewpoint.

4. Conclusions

The suspension containing the chitosan (CHI)-stabilized Ni⁰-Fe⁰ nanoparticles denoted as bNP/CHI_(susp.) is very active for promoting the removal/transformation of nimesulide present in water. The stabilising agent (CHI) prevented the agglomeration phenomenon thus strongly increasing the redox activity of the bimetallic nanoparticles for the reductive degradation of nimesulide. It was verified that the best composition of the bimetallic system contains 17 wt.% Ni and 83 wt.% Fe (e.g., 17-bNP/CHI_(susp.)). The XRD and Mössbauer analyses revealed the predominance of amorphous structures for iron-rich phases containing Fe⁰ and Fe₂O₃.

The presence of the catalyst (Ni⁰) is essential for promoting the reductive degradation of nimesulide where the functional groups of this substance are converted/modified by incorporation of the hydrogen radicals formed during the oxidation of the Fe⁰-centres.

The analysis of the by-product formed during the redox reaction revealed the formation of a substance containing the amine and thioester functionalities. In this sense, the present study suggests that the reductive removal/transformation of nimesulide using the 17-bNP/CHI_(susp.) system can be useful for the reduction of the toxicity intrinsic to this kind of NAC substance.

5. Acknowledgements

L. M. Da Silva wishes to thank the “*Conselho Nacional de Desenvolvimento Científico e Tecnológico* – CNPq” (PQ-2 grant) and “*Fundação de Ampara à Pesquisa do Estado de Minas Gerais* – FAPEMIG” (APQ-02739-17).

6. References

- [1] Campanha, M.B., Awan, A.T., de Sousa, D.N.R. Grosseli, G. M.; Mozeto, A. A.; Fadini, P.S. *Environ. Sci. Pollut. Res.* 22 (2015) 7936-7947. <https://doi.org/10.1007/s11356-014-3929-x>.
- [2] Silveira, M.A.K., Caldas, S.S., Guilherme, J.R., Costa, F.P., Guimarães, B.S., Cerqueira, M.B.R. et al., Quantification of Pharmaceuticals and Personal Care Product Residues in Surface and Drinking Water Samples by SPE and LC-ESI-MS/MS, *J. Braz. Chem. Soc.* 24 (2013) 1385–1395. <https://doi.org/10.5935/0103-5053.20130176>.
- [3] Papageorgiou, M., Kosma, C., Lambropoulou, D., Seasonal occurrence, removal, mass loading and environmental risk assessment of 55 pharmaceuticals and personal care products in a municipal wastewater treatment plant in Central Greece, *Sci. Total Environ.* 543 (2016) 547–569. <https://doi.org/10.1016/j.scitotenv.2015.11.047>.
- [4] Crane, R.A., Scott, T.B., Nanoscale zero-valent iron: future prospects for an emerging water treatment technology, *J. Hazard. Mater.* 211 (2012) 112–125. <https://doi.org/10.1016/j.jhazmat.2011.11.073>.
- [5] Liu, W.-J., Qian, T.-T., Jiang, H., Bimetallic Fe nanoparticles: Recent advances in synthesis and application in catalytic elimination of environmental pollutants, *Chem. Eng. J.* 236 (2014) 448–463. <https://doi.org/10.1016/j.cej.2013.10.062>.
- [6] Gao, Y., Wang, F., Wu, Y., Naidu, R., Chen, Z., Comparison of degradation mechanisms of microcystin-LR using nanoscale zero-valent iron (nZVI) and bimetallic Fe/Ni and Fe/Pd nanoparticles, *Chem. Eng. J.* 285 (2016) 459–466. <https://doi.org/10.1016/j.cej.2015.09.078>.
- [7] Lima, A.B., Chaves, S.C., Da Silva, L.M., Pereira, P.F., Richter, E.M., Santos, W.T.P.,

- Determinação de nimesulida por análise por injeção em fluxo com detecção amperométrica de múltiplos pulsos, *Quim. Nova* 39 (2013) 1296–1302. <https://doi.org/10.1590/S0100-40422013000900004>.
- [8] Bernareggi, A., Clinical pharmacokinetics and metabolism of nimesulide, *Inflammopharmacology* 9 (2001) 81–89. <https://doi.org/10.1163/156856001300248353>.
- [9] Agrawal, A., Tratnyek, P., Reduction of nitro aromatic compounds by zero-valent iron metal, *Environ. Sci. Technol.* 30 (1995) 153–160. <https://doi.org/10.1021/es950211h>.
- [10] Fu, F.; Dionysios, D.D.; Liu, H., The use of zero-valent iron for groundwater remediation and wastewater treatment: A review, *J. Hazard. Mater.* 267 (2014) 194–200. <https://doi.org/10.1016/j.jhazmat.2013.12.062>.
- [11] Kustov, L.M.; Finashina, E.D.; Shuvalova, E.V.; Tkachenko, O.P.; Kirichenko, O.A., Pd–Fe nanoparticles stabilized by chitosan derivatives for perchloroethene dechlorination, *Environ. Int.* 37 (2011) 1044–1052. <https://doi.org/10.1016/j.envint.2011.05.003>.
- [12] Cai, Z.; Fu, J.; Du, P.; Zhao, X.; Hao, X.; Liu, W.; Zhao, D., Reduction of nitrobenzene in aqueous and soil phases using carboxymethyl cellulose stabilized zero-valent iron nanoparticles, *Chem. Eng. J.* 332 (2018) 227–236. <https://doi.org/10.1016/j.cej.2017.09.06>.
- [13] Fang, Z., Chen, J., Qiu, X., Qiu, X., Cheng, W., Zhu, L., Effective removal of antibiotic metronidazole from water by nanoscale zero-valent iron particles, *Desalination* 268 (2011) 60–67. <https://doi.org/10.1016/j.desal.2010.09.051>.
- [14] Franco, D.V., Da Silva, L.M., Jardim, W.F., Reduction of hexavalent chromium in soil and ground water using zero-valent iron under batch and semi-batch conditions, *Water Air Soil Poll.* 197 (2009) 49–60. <https://doi.org/10.1007/s11270-008-9790-0>.
- [15] Franco, D.V., Da Silva, L.M., Jardim, W.F., Chemical reduction of hexavalent chromium and its immobilisation under batch conditions using a slurry reactor, *Water Air Soil Poll.* 203 (2009) 305–315. <https://doi.org/10.1007/s11270-009-0013-0>.
- [16] Cao, J., Xu, R., Tang, H., Tang, S., Cao, M., Synthesis of monodispersed CMC-stabilized Fe-Cu bimetal nanoparticles for in situ reductive dechlorination of 1,2,4-trichlorobenzene, *Sci. Total Environ.* 409 (2011) 2336–2341. <https://doi.org/10.1016/j.jece.2016.09.038>.
- [17] Wang, D.R.Y., Zhou, J., Liu, L., Huang, C.J., Zhou, D., Fu, L., Characterization and toxicology evaluation of chitosan nanoparticles on the embryonic development of zebra fish, *Carbohydr. Polym.* 141 (2016) 204–210. <https://doi.org/10.1016/j.carbpol.2016.01.012>.
- [18] Liu, T., Zhao, L., Sun, D., Tan, X., Entrapment of nanoscale zero-valent iron in chitosan beds for hexavalent chromium removal from wastewater, *J. Hazard. Mat.* 184 (2012) 724–730. <https://doi.org/10.1016/j.jhazmat.2010.08.099>.
- [19] Ruela, A.L.M., Araújo, M.B., Pereira, G.R., Desenvolvimento e validação de um método analítico rápido por cromatografia líquida de alta eficiência para determinação de nimesulida em estudos de liberação in vitro, *Quim. Nova* 32 (2009) 165–168. <https://doi.org/10.1590/S0100-40422009000100031>.
- [20] Lin, Y.-T., Weng, C.-H., Chen, F.-Y., Effective removal of AB24 dye by nano/micro-size zero-valent iron, *Sep. Purif. Technol.* 64 (2008) 26–30. <https://doi.org/10.1016/j.seppur.2008.08.012>.
- [21] Han, Y., Li, W., Zhang, M., Tao, K., Catalytic dechlorination of monochlorobenzene with a new type of nanoscale Ni(B)/Fe(B) bimetallic catalytic reductant, *Chemosphere* 72 (2008) 53–58. <https://doi.org/10.1016/j.chemosphere.2008.02.002>.
- [22] Chen, Z.X., Jin, X.Y., Chen, Z., Megharaj, M., Naidu, R., Removal of methyl orange from aqueous solution using bentonite-supported nanoscale zero-valent iron, *J. Colloid Interface Sci.* 363 (2011) 601–607. <https://doi.org/10.1016/j.jcis.2011.07.057>.
- [23] Weng, X., Lin, S., Zhong, Y., Chen, Z., Chitosan stabilized bimetallic Fe/Ni nanoparticles

- used to remove mixed contaminants-amoxicillin and Cd(II) from aqueous solutions, *Chem. Eng. J.* 229 (2013) 27–34. <https://doi.org/10.1016/j.cej.2013.05.096>.
- [24] Segura, Y., Martínez, F., Melero, J.A., Fierro, J.L.G., Zero valent iron (ZVI) mediated Fenton degradation of industrial wastewater: Treatment performance and characterization of final Composites, *Chem. Eng. J.* 269 (2015) 298–305. <https://doi.org/10.1016/j.cej.2015.01.102>.
- [25] Kuang, Y.; Du, J.; Zhou, R.; Chen, Z.; Megharaj, M.; Naidu, R., Calcium alginate encapsulated Ni/Fe nanoparticles beads for simultaneous removal of Cu (II) and monochlorobenzene, *J. Colloid Interface Sci.* 447 (2015) 85–91. <https://doi.org/10.1016/j.jcis.2015.01.080>.
- [26] Liu, X.; Chen, Z.; Chen, Z.; Megharaj, M.; Naidu, R., Remediation of Direct Black G in wastewater using kaolin-supported bimetallic Fe/Ni nanoparticles, *Chem. Eng. J.* 223 (2013) 764–771. <https://doi.org/10.1016/j.cej.2013.03.002>.
- [27] Liu, Z.; Gu, C.; Ye, M.; Bian, Y.; Cheng, Y.; Wang, F.; Yang, X.; Yang, S.; Jiang, X., Debromination of polybrominated diphenyl ethers by attapulgite-supported Fe/Ni bimetallic nanoparticles: Influencing factors, kinetics and mechanism, *J. Hazard. Mater.* 298 (2015) 328–337. <https://doi.org/10.1016/j.jhazmat.2015.05.032>.
- [28] Lin, C., Shih, Y., MacFarlane, J., Amphiphilic compounds enhance the dechlorination of pentachlorophenol with Ni/Fe bimetallic nanoparticles, *Chem. Eng. J.* 262 (2015) 59–67. <https://doi.org/10.1016/j.cej.2014.09.038>.
- [29] Marchal, G., Mangin, P., Piecuch, M., Janot, C., Mössbauer study of magnetic ordering in amorphous Fe-Si alloys, *J. Physique Colloq.* 37 (1976) C6-763-768. <https://doi.org/10.1051/jphyscol:19766160>.
- [30] Tartaj, P., González-Carreño, T., Bomati-Miguel, O., Serna, C.J., Bonville, P., Magnetic behaviour of superparamagnetic Fe nanocrystals confined inside submicron-sized spherical silica particles, *Phys. Rev. B* 69 (2004) 094401-1-094401-8. <https://doi.org/10.1103/PhysRevB.69.094401>.
- [31] Murad, E., Mössbauer spectroscopy of clays, soils and their mineral constituents, *Clay Minerals* 45 (2010) 413–430. <https://doi.org/10.1180/claymin.2010.045.4.413>.
- [32] van der Kraan, A. M., Mössbauer effect studies of surface ions of ultrafine α -Fe₂O₃ particles, *Phys. Status Solidi A* 18 (1973) 215–226. <https://doi.org/10.1002/pssa.2210180120>.
- [33] Zboril, R., Mashlan, M., Petridis, D., Iron (III) Oxides from Thermal Processes Synthesis, Structural and Magnetic Properties, Mössbauer Spectroscopy Characterization, and Applications, *Chem. Mater.* 14 (2002) 969–982. <https://doi.org/10.1021/cm011107a>.
- [34] Bokare, A.D., Chikate, R.C., Rode, C.V., Paknikar, K.M., Effect of surface chemistry of Fe–Ni nanoparticles on mechanistic pathways of azo dye degradation, *Environ. Sci. Technol.* 41 (2007) 7437–7443. <https://doi.org/10.1021/es071107q>.
- [35] Grieger, K.D.; Fjordbøge A.; Hartmann, N.B.; Eriksson, E.; Bjerg, P.L.; Baun, A., Environmental benefits and risks of zero-valent iron nanoparticles (nZVI) for in situ remediation: Risk mitigation or trade-off? *Journal of Contaminant Hydrology* 118 (2010) 165–183. <https://doi.org/10.1016/j.jconhyd.2010.07.011>.
- [36] Geng, B., Jin, Z., Li, T., Qi, X., Preparation of chitosan-stabilized Fe(0) nanoparticles for removal of hexavalent chromium in water, *Sci. Total Environ.* 407 (2009) 4994–5000. <https://doi.org/10.1016/j.scitotenv.2009.05.051>.

Supplementary Material

Synthesis of chitosan-stabilised iron and nickel nanoparticles and the application in the reductive degradation of nimesulide

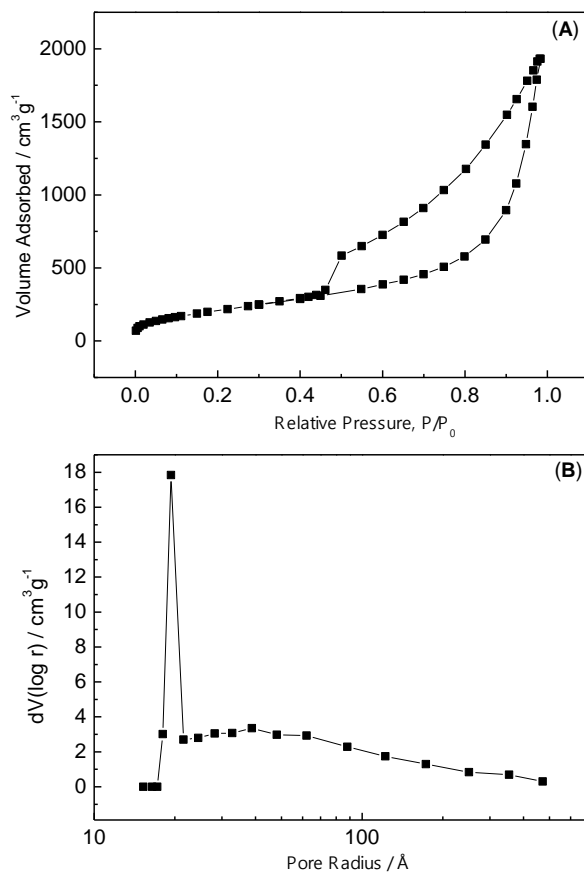


Figure S1. BET analysis: (A) isotherm plot and (B) pore radius distribution obtained for 17-bNP/CHI.

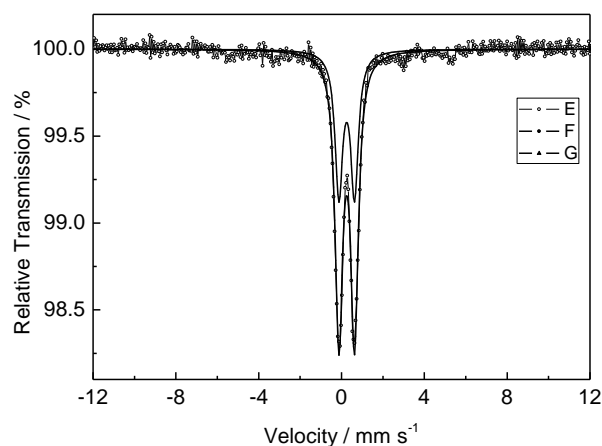


Figure S2. ^{57}Fe Mössbauer spectrum obtained for the 17-bNP/CHI sample at room temperature. The fitted curve is the sum of two signal distributions also shown (displaced on the vertical scale for clarity).

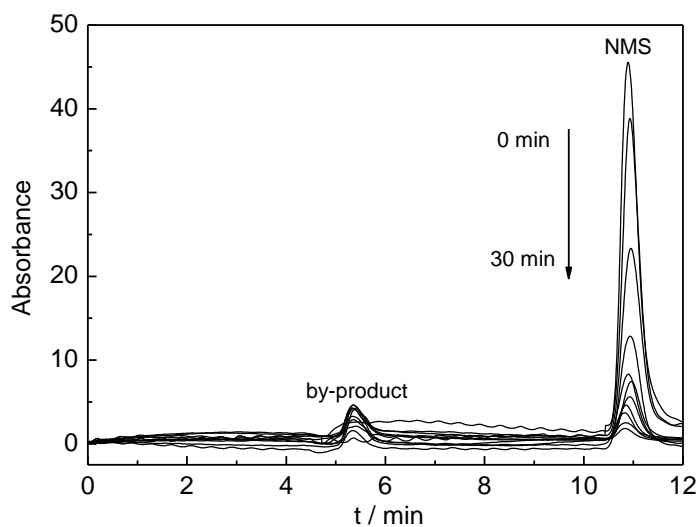


Figure S3. HPLC chromatograms obtained for the treated samples as a function of the reaction time. Conditions: $[\text{NMS}]_0 = 40 \text{ mg L}^{-1}$; $[\text{17-bNP/CHI}]_0 = 0.8 \text{ g L}^{-1}$; $T = 24 \pm 3 \text{ }^\circ\text{C}$.

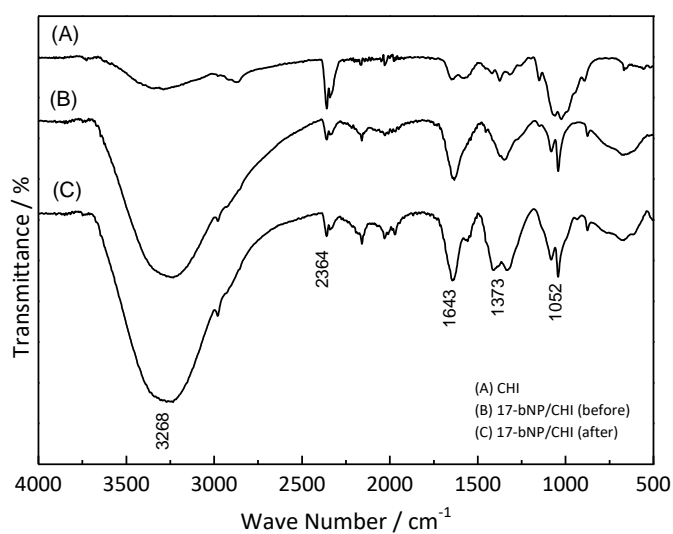


Figure S4. FT-IR spectra obtained for pure CHI and for 17-bNP/CHI, before and after the reductive reaction with NMS.

Photocatalytic degradation of methylene blue using TiO₂ supported in ceramic material

Raul Fernando de Mello Peters¹, Pâmela Andréa Mantey dos Santos¹, Tiele Caprioli Machado², Diosnel Antonio Rodriguez Lopez^{1,2}, Ênio Leandro Machado^{1,3}, Adriane de Assis Lawisch Rodriguez^{1,2+}

¹ University of Santa Cruz do Sul, Postgraduate Program in Environmental Technology, 2293 Independência Av, 96815-900 Santa Cruz do Sul, Rio Grande do Sul, Brazil

² University of Santa Cruz do Sul, Department of Engineering, Architecture and Agricultural Science, 2293 Independência Av, 96815-900 Santa Cruz do Sul, Rio Grande do Sul, Brazil

³ University of Santa Cruz do Sul, Department of Chemistry and Physics, 2293 Independência Av, 96815-900 Santa Cruz do Sul, Rio Grande do Sul, Brazil

+ Corresponding author: Adriane de Assis Lawisch Rodriguez, phone: +55 51 3717-7545, e-mail address: adriane@unisc.br

ARTICLE INFO

Article history:

Received: January 24, 2018

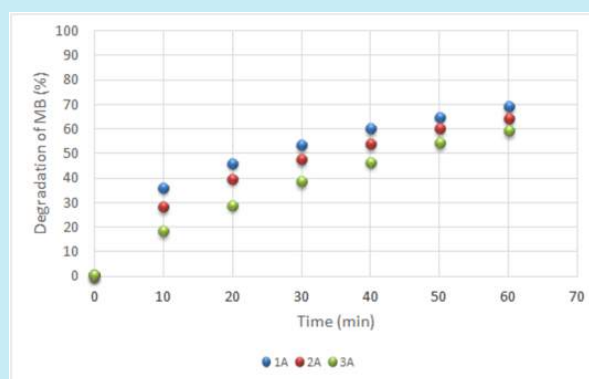
Accepted: April 16, 2018

Published: May 29, 2018

Keywords:

1. porous ceramic
2. residue
3. degradation
4. methylene blue

ABSTRACT: The present work evaluates the use of ceramic material, produced with the aid of industrial waste through the Gel-Casting method, as a support for catalysts in the photocatalytic degradation of Methylene Blue. The analysis was carried out in a reactor containing UVC lamps through batch processing. The results show that the reaction of photocatalytic degradation of the dye presents pseudo-first order kinetics, with values of degradation between 60 and 70 %. The study evaluated the deactivation of the catalysts synthesized and supported in the ceramic material. In this case, it was observed that the larger the mass of deposited catalyst on the ceramic support, the longer the lifespan of the sample, since a larger mass takes longer to deactivate.



1. Introduction

In the midst of a wide range of pollutants and contaminants from a large variety of sources, there is a need for the development of effluent remediation systems, whether liquid or gaseous. Among these pollutants are dyes, which are widely used in the textile, rubber, paper, plastic, and cosmetic industries. Dyes provide a significant share of environmental contamination, since they alter the natural coloration of the ecosystem to which they are released¹. About 30 % of the synthetic dyes used in industry are discarded in the

form of residues². It is also estimated that 280,000 tons of textile dyes are discharged as industrial effluents worldwide each year³. Effluents containing dyes are commonly characterized as having high quantities of salts and organic matter and high toxicity, and a low potential for biodegradation⁴.

Different techniques have been developed for the removal of dyes, including chemical precipitation, chemical oxidation, adsorption, and membrane-based biological treatment techniques⁵. However, these techniques mostly result in environmental liabilities when the dye is inadequately disposed of, therefore generating

damages to the environment. One promising alternative for the treatment of water and industrial effluents, which is especially useful for compounds resistant to conventional technologies, are advanced oxidative processes (AOPs). AOPs are based on the generation of hydroxyl radicals, which are a highly oxidizing and low selective species. Several AOPs have been used for dye degradation, among them heterogeneous photocatalysis.

The heterogeneous photocatalytic processes occur when a light energy falls on a semiconductor, with a wavelength equal to or greater than the band-gap energy of this semiconductor. This generates electron pairs that can undergo subsequent oxidation and reduction reactions with some species. These species can then be adsorbed on the semiconductor surface, generating the necessary products⁶.

Titanium Dioxide (TiO₂) has attracted a great deal of attention because of its semiconductor properties, since it is a non-toxic, stable photo, with high photocatalytic ability to decompose organic compounds present in air or water⁷. For the TiO₂ fixation, ceramic supports are widely used, due to their properties of mechanical resistance, high surface area, and other properties that favor their use⁸.

In this context, this work aims to produce a porous ceramic material, with the aid of industrial waste, impregnated with TiO₂ and applied in the photocatalytic degradation of dye. Methylene blue was used as a model molecule, as it shows similarities with industrial wastewater and is widely used for analysis in bench tests, aiming to observe the behavior and efficiency of photocatalytic systems⁹. Furthermore, the deactivation of the synthesized catalysts was evaluated.

2. Materials and methods

2.1 Synthesis of the ceramic material and impregnation of TiO₂

The TiO₂ catalyst was prepared by the Sol-Gel method using titanium tetraisopropoxide/IV-TIPT (Sigma-Aldrich), as titanium precursor material, and isopropanol PA (Nuclear), which were mixed in a 2:1 ratio and kept under stirring at 60 °C for 1 h on a hotplate (78 HW-1, Biomixer). After, deionized water was added and the mixture was stirred until dry at a temperature of 100 °C.

Subsequently, the material was ground in a mortar and placed in an oven (MB150/6, Marte) at 100 °C for 1 h, and finally calcined at 500 °C for 2 h.

The ceramic materials that served as support for the synthesized TiO₂ catalyst were produced from the Gel-Casting method, a process developed by the Oak Ridge National Laboratory¹⁰. Green sand (5.5 % w/w), clay (27.5 % w/w), corn starch (16.5 % w/w), tobacco powder, 75 % w/w), sunflower stem (0.44 % w/w) and water (47.3 % w/w) were used for the synthesis of the ceramic material. Also, residues were used in the manner in which they were available. It should be noted that green sand, tobacco powder, and sunflower stem are considered waste in industrial processes, originating from the foundry industry, tobacco industry, and biodiesel production, respectively. However, when added to the ceramic support composition, the amount of clay (raw material) used decreases, mitigating the environmental impacts from the extraction and transport of the same concomitant to the aggregation of the value of the waste generated by the industries.

The materials were mixed in a mechanical mixer (Q-250M2, Quimis), poured into molds (62 x 62 x 16 mm) and passed through the greenhouse gelling processes (MB150/6, Marte) to 80 °C for 24 h and quenched in a muffle type oven (9813, Jung Ltda.) at 1175 °C for 2 h. After the heat treatment process, the synthesized ceramic samples were sanded with a file, in order to reveal the porosity of the material and, consequently, to increase the surface area. Finally, the ceramic material was weighed and divided into 3 groups of approximately 50 g each.

For impregnation of the TiO₂ in the ceramic supports, a solution containing 5 g of TiO₂ in 100 mL of deionized water was prepared. For the impregnation of the catalyst in the ceramic material a Dip-Coating device was used. The ceramic samples (50 g) were immersed several times in the TiO₂ solution, for 1 min, in order to standardize the thickness and amount of catalyst adhered to the porous surface of the ceramic materials. After impregnation, the samples were calcined in a muffle type oven (9813, Jung Ltda.) at a temperature of 600 °C for 1 h.

Water absorption (WA) tests were performed by immersing the ceramic samples in water for 24 h. The masses were analyzed before immersion, after immersion and still saturated, with the mass measurement of the sample immersed in water. For this analysis, Equation 1 was used:

$$WA (\%) = \left(\frac{M_u - M_s}{M_s} \right) * 100 \quad (\text{Eq. 1})$$

where M_u (g) is the mass of the sample saturated with water and M_s (g) is the mass of the sample after drying.

For the apparent porosity (AP) tests, the same mass measurements were used that were performed in the water absorption analysis for the samples. The analysis is done based on Equation 2:

$$AP (\%) = \left(\frac{M_u - M_s}{M_u - M_i} \right) * 100 \quad (\text{Eq. 2})$$

where M_u (g) is the mass of the sample saturated in water, M_s (g) is the mass of the sample after drying and M_i (g) is the mass of the sample immersed in water.

2.2 Photocatalytic degradation tests of dye

The tests were carried out in a vertical batch reactor irradiated with a 254 nm ultraviolet lamp (UVC) arranged in the center of the reactor in order to obtain better use of the irradiation area by the dye solution to be tested. A peristaltic pump (AWG 4000, Provitec) was used to inject air into the reactor, which is necessary for a photocatalytic reaction and keeps the dye solution under stirring. Figure 1 shows a schematic of the assembly system used for the degradation assays. The vertical reactor was covered with aluminum foil.

For the reactions of photocatalytic degradation, 3 ceramic samples supported with a photocatalyst were used, labeled samples 1A, 2A, and 3A. These samples were placed in the vertical reactor and added to 300 mL of 5 mg L⁻¹ aqueous methylene blue solution. The analysis of each of the samples lasted 60 minutes and, every ten minutes, aliquots of the material containing the dye were collected using a syringe and analyzed in a spectrophotometer (V1200, Pró-Análise) through measurements of absorbance, at the wavelength of 665 nm (maximum absorbance of methylene blue). In addition, the deactivation of the synthesized catalysts was evaluated, for which 3 subsequent reactions were carried out with the same catalyst.



Figure 1. Photo of the vertical reactor used in the experiments: a) peristaltic pump and b) vertical reactor containing the UVC lamp (schematic).

3. Results and discussion

3.1 Synthesized catalysts

The ceramic samples were weighed before and after impregnation with TiO₂ (Figure 2) to determine the mass of catalyst adhered to the carrier. The mass values before and after the impregnation are presented in Table 1. It can be seen that, on average, 0.4 g of TiO₂ mass was deposited in each of the samples.



Figure 2. Ceramic samples impregnated with TiO₂.

Table 1. Mass values of samples before and after impregnation

Sample	Weight of ceramic material (g)	Weight of TiO ₂ (g)
Sample 1A		
Without TiO ₂	50.37	0.38
With TiO ₂	50.75	
Sample 2A		
Without TiO ₂	50.36	0.39
With TiO ₂	50.75	
Sample 3A		

Without TiO ₂	50.34	0.47
With TiO ₂	50.81	

The mean values of absolute porosity and water absorption for the synthesized catalysts are approximately 35.0 % and 22.5 %, respectively. Sifontes *et al.*¹¹, in his study, achieved a porosity of approximately 67 % for ceramic supports obtained from the replica method with polyurethane foam. This difference in the porosity is mainly due to the method for obtaining the samples. In the method used in the present study, the porosity is obtained by burning the loading material and also by the organization of the structure in the burning process. However, in the replicate method, the ceramic material copies the porosity already existing in the base material, thus leaving it with greater porosity. According to Menezes, Neves and Ferreira¹² the water absorption of ceramic materials, where there are ceramic flux residues, is between 5 and 18 %. The value obtained in this work is due to the fact that it contains other elements in the composition that alter its absorption property.

3.2 Photocatalytic degradation tests of methylene blue

The process of direct photolysis with ultraviolet radiation is one in which the only source capable of decomposing or dissociating the dye is light. Experiments were performed with the methylene blue only in the presence of UVC radiation, without the presence of the catalyst, to quantify the contribution of photolysis. The results are shown in Figure 3. The degradation of the methylene blue by photolysis was observed to be approximately 16 %.

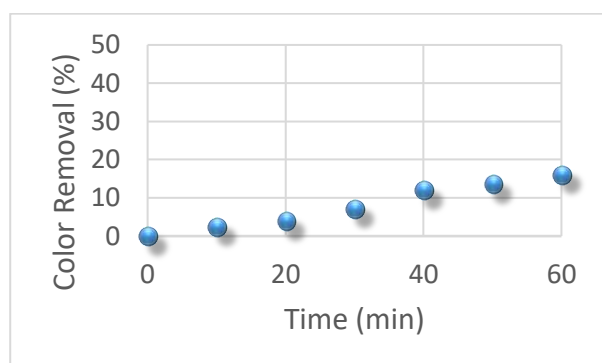


Figure 3. Percentage of color removal for methylene blue due to photolysis.

For the photocatalytic degradation reactions of methylene blue, the three ceramic material

supported with synthesized catalyst TiO₂ were used, labeled 1A, 2A and 3A. Figure 4 presents the triplicate data analyzes for TiO₂ supported in ceramic material. For each one of the three analyzes were used ceramic material with TiO₂ supported without previous use, under UVC radiation. The methylene blue photocatalytic degradation values for the synthesized catalyst samples were between 60 and 70 % for 60 minutes of reaction, that is, on average 65 % of degradation. These results show a good reproducibility in the synthesis of these ceramic samples supported with TiO₂ photocatalyst.

Xu, Rangaiah and Zhao¹³ also studied the photocatalytic degradation of methylene blue with a TiO₂ catalyst and obtained values of dye degradation of approximately 100 % for 65 minutes of reaction. This difference of degradation is possibly due to ultraviolet radiation used in the experiments. The results of these authors were obtained through the use of a 500 W mercury vapor lamp with a wavelength of 365 nm. According to Lan, Lu and Ren¹⁴, the activation range of the TiO₂ catalyst is 280-400 nm and in the present work a UVC lamp with a wavelength of 254 nm was used, which probably explains the lower degradation obtained, on average 65 %.

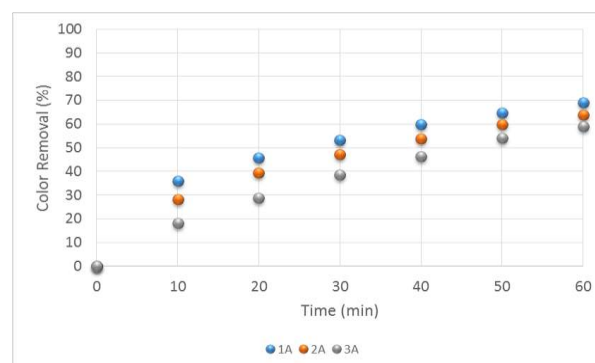


Figure 4. Photocatalytic degradation of methylene blue for samples 1A, 2A, and 3A without prior use.

In order to evaluate the kinetics of the photocatalytic degradation reaction of methylene blue, it was hypothesized that this reaction follows pseudo-first order kinetics, since the dye is sufficiently diluted. Figure 5 shows the results obtained for photocatalytic degradation of the dye in the presence of the synthesized catalyst 3A and UVC radiation. This is verified with a line that passes through the origin, with a coefficient of adjustment equal to 0.9923, proving that the

hypothesis is true. Thus, the specific rate of reaction, k , for these conditions is 0.0155 min^{-1} .

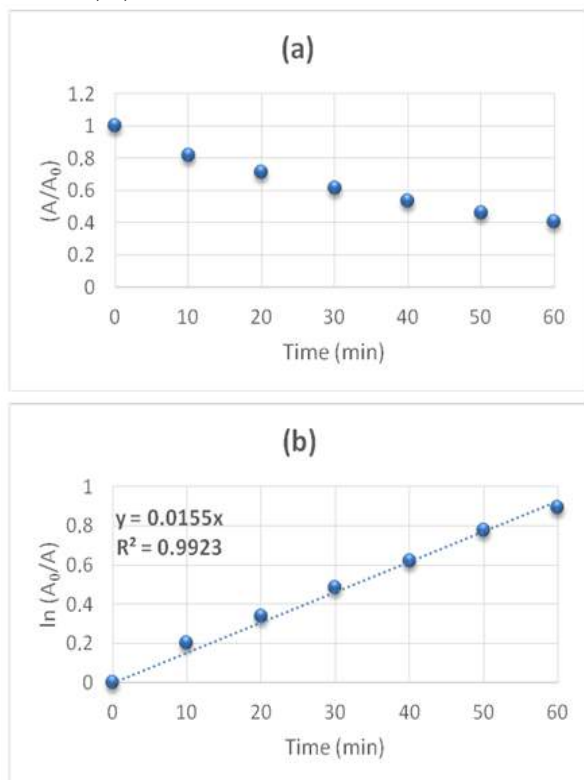


Figure 5. Pseudo-first order kinetics for photocatalytic degradation of the dye: (a) Variation of the absorbance of the dye with the reaction time (b) Linear adjustment of a pseudo-first order reaction.

The catalysts lose their activity during the reaction time. Catalytic deactivation can be caused by aging or sintering, clogging or coke formation, or by poisoning¹⁵. In order to evaluate the deactivation of the synthesized catalysts, three subsequent tests were carried out with each sample of ceramic material supported with TiO_2 (Figure 6).

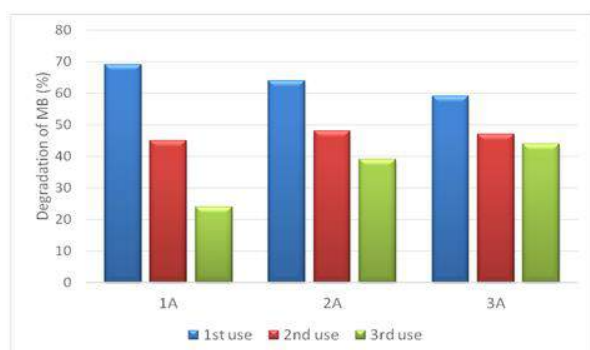


Figure 6. Influence of reuse cycles for ceramics material supported with TiO_2 for degradation of new solutions of methylene blue.

Figure 6 presents the results of photocatalysis for TiO_2 supported in ceramic materials previously used and now in a second and third reuse cycle to verify their potential and behavior for photocatalysis. It is possible to observe that the samples 1A, 2A and 3A presented a very similar behavior concerning their reuse cycles for methylene blue degradation. The sample 1A presented higher percentage for degradation of methylene blue in the first use and presented greater deactivation, losing about 24 % of its photocatalytic activity in the second use and 45 % in the third use. However, sample 3A, which presented lower degradation of the dye in the first use, maintained higher photocatalytic activity during reuse, obtaining in the third use a dye degradation of 44 %, comparable to the degradation obtained by sample 1A in the second use (45 %). The difference of the percentage of degradation of methylene blue for the three samples is due the heterogeneity of the ceramic samples produced. The porosity is an important factor for supporting photocatalytic material as well as the parameters related to operational control and sample reconditioning. Also, it is possible that saturation of adsorbed species that are usually ions do not desorb and are associated as by products in photocatalysis.

According to Rodrigues¹⁶, the higher the mass of catalyst deposited on the support, the longer the lifespan of the sample, since a larger mass takes more time to deactivate, justifying the smaller deactivation of the synthesized catalyst in sample 3A, which presented a higher impregnated TiO_2 mass than catalysts 1A and 2A.

4. Conclusions

The present work studied the application of a porous ceramic material produced from the use of industrial waste and supported with a TiO_2 photocatalyst in the photocatalytic degradation of methylene blue. Furthermore, the deactivation of the synthesized catalysts was evaluated. The experiments were carried out in a batch reactor irradiated by a UVC lamp. The results show that the reaction of photocatalytic degradation of the dye followed pseudo-first order kinetics, with degradation values between 60 and 70 % of the dye in 60 minutes of reaction. The evaluation of the deactivation of the catalysts synthesized showed that catalyst 1A, which obtained the greatest

degradation, presented the greatest loss of photocatalytic activity, about 45 % in the third use. While catalyst 3A, with a higher impregnated TiO₂ mass, maintained greater photocatalytic activity during the second and third uses, losing only 15 % of the activity in the third use. Ceramic material was an important factor for supporting TiO₂ and was easy to handle avoiding its use in liquid media and porosity of ceramic material plays an important role to operational control and sample reconditioning for reuse cycles for methylene blue degradation.

5. Acknowledgments

The authors would like to thank Brazilian funding agencies CAPES and CNPq (proc. n° 427402/2016-6) for financial support.

6. References

- [1] Galindo, C., Jacques, P., Kalt, A., Photooxidation of the phenylazonaphthol AO20 on TiO₂: kinetic and mechanistic investigations, *Chemosphere*, 45 (2001) 997-1005. [https://doi.org/10.1016/S0045-6535\(01\)00118-7](https://doi.org/10.1016/S0045-6535(01)00118-7).
- [2] Mourão, H., Mendonça, V. R., Malagutti, A. R., Ribeiro, C., Nanoestruturas em fotocatalise: uma revisão sobre estratégias de síntese de fotocatalisadores em escala nanométrica, *Quím. Nova*, 32 (2009) 2181-2190. <https://doi.org/10.1590/S0100-40422009000800032>.
- [3] Wawrzekiewicz, M., Wiśniewska, M., Gun'ko, V. M., Zarko, V. I., Adsorptive removal of acid, reactive and direct dyes from aqueous solutions and wastewater using mixed silica–alumina oxide, *Powder Technol.* 278 (2015) 306-315. <https://doi.org/10.1016/j.powtec.2015.03.035>.
- [4] Rosales, E., Pazos, M., Sanromán, M. A., Comparative efficiencies of the decolourisation of leather dyes by enzymatic and electrochemical treatments, *Desalination*, 278 (2011) 312-317. <https://doi.org/10.1016/j.desal.2011.05.041>.
- [5] Su, C.-C., Pukdee-Asa, M., Ratanatamskul, C., Lu, M.-C., Effect of operating parameters on decolorization and COD removal of three reactive dyes by Fenton's reagent using fluidized-bed reactor, *Desalination*, 278 (2011) 211-218. <https://doi.org/10.1016/j.desal.2011.05.022>.
- [6] Chatterjee, D., Dasgupta, S., Visible light induced photocatalytic degradation of organic pollutants, *J. Photoch. Photobio. C* 6 (2005) 186-205. <https://doi.org/10.1016/j.jphotochemrev.2005.09.001>.
- [7] El-Roz, M., Haidar, Z., Lakiss, L., Toufaily, J., Thibault-Starzyk, F., Immobilization of TiO₂ nanoparticles on natural *Luffa cylindrica* fibers for photocatalytic applications, *RSC Adv.* 3 (2013) 3438-3445. <https://doi.org/10.1039/C2RA22438K>.
- [8] Vargová, M., Plesch, G., Vogt, U. F., Zahoran, M., Gorbár, M., Jesenák, K., TiO₂ thick films supported on reticulated macroporous Al₂O₃ foams and their photoactivity in phenol mineralization, *Appl. Surf. Sci.* 257 (2011) 4678-4684. <https://doi.org/10.1016/j.apsusc.2010.12.121>.
- [9] Houas, A., Lachheb, H., Ksibi, M., Elaloui, E., Guillard, C., Herrmann J.-M., Photocatalytic degradation pathway of methylene blue in water, *Appl. Catal. B-Environ.* 31 (2001) 145-157. [https://doi.org/10.1016/S0926-3373\(00\)00276-9](https://doi.org/10.1016/S0926-3373(00)00276-9).
- [10] Johnson, C. K., Ortep, II, Oak Ridge National Laboratory, Oak Ridge, TN, (1976).
- [11] Sifontes, A. B., Urbina, M., Fajardo, F., Melo, L., García, L., Mediavilla, M., Carrión, N., Brito, J. L., Hernández, P., Solano, R., Mejias, G., & Quintero, A. Preparation of gamma-alumina foams of high surface area employing the polyurethane sponge replica method. *Latin Ame Appl Res.* 40 (2010) 185-191. Available from: http://www.scielo.org.ar/scielo.php?pid=S0327-07932010000200013&script=sci_arttext&tlng=pt.
- [12] Menezes, R. R., Neves, G. A., Ferreira, H. C., O estado da arte sobre o uso de resíduos como matérias-primas cerâmicas alternativas, *Rev. Bras. Eng. Agr. Amb.* 6 (2002) 303-313. <https://doi.org/10.1590/S1415-43662002000200020>.
- [13] Xu, C., Rangaiyah, G. P., Zhao, X. S., Photocatalytic degradation of methylene blue by titanium dioxide: experimental and modeling






study, *Ind. Eng. Chem. Res.*, 53 (2014) 14641-14649. <https://doi.org/10.1021/ie502367x>.

[14] Lan, Y., Lu, Y., Ren, Z., Mini review on photocatalysis of titanium dioxide nanoparticles and their solar applications, *Nano Energy*, 2 (2013) 1031-1045. <https://doi.org/10.1016/j.nanoen.2013.04.002>.

[15] Fogler, H. S., *Elementos de engenharia das reações químicas: Comsol Multiphysics*, LTC2009.

[16] Rodrigues, M. M., *Preparação e caracterização de fotocatalisadores imobilizados em vidro*, (2007). Available from: <http://hdl.handle.net/10183/35972>.

Antifungal piperamides from *Piper mollicomum* Kunth (Piperaceae)

Herlle Aparecido da Silva¹, Lydia Fumiko Yamaguchi², Maria Cláudia Marx Young³, Clécio Souza Ramos⁴,
André Márcio Araújo Amorim⁵, Massuo Jorge Kato², Ronan Batista⁶⁺

¹ State University of Southeast of Bahia, BR 415 Hwy, Km 03, Itapetinga, Bahia, Brazil

² University of São Paulo (USP), Institute of Chemistry, 748 Prof. Lineu Prestes Av, São Paulo, São Paulo, Brazil

³ Institute of Botany, 3687 Miguel Stéfano Av, São Paulo, São Paulo, Brazil

⁴ Federal Rural University of Pernambuco (UFRPE), Dom Manoel de Medeiros St, Recife, Pernambuco, Brazil

⁵ State University of Santa Cruz (UESC), Ilhéus-Itabuna Hwy, Km 16, Ilhéus, Bahia, Brazil

⁶ Federal University of Bahia (UFBA), Barão de Jeremoabo St, Salvador, Bahia, Brazil

+ Corresponding author: Ronan Batista, phone: +55 71 3283-6841, e-mail address: ronbatis@ufba.br

ARTICLE INFO

Article history:

Received: January 26, 2018

Accepted: April 20, 2018

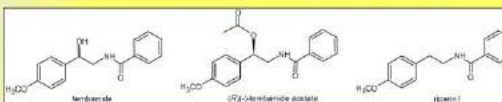
Published: May 29, 2018

Keywords:

1. Piperaceae
2. *Piper mollicomum*
3. antifungal compounds
4. direct bioautography
5. piperamides

ABSTRACT: The phytochemical study on dichlorometane extracts of leaves, stem and roots of *Piper mollicomum* Kunth (Piperaceae) led to isolation of the known piperamides tembamide (1), (*R*)-(-)-tembamide acetate (2) and riparin I (3). Compounds 1 and 2 displayed moderate *in vitro* antifungal activity against *Cladosporium cladosporioides* (5.0 µg) and *Cladosporium sphaerospermum* (1.0 µg) by direct bioautographic analyses and compound 3 was inactive up to 100.0 µg.

Antifungal piperamides from *Piper mollicomum* Kunth (Piperaceae) were isolated and fully characterized by usual spectroscopic methods.



1. Introduction

Piperaceae family belongs to the Piperales order and it is one of the most primitive families among Angiosperms. It is predominantly a tropical family, comprising the genera *Piper*, *Peperomia*, *Sarchorhachis* and *Ottonia*, from which *Piper* and *Peperomia* are the most representative ones with approximately 2000 and 1700 species, respectively^{1,2}. Piperaceae species have long been used as food additive and folk medicine agents

mainly due to their antimicrobial properties, including potent fungicidal action³.

Piper species usually possess strong and pleasant aroma and spicy flavor, which explain their use as condiments, flavorings and medicinal materials. *Piper* compounds are often grouped into seven general classes, including amides, lignans, neolignans, flavonoids, kavalactones, butenolides, and volatile oils^{4,5}. Amides are one of the most characteristic constituents of *Piper* species⁶. The biological activities presented by *Piper*'s amides (also known as “piperamides”) have inspired

synthetic studies towards the preparation of analogs of these substances, in order to evaluate their potential for commercial and medical use⁷. As result, many of these analogs revealed promising antifungal and insecticidal properties^{3, 8-10}.

Known as “jaborandi-manso” or simply “jaborandi”, the species *Piper mollicomum* Kunth is a small shrub of 1.0 to 1.5 m in height, found in Brazil in the states of São Paulo, Minas Gerais, Rio de Janeiro, Espírito Santo, Bahia, Santa Catarina, Ceará, Paraíba, Pernambuco, Mato Grosso and Goiás. The fruits of *P. mollicomum* Kunth are popularly used to treat stomach problems, and its roots, when chewed, are useful for anesthetizing toothaches¹¹. Nevertheless, few studies with *P. mollicomum* Kunth have been performed so far. From *P. mollicomum* methanolic extracts, the

chromenes methyl 2,2-dimethyl-2*H*-chromene-6-carboxylate (4) and methyl 8-hydroxy-2,2-dimethyl-2*H*-chromene-6-carboxylate (5), along with the dihydrochalcone 2',6'-dihydroxy-4'-methoxychalcone (6), were isolated and displayed antifungal properties against the fungi *Cladosporium cladosporioides* and *Cladosporium sphaerospermum*¹².

The present study aimed to further investigate the chemical composition of *P. mollicomum* Kunth dichlorometane extracts. The compounds tembamide (1), (*R*)-(-)-tembamide acetate (2) and riparin I (3) were isolated and characterized and compounds 1 and 2 were found to display *in vitro* antifungal activity against *Cladosporium cladosporioides* and *C. sphaerospermum*.

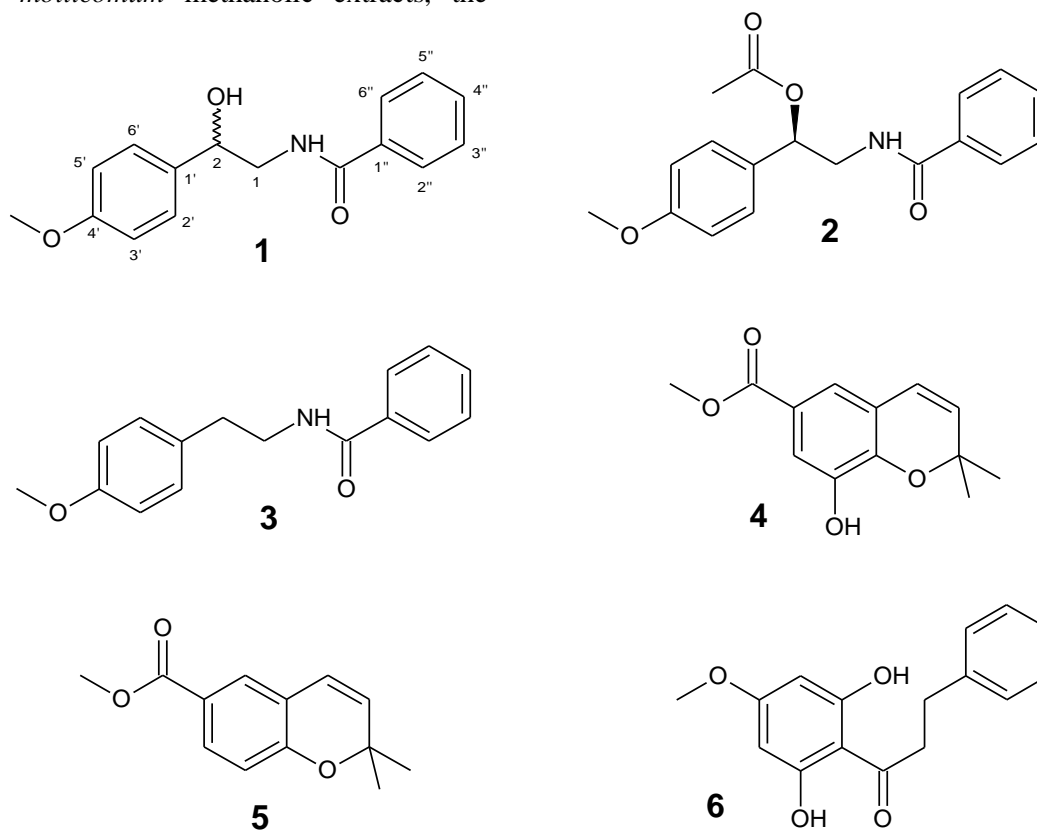


Figure 1. Tembamide (1), (*R*)-(-)-tembamide acetate (2), riparin I (3), methyl 2,2-dimethyl-2*H*-chromene-6-carboxylate (4), methyl 8-hydroxy-2,2-dimethyl-2*H*-chromene-6-carboxylate (5) and 2',6'-dihydroxy-4'-methoxychalcone (6) isolated from *Piper mollicomum* Kunth.

2. Experimental

2.1 General procedures

Optical rotation was measured on a Perkin-Elmer 241 polarimeter. ¹H and ¹³C NMR spectra were recorded at 500 and 125 MHz, respectively,

on a Bruker DRX. CDCl₃ (Aldrich) was used as solvent and TMS as internal standard. Chemical shifts were reported in δ units (ppm) and coupling constants (*J*) in Hz. MS spectra were obtained on a GGEM SHIMADZU mass spectrometer (70 eV) apparatus GCMS-QP5050A, equipped with BPX5 capillary column (30m x 0.25mm ID). Silica gel

(Macherey-Nagel, 70–230 mesh) was used for column chromatographic separations, while silica gel 60G (Acros Organic) was used for analytical TLC chromatography.

2.2 Plant material

The plant was collected in Firmino Alves, southern Bahia, Brazil, in April 2009, and a voucher specimen was housed in the Herbarium of the Executive Committee of the Cacao Plan (CEPLAC) in Ilhéus, Bahia, under the code “PIPER-007”, and identified as *Piper mollicomum* Kunth by Dr. André Márcio Araújo Amorim (Bahia State University of Santa Cruz – UESC). The collected material was dried in an oven (50 °C) for 48 hours, and their separated parts (stem, leaf and root) were pulverized in a knife mill.

2.3 Obtaining extracts

The dried and pulverized leaves (28 g), stem (128 g) and roots (200 g) were thoroughly extracted by maceration with dichloromethane, and then concentrated under reduced pressure (38 °C) until complete removal of the solvent, affording the dichloromethane extracts of the roots (1.68 g), stem (1.31 g) and leaves (1.19 g).

2.4 Fractionating extracts

The crude extract from roots (1.68 g) was subjected to silica gel column chromatography (Si-CC) eluting with mixtures of hexane, ethyl acetate (EtOAc) and methanol (MeOH) with increasing polarities, yielding a total of 55 fractions. Two fractions eluted with EtOAc were further processed. The fraction 24 (45 mg) was treated with ethyl ether to provide (*R*)-(-)-tembamide acetate (2, 28 mg), and the fraction 26 (245 mg) was submitted again to Si-CC (hexane-EtOAc, 1:1) to produce tembamide (1, 31 mg). Additional amounts of 1 (6 mg) and 2 (5 mg) were isolated when crude extracts from stems (1.31 g) were fractionated by similar procedure.

The crude dichloromethane extract from leaves (1.19 g) was also submitted to Si-CC using mixtures of hexane, EtOAc and MeOH with increasing polarities to afford 87 fractions. Fractions 76 to 80, eluted with hexane-EtOAc (7:3), were grouped (13 mg) and submitted to prep-TLC (hexane-EtOAc, 6:4) to yield riparin I (3, 5 mg).

Tembamide (1). ¹H NMR (500 MHz, CDCl₃): δ 7.75 (d, 2H, *J* = 8.0 Hz), 7.51 (dd, 1H, *J* = 7.5, 7.0 Hz), 7.43 (dd, 2H *J* = 8.0, 7.0 Hz), 7.33 (d, 2H, *J* = 8.5 Hz), 6.90 (d, 2H, *J* = 8.5 Hz), 6.59 (br. s, 1H), 4.91 (dd, 1H, *J* = 8.0, 3.5 Hz), 3.90 – 3.86 (m, 1H), 3.81 (s, 3H), 3.54 – 3.49 (m, 1H); ¹³C NMR (125 MHz, CDCl₃): δ 168.53, 159.18, 134.12, 133.85, 131.67, 128.60, 127.09, 126.96, 113.99, 73.33, 55.30 and 47.73; EM-IES (*m/z*): 294.1124 (M + Na)⁺; [C₁₆H₁₇NO₃ requires (M + Na)⁺ = 294.1095].

(*R*)-(-)-*Tembamide acetate* (2). [α]_D = -43.9° (*c* 0.55), CHCl₃. ¹H NMR (500 MHz, CDCl₃): δ 7.72 (d, *J* = 8.0 Hz, 2H), 7.50 (t, *J* = 7.0 Hz, 1H), 7.43 (dd, *J* = 8.0, 7.0 Hz, 2H), 7.33 (d, *J* = 8.5 Hz, 2H), 6.91 (d, *J* = 8.5 Hz, 2H), 6.41 (br. s, 1H), 5.94 (dd, *J* = 7.5, 5.5 Hz, 1H), 3.82 – 3.85 (m, 2H), 3.81 (s, 3H), 2.10 (s, 3H). ¹³C NMR (125 MHz, CDCl₃): δ 170.76, 167.43, 159.76, 134.27, 131.58, 129.65, 128.62, 127.94, 126.86, 114.14, 74.34, 55.30, 45.01, 21.23; EM-IES (*m/z*): 336.1204 (M + Na)⁺; [C₁₈H₁₉NO₄ requires (M + Na)⁺ = 336.1201].

Riparin I (3). ¹H NMR (500 MHz, CDCl₃): δ 7.67-7.70 (m, 2H), 7.16 (d, *J* = 8.5 Hz, 2H), 7.46-7.49 (m, 1H), 7.38-7.42 (m, 2H), 6.87 (d, *J* = 8.5 Hz, 2H), 6.10 (br. s, 1H), 3.80 (s, 3H), 3.68 (q, *J* = 7.0 Hz, 2H), 2.88 (t, *J* = 7.0 Hz, 2H); ¹³C NMR (125 MHz, CDCl₃): δ 167.42, 158.35, 134.69, 131.37, 130.83, 129.75, 128.55, 126.77, 114.14, 52.27, 41.27, 34.77; EM-IES (*m/z*): 255.1209 (M)⁺, 256.1322 (M + 1)⁺, 254.1201 referring to [(M – 2H) + 1]⁺; [C₁₆H₁₇NO₂ requires (M)⁺ = 255.1254, (M + 1)⁺ = 256.1332, and (M-1)⁺ = 254.1176].

2.5 Antifungal assay by direct bioautography

The microorganisms used in the antifungal assays *Cladosporium cladosporioides* (Fresen.) de Vries SPG 140 and *C. sphaerospermum* (Penzig) SPC 491 were grown in Sabouraud dextrose agar, and maintained at the Instituto de Botânica, São Paulo, SP, Brazil. Both fungi were cultured in Sabouraud medium before the assay. Direct bioautography assays were performed in triplicate in agreement with the literature procedure^{9, 13}. Ten microliters of dichloromethane solutions prepared for each pure compound, corresponding to 100, 50, 25, 10, 5, and 1 µg, were applied to TLC plates and eluted with hexanes-EtOAc (7:3) followed by complete removal of the solvent at room temperature. The chromatograms were then sprayed with a spore suspension (3 x 10⁶ cells/mL) in glucose and salt solution and incubated for 48 h in the darkness in a moistened chamber at 25 °C.

Clear inhibition zones appeared against a dark background, indicating the minimal amount of compound required to inhibit the growth of each fungus (Table 1). Nystatin was used as the positive control (detection limit 1 µg).

3. Results and discussion

The phytochemical study on dichloromethane extracts of the leaves, stem and roots of *Piper mollicomum* Kunth led to the isolation of the known compounds tembamide (1), (*R*)-(-)-tembamide acetate (2) and riparin I (3) (Figure 1), from which only 1 and 2 were found to exhibit remarkable antifungal properties against *Cladosporium cladosporioides* (5 µg) and *C. sphaerospermum* (1 µg) through direct bioautography analyses. When tested against *C. sphaerospermum*, compounds 1 and 2 were shown to be as potent as nystatin, the positive control (Table 1). The acetate 2 could be easily hydrolysed by fungal enzymes and this could be one likely explanation for the same antifungal activity observed for both compounds 1 and 2. In spite of being already known chemical entities, the compounds 1-3 are reported here, for the first time, as chemical constituents of *P. mollicomum* Kunth. In addition, bearing in mind that only 1 and 2 were active against the assayed fungi, but not 3, one can hypothesize that such antifungal activity may be

related to the oxygenation at the benzylic carbon, explaining why 3 was inactive against the both fungi assayed.

Tembamide is widely described as a chemical constituent of plants belonging to the Rutaceae family, such as *Clausena brevistyla* Oliver¹⁴, *Zanthoxylum ekmanii* (URB.) ALAIN¹⁵, *Aegle marmelos*¹⁶, *Clausena lansium*¹⁷, and *Feroniella lucida*¹⁸. This amide was also obtained by hydrolysis from tembamide acetate isolated from the dichloromethane fraction of *Piper guayranum* (Piperaceae)¹⁹, a plant species traditionally used in Indian medicine due to its hypoglycemic activity²⁰. In addition, tembamide displayed one of the most potent activities against HIV virus among 67 substances isolated from the bark and root of *Zanthoxylum ailanthoides* (Rutaceae)²¹. Isolated from *Zanthoxylum capense* (Rutaceae), tembamide was also evaluated along with (*R*)-(+)-tembamide acetate in tests of antibiotic modulators²². Its synthesis has been previously described by Aguirre et al. (2001) and Kamal et al. (2004)^{23, 24}. According to literature data, riparine I, isolated from the fruits of *Aniba riparia* (Nees) Mez (Lauraceae), presented anxiolytic effects²⁵ and it was shown to be a potent muscle relaxant²⁶.

Our findings call attention to the importance of *P. mollicomum* Kunth as a source of bioactive natural compounds for further studies on promising antimicrobial and pharmacological agents.

Table 1. Antifungal activity of compounds from *P. mollicomum* Kunth against *Cladosporium* species.

compounds	Antifungal Activity (µg) ^a	
	<i>C. cladosporioides</i>	<i>C. sphaerospermum</i>
Tembamide (1)	5.0	1.0
(<i>R</i>)-(-)-Tembamide acetate (2)	5.0	1.0
Riparin I (3)	> 100.0	> 100.0
Nystatin	1.0	1.0

^a Minimum amount required for inhibition of fungal growth on thin layer chromatography (TLC) plate.

4. Conclusions

The present study reports on the chemical constituents of *Piper mollicomum* Kunth, in which

the piperamides tembamide, (*R*)-(-)-tembamide acetate and riparin I, bioactive compounds commonly isolated from Rutaceae species. Tembamide and (*R*)-(-)-tembamide acetate showed antifungal activity as potent as nystatin

against *Cladosporium* strains by means of direct bioautographic analyses.

5. Acknowledgements

The authors are grateful to the Brazilian agencies FAPESB (DCR0051/20107) and FAPESP (2005/51850-9 and 2014/50316-7) for grants and financial support.

6. References

- [1] Mabberley, D. J., The plant-book - a portable dictionary of the higher plants, Cambridge University Press, New York, 1997.
- [2] Souza, V. C., Botânica Sistemática: guia ilustrado para identificação das famílias de Angiosperma da flora brasileira baseado em APG II, Instituto Plantarum, Nova Odessa, 2005.
- [3] Navickiene, H. M. D., Miranda, J. E., Bortoli, S. A., Kato, M. J., Bolzani, V. S., Furlan, M., Toxicity of extracts and isobutyl amides from *Piper tuberculatum*: potent compounds with potential for the control of the velvet bean caterpillar *Anticarsia gemmatilis*, Pest Manag. Sci. 63 (2007) 399-403. <https://doi.org/10.1002/ps.1340>.
- [4] Rorig, L. R., Poser, G. L. von, Investigação fitoquímica em espécies de Piperaceae, Rev. Bras. Farm. 72 (1) (1991) 15-17.
- [5] Scott, I. M., Jensen, H. R., Philogène, B. J. R., Arnason, J. T., A review of *Piper spp.* (Piperaceae): phytochemistry, insecticidal activity and mode of action, Phytochem. Rev. 7 (2008) 65-75. <https://doi.org/10.1007/s11101-006-9058-5>.
- [6] Srinivasan, K., Black pepper and its pungent principle-piperine: a review of diverse physiological effects, Crit. Rev. Food Sci. 47 (2007) 735-748. <https://doi.org/10.1080/10408390601062054>.
- [7] Dyer, L. A., Palmer, A. N., *Piper*: a model genus for studies of evolution, chemical ecology and tropic interactions, Klumer Academic Publishers, New York, 2004, ch7.
- [8] Alécio, A. C., Bolzani, V. D., Young, M. C. M., Kato, M. J., Furlan, M., Antifungal amide from leaves of *Piper hispidum*, J. Nat. Prod. 61 (1998) 637-639. <https://doi.org/10.1021/np9703656>.
- [9] Marques, J. V., Kitamura, R. O. S., Lago, J. H. G., Young, M. C. M., Guimaraes, E. F., Kato, M. J., Antifungal amides from *Piper scutifolium* and *Piper hoffmanseggianum*, J. Nat. Prod. 70 (2007) 2036-2039. <https://doi.org/10.1021/np070347g>.
- [10] Navickiene, H. M. D., Alécio, A. C., Kato, M. J., Bolzani, V. S., Young, M. C. M., Cavalheiro, A. J., Furlan, M., Antifungal amides from *Piper hispidum* and *Piper tuberculatum*, Phytochemistry 55 (2) (2000) 621-626. [https://doi.org/10.1016/S0031-9422\(00\)00226-0](https://doi.org/10.1016/S0031-9422(00)00226-0).
- [11] Guimarães, E. F., Giordano, L. C. S., Piperaceae do Nordeste Brasileiro I: estado do Ceará, Rodriguesia 55 (2004) 21-46. <https://doi.org/10.1590/2175-78602004558402>.
- [12] Lago, J. H. G., Young, M. C. M., Reigada, J. B., Soares, M. G., Roesler, B. P., Kato, M. J., Antifungal derivatives from *Piper mollicomum* and *P. lhotzkyanum* (Piperaceae), Quím. Nova 30 (5) (2007) 1222-1224. <https://doi.org/10.1590/S0100-40422007000500032>.
- [13] Santos, R. A., Ramos, C. S., Young, M. C. M., Pinheiro, T. G., Amorim, A. M., Kato, M. J., Batista, R., Antifungal constituents from the roots of *Piper dilatatum* Rich., J. Chem. article 160165 (2013) 1-5. <https://doi.org/10.1155/2013/160165>.
- [14] Johns, S. R., Lamberton, J. A., Price, J. R., (±)-N-Benzoyl[2-Hydroxy-2-(4'-methoxyphenyl)]ethylamine from *Clausena Brevistyla* Oliver (Family Rutaceae), Aust. J. Chem. 20 (1967) 2795-2797. <https://doi.org/10.1071/CH9672795>.
- [15] Facundo, V. A., da Silveira, A. S. P., Braz Filho, R., Pinto, A. C., Rezende, C. M., Constituintes químicos de *Zanthoxylum ekmanii* (Urb.) Alain. Quím. Nova 28 (2) (2005) 224-225. <https://doi.org/10.1590/S0100-40422005000200010>.
- [16] Phuwapraisirisan, P., Puksasook, T., Jong-Aramruang, J., Kokpol, U., Phenylethyl cinnamides: a new series of α -glucosidase

- inhibitors from the leaves of *Aegle marmelos*, *Bioorg. Med. Chem. Lett.* 18 (2008) 4956-4958. <https://doi.org/10.1016/j.bmcl.2008.08.024>.
- [17] Song, W-W., Zeng, G-Z., Peng, W-W., Chen, K-X., Tan, N-H., Cytotoxic amides and quinolones from *Clausena lansium*, *Helv. Chim. Acta* 97 (2014) 29.8-305. <https://doi.org/10.1002/hlca.201300323>.
- [18] Sriyatep, T., Chakthong, S., Leejae, S., Voravuthkunchai, S. P., Two lignans, one alkaloid, and flavanone from the twigs of *Feroniella lucida*, *Tetrahedron* 70 (2014) 1773-1779. <https://doi.org/10.1016/j.tet.2014.01.023>.
- [19] Maxwell, A., Ramprasad, D., β -Phenylethylamine-derived amides from *Piper guayranum*, *J. Nat. Prod.* 52 (2) (1989) 411-414. <https://doi.org/10.1021/np50062a037>.
- [20] Shoeb, A., Kapil, R. S., Popli, S. P., Coumarins and alkaloids of *Aegle marmelos*, *Phytochemistry* 12 (1973) 2071-2072. [https://doi.org/10.1016/S0031-9422\(00\)91550-4](https://doi.org/10.1016/S0031-9422(00)91550-4).
- [21] Singh, I. P., Bodiwala, H. S., Recent advances in anti-HIV natural products, *Nat. Prod. Rep.* 27 (2010) 1781-1800. <https://doi.org/10.1039/c0np00025f>.
- [22] Cabral, V., Luo, X., Junqueira, E., Costa, S. S., Mulhovo, S., Duarte, A., Couto, I., Viveiros, M., Ferreira, M-J. U., Enhancing activity of antibiotics against *Staphylococcus aureus*: *Zanthoxylum capense* constituents and derivatives, *Phytomedicine* 22 (2015) 469-476. <https://doi.org/10.1016/j.phymed.2015.02.003>.
- [23] Aguirre, G., Salgado-Rodríguez, A., Flores-López, L. Z., Parra-Hake, M., Somanathan, R., Asymmetric synthesis of naturally occurring β -hydroxyamides (*R*)-tembamide and (*R*)-aegeline, *Rev. Soc. Quím. Mex.* 45 (1) (2001) 21-24. Available from: http://www.scielo.org.mx/scielo.php?script=sci_arttext&pid=S0583-76932001000100005&lng=en&nrm=iso&tlng=en.
- [24] Kamal, A., Shaik, A. A., Sandbhor, M., Malik, S. M., Chemoenzymatic synthesis of (*R*)- and (*S*)-tembamide, aegeline and denopamine by a one-pot lipase resolution protocol, *Tetrahedron: Asymm.* 15 (2004) 3939-3944. <https://doi.org/10.1016/j.tetasy.2004.11.013>.
- [25] Sousa, F. C. F., Monteiro, A. P., Melo, C. T. V., Oliveira, G. R., Vasconcelos, S. M. M., Fonteles, M. M. F., Gutierrez, S. J. C., Barbosa-filho, J. M., Viana, G. S. B., Antianxiety effects of riparin I from *Aniba riparia* (Nees) Mez (Lauraceae) in mice, *Phytother. Res.* 19 (2005) 1005-1008. <https://doi.org/10.1002/ptr.1771>.
- [26] Castelo-Branco, U. V., Castelo-Branco, U. J. V., Thomas, G., Araújo, C. C., Barbosa-Filho, J. M., Preliminary pharmacological studies on three benzoyl amides, constituents of *Aniba riparia* (Nees) Mez (Lauraceae), *Acta Farm. Bon.* 19 (3) (2000) 197-202.

Advantages of the use of heterogeneous catalyst for Huisgen cycloaddition reaction: synthesis and application of new metalorganic material capable of regeneration and reuse

Mônica Freire Belian⁺¹, Wagner Eduardo da Silva¹, Moara Targino da Silva¹, Aline de Andrade Alves¹, Ronaldo Nascimento de Oliveira¹,

¹ University Federal Rural de Pernambuco (UFRPE), Dom Manuel Medeiros St, Recife, Pernambuco, Brazil

⁺ Corresponding author: Mônica Freire Belian, phone: +55 81 3320 6370, e-mail address: monica.freirebelian@ufrpe.br

ARTICLE INFO

Article history:

Received: December 28, 2017

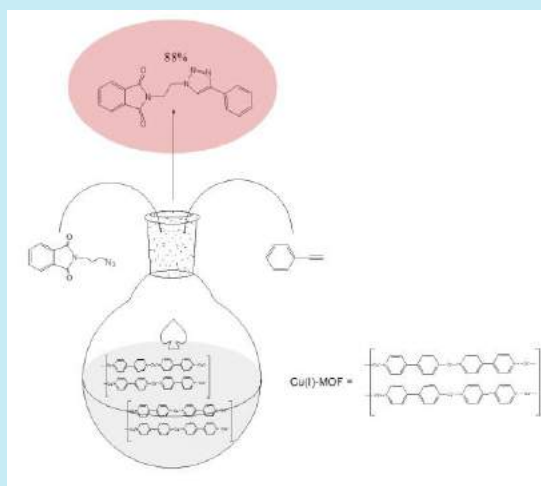
Accepted: May 18, 2018

Published: May 29, 2018

Keywords:

1. Huisgen cycloaddition
2. copper catalysis
3. triazole
4. click chemistry

ABSTRACT: This work evaluates the catalytic capacity of metalorganic materials synthesized, based on Cu⁺ and ambidentate ligand in Huisgen cycloaddition reaction. The synthesis of 1,2,3-triazole was made using CuCl and CuI salts, and the [Cu(4,4'-dipy)]Cl and [Cu(4,4'-dipy)]I compounds as catalysts, with or without base catalysis by triethylamine. The copper salts and compounds lead to formation of the desired triazole product; however, in the synthesis mediated by [Cu(4,4'-dipy)]I does not generate the product, even after 48 h of reaction. The reaction with [Cu(4,4'-dipy)]Cl mediated or not by triethylamine showed high yields of 88 % and 70 %, respectively. The [Cu(4,4'-dipy)]Cl compounds was reused five times, and regenerated by ascorbic acid, maintaining thus, the same reaction yield.



1. Introduction

Metalorganic materials have attracted attention owing to their potential applications in gas separation and storage¹, as sensors², in drug storage and delivery³, templated low-dimensional material preparations⁴, and principally, as catalysts⁵. Due to their high surface areas, pore sizes, ease and diversity of their ability to process, these compounds can be used in catalysis. The literature reports on several works that describe very recently the use of metalorganic materials as catalysts in

solid-phase organic reactions, such as in Friedel-Crafts alkylation and acylation⁶⁻⁸, oxidation⁹⁻¹⁴, alkene epoxidation¹⁵⁻¹⁷, hydrogenation¹⁸, Suzuki cross-coupling^{19, 20}, the Sonogashira reaction²¹, transesterification reaction²², the Knoevenagel condensation²³⁻²⁵, aldol condensation^{26, 27} and 1,3-dipolar cycloaddition reactions²⁸. The Huisgen azide-alkyne 1,3-dipolar cycloaddition afford 1,2,3-triazole derivatives, through solid-phase catalyst that has a number of advantages, such as low consumption of reagents and solvents, possibility of regeneration and removal of the

catalyst from the reaction medium. In this context, metalorganic materials are widely used because of these advantages. The literature describes the use of these compounds, for instance in cyclization reaction²⁹; however, some catalysts, it is shown low yields, difficulty in the removal of residues, as well as the impossibility of catalyst reuse. An explanation for these problems is the use of copper (II) ion, to constitute the metalorganic structure, since the 1,3-dipolar cycloaddition reaction needs the presence of copper(I) ions. The copper(I) catalyst promotes the formation of 1,2,3-triazoles from azides and terminal alkynes, with high yields, mild conditions and excellent regioselectivity^{30, 31}. Generally, in this reaction, the desired product is isolated by chromatography and the copper(I) residues are removed by an extraction process, using successive washes with ammonium hydroxide^{32, 33}.

In this work were synthesized and characterized copper(I) complexes containing 4,4'-dipyridyl (4,4'-dipy) as ligand, and CuCl or CuI as copper (I) font. To reduce the number of extraction steps and low yields, and to promote the reuse of the catalyst, we used two copper(I) compounds as catalysts in solid-phase for reaction between phenylacetylene (PhA) and 2-[2-azido-ethyl]-isoindole-1,3-dione (AID) in the presence or absence of base (triethylamine). The reactions were repeated five times and the catalyst was reuse, through of the regeneration process by ascorbic acid.

2. Materials and methods

The copper(I) chloride, copper(I) iodide, 4,4'-dipyridyl, triethylamine, dichloromethane, phenylacetylene and 2-[2-azido-ethyl]-isoindole-1,3-dione (all from Aldrich) were all used as received. Carbon, nitrogen and hydrogen percentages for the two metalorganic compounds and 1,2,3-triazole were determined by analysis of the elements, using a Perkin-Elmer Model 240 microanalyzer. The infrared spectra were obtained with a KBr tablet using a *Fourier* transform IF66 model spectrophotometer in the 4000–400 cm^{-1} range, with a spectral resolution of 4 cm^{-1} . The NMR spectrum was obtained using VARIAN Unity Plus 300 equipment, at frequencies of 400

MHz to ^1H in DMSO and 75.5 MHz to ^{13}C in CDCl_3 .

2.1 Synthesis of Copper(I) complexes

The optimized synthesis of copper(I) complexes in the reactor system ($V_{\text{max}} = 5.0$ mL per Teflon insert) is as follows: 0.5 mmol of CuCl (49.5 mg) or CuI (95.25 mg) and 0.5 mmol of 4,4'-dipyridyl (78.0 mg) were dissolved in 4 mL dried ethanol (0.068 mmol). The reactor was heated for 24 h at 120 °C. After the reaction, the resultant solid was filtered and washed with water and ethanol three times. The powder obtained was then dried at room temperature in a fume hood and then dried under vacuum at 40 °C for 4 h.

2.2 Synthesis of 1,4-disubstituted 1,2,3-triazole

In a test tube, 100 mg (0.5 mmol) of 2-[2-azido-ethyl]-isoindole-1,3-dione, 71 mg (1.5 mmol) of phenylacetylene, 10 mol% (12 mg) of catalyst ($[\text{Cu}(4,4'\text{-dipy})]\text{Cl}$, $[\text{Cu}(4,4'\text{-dipy})]\text{I}$, CuCl or CuI) and 10 mol % (6 mg ~1 drop) triethylamine or (8 mg) ascorbic acid were mixed together in 1.2 mL of dichloromethane (see Scheme 1). The same mixture was used either without the base or without the acid. Each mixture was stirred at room temperature (298 K) in an argon atmosphere; and monitored by TLC (Hexane:EtOAc, 8:2). After the consumption of the starting material, the mixture was decanted using centrifugation and washed. Thereafter, the supernatant was subjected to drying by adding sodium sulfate, and then filtered. The filtrate was crystallized and the final product was analyzed by ^1H and ^{13}C NMR, infrared spectroscopy and elemental analysis to verify the synthesis of triazole by use of metalorganic compounds.

3. Results and discussion

In the synthesis of copper(I) complexes, a light green (from CuCl reagent) and a red (from CuI reagent) precipitant with crystalline characteristics were generated. The elemental analysis data of the $[\text{Cu}(4,4'\text{-dipy})]\text{Cl}$ and $[\text{Cu}(4,4'\text{-dipy})]\text{I}$ complexes are shown in Table 1.

Table 1. Elemental analysis data of copper(I) complexes

Minimal Formulae	%C		%H		%N	
	E	T	E	T	E	T
$[\text{Cu}_x(4,4'\text{-dipy})]_n\text{Cl}_x$	47.10	47.06	3.16	3.14	11.02	10.98
$[\text{Cu}_x(4,4'\text{-dipy})]_n\text{I}_x$	34.65	34.63	2.31	2.31	8.12	8.08

* 4,4'-dipy = 4,4'-dipyridyl, E =Experimental and T = Theoretical.

The CHN elemental analysis results are in good agreement with the proposed formulas for the copper(I) complexes; with an error level less than 0.4 % (Table 1). The infrared spectroscopy was complementarily used through the assignment of bands to functional groups of the free ligands as well as with the possible band shifts which could be correlated with the copper ion coordination. In Figure 1, the infrared overlapped spectra of the $[\text{Cu}(4,4'\text{-dipy})]\text{Cl}$ and 4,4'-dipyridyl ligand are presented. Since the $[\text{Cu}(4,4'\text{-dipy})]\text{I}$ had the same spectral profile, this has not been dealt with in this text.

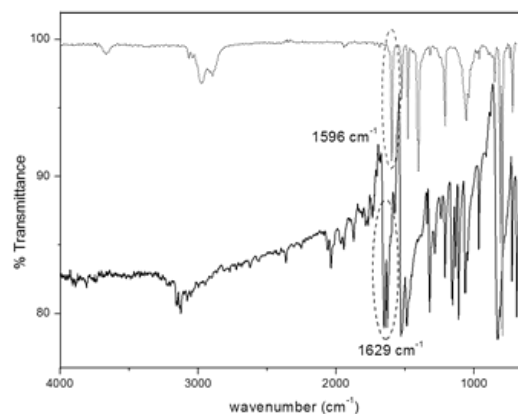


Figure 1. Infrared spectra of 4,4'-dipyridyl (in black) and $[\text{Cu}(4,4'\text{-dipy})]\text{Cl}$ complex (in gray).

It can be observed that the C=N stretch of the $[\text{Cu}(4,4'\text{-dipy})]\text{Cl}$ complex (1596 cm^{-1}) are shifted to the red region in comparison to the free ligand (1629 cm^{-1}), suggesting coordination with the copper (I) ion. In the absence of an X-ray structural analysis, because the mixture had polycrystalline properties, structure based on elemental analysis data and infrared spectroscopy could be suggested (see Figure 2).

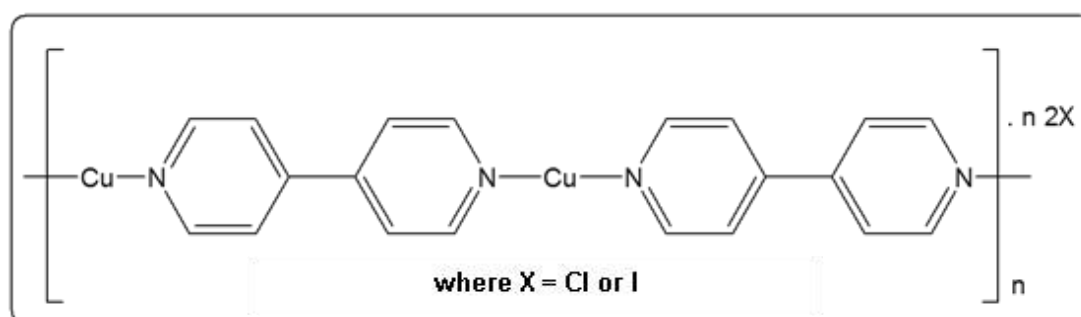
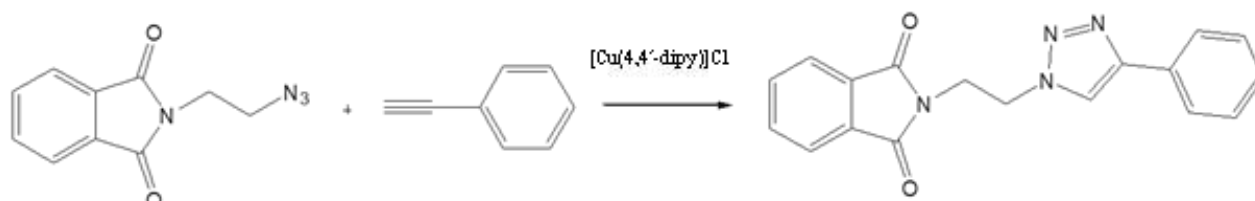


Figure 2. Structure proposed for the $[\text{Cu}(4,4'\text{-dipy})]\text{Cl}$ complex from the data of infrared spectroscopic and elemental analysis.

After the synthesis and characterization of copper(I) complexes, the 1,4-disubstituted 1,2,3-triazole were synthesized. The result was then analyzed by ^1H NMR and demonstrated the following signals: a singlet at 8.64 ppm referring to

the H-triazolic multiples between 7.87 and 7.32 ppm, referring to the protons of the aromatic ring, and two triplets referring to the alkyl groups, the first being at 4.75 ppm, and the second at 4.21 ppm. The ^{13}C NMR spectrum makes it possible to

observe a signal at 167.6, referring to the carbonyls and a signal at 148.0 referring to the carbon on the triazolic ring, signals between 134.2 and 119.8 referring to the aromatic carbons; and two signals at 47.8 and 37.6 referring to the alkyl carbons.



Scheme 1. Synthesis of 1,2,3-triazole catalyzed by [Cu(4,4'-dipy)]Cl complex.

2-[2-(4-Phenyl-[1,2,3]triazol-1-yl)-ethyl]-isoindole-1,3-dione: ^1H NMR (400 MHz, DMSO- d_6): δ 8.64 (s, 1H, H_{triaz}), 7.87-7.82 (m, 4H, Phth), 7.77 (d, 2H, $J = 8.0$ Hz, H_{arom}), 7.43 (dd, 2H, $J = 7.6, 7.6$ Hz, H_{arom}), 7.32 (dd, 1H, $J = 7.6, 7.6$ Hz, H_{arom}), 4.69 (t, 2H, $J = 6.0$ Hz, NCH_2), 4.06 (t, 2H, $J = 5.6$ Hz, NCH_2). ^{13}C NMR (75.5 MHz, CDCl_3): δ 37.6, 47.8, 119.8, 123.5, 125.7, 128.1, 128.7, 130.3, 131.6, 134.2, 148.0, 167.6.

The copper (I) chloride and iodide were used to make the same synthesis in order to compare their catalytic capacity with regard to copper(I) complexes. After 23 h, the azide has been completely consumed and the mixture which had suffered reaction was then treated with NH_4OH to remove the copper residues. When copper (I or II) salts are used, the NH_4OH extraction step is always necessary, which generates soluble copper residues in the water, leading to a greater environmental

contamination. These results indicate that the desired triazole had been synthesized and the ^1H and ^{13}C NMR are in accordance with literature³⁴.

The yield on the synthesis obtained by using copper (I) chloride with or without a base were 38.4 % and 16.3 %, respectively. With copper (I) iodide, with or without a base, they were 92.8 % and 54.8 %, respectively.

In the synthesis using [Cu(4,4'-dipy)]Cl complex, the reaction time varied between 19 and 22 h. In all the cases, the catalyst was removed by centrifugation process, eliminating the extraction step with NH_4OH . The synthesis using a base led to improved the yield, but not enough to justify their use. Table 2 shows the reaction yields with [Cu(4,4'-dipy)]Cl complex, with or without addition of base. On the other hand, the same reaction using [Cu(4,4'-dipy)]I complex even after it has been stirred for 48 h, did not promote the formation of the desired product.

Table 2. Yields for the synthesis of 1,2,3-triazole in the presence or absence of base catalyzed by CuCl , CuI , [Cu(4,4'-dipy)]Cl and [Cu(4,4'-dipy)]I complexes

Reaction Yield (%)							
CuCl		CuI		[Cu(4,4'-dipy)]Cl		[Cu(4,4'-dipy)]I	
Et_3N^*	No Base	Et_3N^*	No Base	Et_3N^*	No Base	Et_3N^*	No Base
38.4	16.3	92.8	54.8	88.0	70.0	0%	0%

* Et_3N = triethylamine.

In order to evaluate the capacity for reuse of the catalyst ([Cu(4,4'-dipy)]Cl complex), the reaction was repeated five times, recovering the catalyst by centrifugation and adjusting the amount of reagents (azide and alkyne). Before reuse, the catalyst was washed (5x) with dichloromethane to remove

possible interferences. When triethylamine was used, after 5 cycles of reactions, the yield decreased to 33.5 % (Table 3, cycle 5). In the case of reactions which did not use the base, the yields lessened to 49.8 % after five cycles.

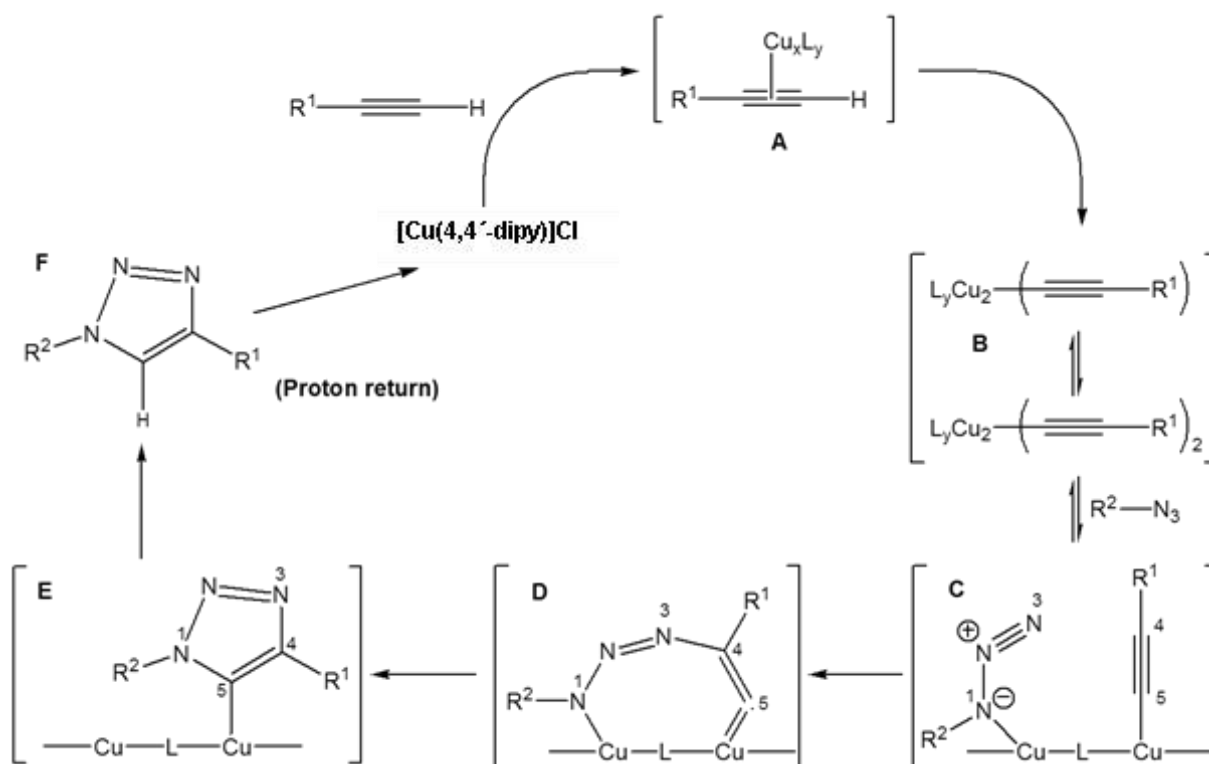
Table 3. Recycling Steps of [Cu(4,4'-dipy)]Cl complex

[Cu(4,4'-dipy)]Cl / Reaction Yield (%)		
Cycle	Et ₃ N*	No Base
1	88.0	70.0
2	78.8	68.9
3	66.6	66.5
4	59.9	63.0
5	33.5	49.8
6 ^a	86.4	71.9

^a After added ascorbic acid (10 mol %).

To explain our poor results after five cycles, however, we need to have some considerations. The viability of the reductive elimination process (restitution of the copper to its lowest value oxidative) and the quality of the solvents used (type of oxidants present). Supposing the copper (II) generation, which would justify the reduction of active sites, Cu(I), as a reaction promoter, ascorbic acid was used as a reducing agent for recuperation of the catalyst. In both cases, with or without the use of a base, after use of ascorbic acid, the yields

were restored. In the case of the drastic lessening of yields when triethylamine was used, it can be accounted for because of the base, before acting as a deprotonate of alkyne and after oxidation of copper (I) to the form (II), could be added as a ligand in the coordination sphere of the first cupric ion, since the typical coordination numbers of these ions copper (I) and (II) are 2 and 4, respectively. The [Scheme 2](#) shows the mechanism proposed to create the reaction using [Cu(4,4'-dipy)]Cl complex.



Scheme 2. Mechanism proposed for the Huisgen cycloaddition reaction mediated by [Cu(4,4'-dipy)]Cl complex.

Based on data in literature indicating that Cu(I) catalyzed alkyne-azide coupling begins with π complex **A** ([Scheme 2](#)), this first step was also

proposed for the [Cu(4,4'-dipy)]Cl complex³⁰⁻³⁶. Some works suggest that an energetic compensation can occur depending on the solvent

used in this reaction, i.e. an improvement can be perceived, concerning copper species formation **B** (Scheme 2), and then this copper coordination can reduce the C-H alkyne pK_a , facilitating the deprotonation in aqueous systems without the use of a base³⁷. In the case of the current work, the reaction was carried out, using dichloromethane (CH_2Cl_2) as the solvent, in the presence and absence of the base (triethylamine), in both cases the final product was obtained with yields of (88 %) and (70 %), respectively. This last reactional condition, using CH_2Cl_2 , invites more significant studies, experimental and/or theoretical, involving different solvents and their interference on the catalytic cycle. In comparison with the usual mechanistic studies³⁷⁻³⁹, the current $[Cu(4,4'-dipy)]I$ complex reinforces and represent well the requirement of two catalytic copper atoms, here can be spaced by a 4,4'-dipyridyl ligand, which were part of an alkyne-azide cycloaddition. The first one changed the alkyne (acetylide complex) reaction and the second served as an azide activator which led to the **D** cyclization (Scheme 2).

Some works have suggested that the size of the ring which surrounds the two acid centers of copper **D** may be easily converted into a copper triazole ring **E** (Scheme 2)³⁷. There is a considerable need for experimental work to confirm the true proton source responsible for the protonation of the type shown in **E**, which will converge on the composite **F**, which may be the reaction which occurs in the presence or absence of a base^{40, 41}. Even with the extensive use of copper salts capable of catalyzing alkyne-azide coupling reactions, the anions of which generally look like sulfate and halogens (generally Cl, Br and I), the study of the influence of these anions as reactors have not been entirely understood by the scientific community. Thus we must emphasize that in the present study, the use of metalorganic compounds, $[Cu(4,4'-dipy)]Cl$ and $[Cu(4,4'-dipy)]I$ complexes, synthesized from the known types of copper salts, CuCl and CuI respectively, showed that the reaction yield was extremely dependent on the anion present in these complexes. In other words, the difference of these counter-ions (anions) present in the complexes were the determining factor as to the catalytic force of the same, making the type $[Cu(4,4'-dipy)]I$ complex not viable for catalyzing the reaction proposed in this study (Scheme 1). Further studies need to be made to confirm which anions work best for high yields in copper(I)-catalyzed reaction.

4. Conclusions

The copper(I) complexes compounds were synthesized and characterized by elemental analysis and infrared spectroscopy; and applied as catalysts in the Huisgen reaction. There was a high yield from the reactions catalyzed by CuI (92.8 %) and $[Cu(4,4'-dipy)]Cl$ complex (96 %). In the case of the same reaction catalyzed by CuCl (38 %) the yields were low. No product was obtained using $[Cu(4,4'-dipy)]I$ complex. Reuse of the $[Cu(4,4'-dipy)]Cl$ catalyst was proven through a cycle of five consecutive syntheses, resulting in the desired product. The yield from the reactions, however, diminished gradually. The synthetic cycle's maintainer the same reactive good yields through a process of copper (II) ion reduction, which had generated in the complex structure after used ascorbic acid, justifying the preferential use of this matrix as the catalyst in Huisgen 1,3-dipolar cycloaddition reaction.

5. References

- [1] Chen, J.C., Luo, W.Q., Wang, H.D., Xiang, J.M., Jin, H.F., Chen, F., Cai, Z.W., A versatile method for the preparation of end-functional polymers onto SiO₂ nanoparticles by a combination of surface-initiated ATRP and Huisgen [3 + 2] cycloaddition, *Applied Surface Science* 256 (8) (2010) 2490–2495. <https://doi.org/10.1016/j.apsusc.2009.10.093>.
- [2] Li, H., Eddaoudi, M., O'Keeffe, M., Yaghi, O.M., Design and synthesis of an exceptionally stable and highly porous metal-organic framework, *Nature* 402 (1999) 276–279. <https://doi.org/10.1038/46248>.
- [3] Rowsell, J.L.C., Yaghi, O. M., Metal-organic frameworks: a new class of porous materials, *Micropor. Mesopor. Mater.* 73 (1-2) (2004) 3–14. <https://doi.org/10.1016/j.micromeso.2004.03.034>.
- [4] Li, Z.-Q., Qiu, L.-G., Xu, T., Wu, Y., Wang, W., Wu, Z.-Y., Jiang, X., Ultrasonic synthesis of the microporous metal-organic framework Cu₃(BTC)₂ at ambient temperature and pressure: An efficient and environmentally friendly method, *Mater. Lett.* 63 (1) (2009) 78–80. <https://doi.org/10.1016/j.matlet.2008.09.010>.

- [5] Dhakshinamoorthy, A., Alvaro, M., Corma, A., Garcia, H., Delineating similarities and dissimilarities in the use of metal organic frameworks and zeolites as heterogeneous catalysts for organic reactions, *Dalton Trans.* 40 (2011) 6344–6360. <https://doi.org/10.1039/c1dt10354g>.
- [6] Phan, N. T. S., Le, K. K. A., Phan, T. D., MOF-5 as an efficient heterogeneous catalyst for Friedel–Crafts alkylation reactions, *Appl. Catal. A: Gen.* 382 (2) (2010) 246–253. <https://doi.org/10.1016/j.apcata.2010.04.053>.
- [7] Ravon, U., Savonnet, M., Aguado, S., Domine, M.E., Janneau, E., Farrusseng, D., Engineering of coordination polymers for shape selective alkylation of large aromatics and the role of defects, *Micropor. Mesopor. Mater.* 129 (3) (2010) 319–329. <https://doi.org/10.1016/j.micromeso.2009.06.008>.
- [8] Nguyen, L. T. L., Nguyen, C. V., Dang, G. H., Le, K. K. A., Phan, N. T. S., Towards applications of metal–organic frameworks in catalysis: Friedel–Crafts acylation reaction over IRMOF-8 as an efficient heterogeneous catalyst, *J. Mol. Catal. A. Chem.* 349 (1-2) (2011) 28–35. <https://doi.org/10.1016/j.molcata.2011.08.011>.
- [9] Dhakshinamoorthy, A., Alvaro, M., Garcia, H., Aerobic Oxidation of Benzylic Alcohols Catalyzed by Metal–Organic Frameworks Assisted by TEMPO, *ACS Catal.* 1 (1) (2011) 48–53. <https://doi.org/10.1021/cs1000703>.
- [10] Xamena, F. X. L. I., Casanova, O., Tailleur, R. G., Garcia, A. C. H., Metal organic frameworks (MOFs) as catalysts: A combination of Cu²⁺ and Co²⁺ MOFs as an efficient catalyst for tetralin oxidation, *J. Catal.* 255 (2) (2008) 220–227. <https://doi.org/10.1016/j.jcat.2008.02.011>.
- [11] Liu, H., Liu, Y., Li, Y., Tang, Z., Jiang, H., Metal–Organic Framework Supported Gold Nanoparticles as a Highly Active Heterogeneous Catalyst for Aerobic Oxidation of Alcohols, *J. Phys. Chem. C* 114 (2010) 13362–13369. <https://doi.org/10.1021/jp105666f>.
- [12] Kleist, W., Maciejewski, M., Baiker, A., MOF-5 based mixed-linker metal–organic frameworks: Synthesis, thermal stability and catalytic application, *Thermochim. Acta* 499 (1-2) (2010) 71–78. <https://doi.org/10.1016/j.tca.2009.11.004>.
- [13] Dhakshinamoorthy, A., Alvaro, M., Garcia, H., Metal organic frameworks as efficient heterogeneous catalysts for the oxidation of benzylic compounds with t-butylhydroperoxide, *J. Catal.* 267 (1) (2009) 1–4. <https://doi.org/10.1016/j.jcat.2009.08.001>.
- [14] Wang, W., Li, Y., Zhang, R., He, D., Liu, H., Liao, S., Metal-organic framework as a host for synthesis of nanoscale Co₃O₄ as an active catalyst for CO oxidation, *Catal. Commun.* 12 (10) (2011) 875–879. <https://doi.org/10.1016/j.catcom.2011.02.001>.
- [15] Song, F., Wang, C., Falkowski, J. M., Ma, L., Lin, W., Isoreticular Chiral Metal–Organic Frameworks for Asymmetric Alkene Epoxidation: Tuning Catalytic Activity by Controlling Framework Catenation and Varying Open Channel Sizes, *J. Am. Chem. Soc.* 132 (43) (2010) 15390–15398. <https://doi.org/10.1021/ja1069773>.
- [16] Cho, S.-H., Ma, B., Nguyen, S. T., Hupp, J. T., Albrecht-Schmitt, T. E., A metal–organic framework material that functions as an enantioselective catalyst for olefin epoxidation, *Chem. Commun.* (24) (2006) 2563–2565. <https://doi.org/10.1039/B600408C>.
- [17] Brown, K., Zolezzi, S., Aguirre, P., Venegas-Yazigi, D., Paredes-García, V., Baggio, R., Novak, M. A., Spodine, E., [Cu(H₂btec)(bipy)]_∞: a novel metal organic framework (MOF) as heterogeneous catalyst for the oxidation of olefins, *Dalton Trans.* (2009) 1422–1427. <https://doi.org/10.1039/B810414J>.
- [18] Opelt, S., Turk, S., Dietzsch, E., Henschel, A., Kaskel, S., Klemm, E., Preparation of palladium supported on MOF-5 and its use as hydrogenation catalyst, *Catal. Commun.* 9 (2008) 1286–1290. <https://doi.org/10.1016/j.catcom.2007.11.019>.
- [19] Xamena, F. X. L. I., Abad, A., Corma, A., Garcia, H., MOFs as catalysts: Activity, reusability and shape-selectivity of a Pd-containing MOF, *J. Catal.* 250 (2007) 294–298. <https://doi.org/10.1016/j.jcat.2007.06.004>.

- [20] Huang, Y., Zheng, Z., Liu, T., Lü, J., Lin, Z., Li, H., Cao, R., Palladium nanoparticles supported on amino functionalized metal-organic frameworks as highly active catalysts for the Suzuki–Miyaura cross-coupling reaction, *Catal. Commun.* 14 (2011) 27–31. <https://doi.org/10.1016/j.catcom.2011.07.004>.
- [21] Gao, S., Zhao, N., Shu, M., Che, S., Palladium nanoparticles supported on MOF-5: A highly active catalyst for a ligand- and copper-free Sonogashira coupling reaction, *Appl. Catal. A: Gen.* 388 (2010) 196–201. <https://doi.org/10.1016/j.apcata.2010.08.045>.
- [22] Zhou, Y., Song, J., Liang, S., Hu, S., Liu, H., Jiang, T., Han, B., Metal-organic frameworks as an acid catalyst for the synthesis of ethyl methyl carbonate via transesterification, *J. Mol. Catal. A* 308 (2009) 68–75. <https://doi.org/10.1016/j.molcata.2009.03.027>.
- [23] Neogi, S., Sharma, M. K. and Bharadwaj, P. K., Knoevenagel condensation and cyanosilylation reactions catalyzed by a MOF containing coordinatively unsaturated Zn(II) centers, *J. Mol. Catal. A* 299 (1-2) (2009) 1–4. <https://doi.org/10.1016/j.molcata.2008.10.008>.
- [24] Gascon, J., Aktay, U., Hernandez-Alonso, M. D., Klink, G. P. M. V., Kapteijn, F., Amino-based metal-organic frameworks as stable, highly active basic catalysts, *J. Catal.* 261 (2009) 75–87. <https://doi.org/10.1016/j.jcat.2008.11.010>.
- [25] Oxford, G. A. E., Dubbeldam, D., Broadbelt, L. J., Snurr, R. Q., Elucidating steric effects on enantioselective epoxidation catalyzed by (salen)Mn in metal-organic frameworks, *J. Mol. Catal. A: Chem.* 334 (1-2) (2011) 89–97. <https://doi.org/10.1016/j.molcata.2010.11.001>.
- [26] Dewa, T., Saiki, T., Aoyama, Y., Enolization and Aldol Reactions of Ketone with a La³⁺-Immobilized Organic Solid in Water. A Microporous Enolase Mimic, *J. Am. Chem. Soc.* 123 (2001) 502–503. <https://doi.org/10.1021/ja001140b>.
- [27] Vermoortele, F., Ameloot, R., Vimont, A., Serre, C., Vos, D. D., An amino-modified Zr-terephthalate metal–organic framework as an acid–base catalyst for cross-aldol condensation, *Chem. Commun.* 47 (5) (2011) 1511–1523. <https://doi.org/10.1039/C0CC03038D>.
- [28] Luz, I., Xamena, F. X. L. I., Corma, A., Bridging homogeneous and heterogeneous catalysis with MOFs: “Click” reactions with Cu-MOF catalysts, *J. Catal.* 276 (2010) 134–140. <https://doi.org/10.1016/j.jcat.2010.09.010>.
- [29] Luz, I., Xamena, F. X. L. I., Corma, A., Bridging homogeneous and heterogeneous catalysis with MOFs: Cu-MOFs as solid catalysts for three-component coupling and cyclization reactions for the synthesis of propargylamines, indoles and imidazopyridines, *J. Catal.* 285 (2012) 285–291. <https://doi.org/10.1016/j.jcat.2011.10.001>.
- [30] Rostovtsev, V. V., Green, L. G., Fokin, V. V., Sharpless, K. B., *Angew. A Stepwise Huisgen Cycloaddition Process: Copper(I)-Catalyzed Regioselective “Ligation” of Azides and Terminal Alkynes*, *Chem. Int. Ed.* 41 (2002) 2596 – 2599. [https://doi.org/10.1002/1521-3773\(20020715\)41:14%3C2596::AID-ANIE2596%3E3.0.CO;2-4](https://doi.org/10.1002/1521-3773(20020715)41:14%3C2596::AID-ANIE2596%3E3.0.CO;2-4).
- [31] Tornøe, C. W., Christensen, C., Meldal, M., Peptidotriazoles on Solid Phase: [1,2,3]-Triazoles by Regiospecific Copper(I)-Catalyzed 1,3-Dipolar Cycloadditions of Terminal Alkynes to Azides, *J. Org. Chem.* 67 (2002) 3057–3064. <https://doi.org/10.1021/jo011148j>.
- [32] da Silva, M. T., de Oliveira, R. N., Valença, W. O., Barbosa, F. C. G., da Silva, M. G., Camara, C.A., Synthesis of N-Substituted Phthalimidoalkyl 1H-1,2,3-Triazoles: A Molecular Diversity Combining Click Chemistry and Ultrasound Irradiation, *J. Braz. Chem. Soc.* 23 (2012) 1839–1843. <https://doi.org/10.1590/S0103-50532012005000053>.
- [33] Barbosa, F. C. G., de Oliveira, R. N., Synthesis of a New Class of Triazole-Linked Benzoheterocycles via 1,3-Dipolar Cycloaddition, *J. Braz. Chem. Soc.* 22 (2011) 592–597. <https://doi.org/10.1590/S0103-50532011000300025>.
- [34] Sirion U., Lee, J. H., Bae, Y. J., Kim, H. J., Lee, B. S., Chi, D. Y., Azide/alkyne resins for quick preparation of 1,4-disubstituted 1,2,3-

triazoles, *Bull. Korean Chem. Soc.* 31 (2010) 1843-1847.

<https://doi.org/10.5012/bkcs.2010.31.7.1843>.

[35] For a review of transition metal-catalyzed acetylenic coupling, see: Siemsen, P., Livingston, R. C. and Diederich, F., *Acetylenic Coupling: A Powerful Tool in Molecular Construction*, *Angew. Chem. Int. Ed.* 39 (2000) 2632–2657. [https://doi.org/10.1002/1521-3773\(20000804\)39:15<2632::AID-ANIE2632>3.0.CO;2-F](https://doi.org/10.1002/1521-3773(20000804)39:15<2632::AID-ANIE2632>3.0.CO;2-F).

[36] For a common example, see: Sonogashira, K., Tohda, Y., Hagihara, N., *A convenient synthesis of acetylenes: catalytic substitutions of acetylenic hydrogen with bromoalkenes, iodoarenes and bromopyridines*, *Tetrahedron Lett.* 16 (1975) 4467 – 4470. [https://doi.org/10.1016/S0040-4039\(00\)91094-3](https://doi.org/10.1016/S0040-4039(00)91094-3).

[37] Himo, F., Lovell, T., Hilgraf, R., Rostovtsev, V. V., Noodleman, L., Sharpless, K. B., Fokin, V. V., *Copper(I)-Catalyzed Synthesis of Azoles. DFT Study Predicts Unprecedented Reactivity and Intermediates*, *J. Am. Chem. Soc.* 127 (2005) 210–216. <https://doi.org/10.1021/ja0471525>.

[38] J. Bastide, O. Henri-Rousseau, in *Chemistry of the Carbon–Carbon Triple Bond* (Ed.: S. Patai), Interscience Publishers, London, 1978, p. 447–552.

[39] Collman, J. P., Devaraj, N. K., Chidsey, C. E. D., “Clicking” Functionality onto Electrode Surfaces, *Langmuir* 20 (2004) 1051–1053. <https://doi.org/10.1021/la0362977>.

[40] Rodinov, V. O., Fokin, V. V., Finn, M. G., *Mechanism of the ligand-free CuI-catalyzed azide-alkyne cycloaddition reaction*, *Angew. Chem. Int. Ed.* 44 (2005) 2210–2215. <https://doi.org/10.1002/anie.200461496>.

[41] Bock, V. D., Hiemstra, H., Maarseveen, J. H., *CuI-Catalyzed Alkyne–Azide “Click” Cycloadditions from a Mechanistic and Synthetic Perspective*, *Eur. J. Org. Chem.* (2006) 51–68. <https://doi.org/10.1002/ejoc.200500483>.

Removal of textile dye by adsorption on the cake as solid waste from the press-extraction of the macaúba (*Acrocomia aculeata*) kernel oil

Alice Santos Caldeira¹, José Domingos Fabris¹, David Lee Nelson¹, Sandra Matias Damasceno¹⁺ 

¹ Federal University of Vales do Jequitinhonha e Mucuri (UFVJM), 5000 MGT 367 Hwy, Km 583, Diamantina, Minas Gerais, Brazil

+ Corresponding author: Sandra Matias Damasceno, e-mail address: sandra.matias@ict.ufvjm.edu.br

ARTICLE INFO

Article history:

Received: March 12, 2018

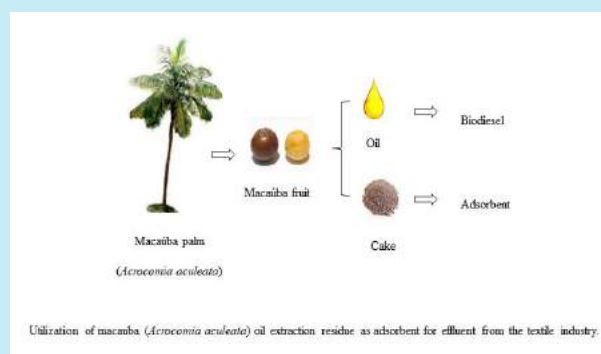
Accepted: May 14, 2018

Published: May 29, 2018

Keywords:

1. adsorbent
2. textile industry
3. isotherms
4. wastewater

ABSTRACT: The textile industries face difficulties in removing dyes from the liquid effluent, even after what is thought to be conventional cleaning treatments. The use of adsorbents to retain dyes in textile effluents has been showing to be a simple and promisingly efficient method. The objective of this research was to test the macaúba (*Acrocomia aculeata*) kernel cake as adsorbent to remove Remazol Brilliant Blue dye in batch adsorption tests. The obtained adsorption kinetic data at equilibrium were modeled by assuming both the Langmuir and the Freundlich isotherms. The values were better fitted with the Langmuir model ($R^2 = 0.983$), with a maximum adsorption capacity of 3.5 mg g^{-1} monolayer. This essay showed that the macaúba cake is an effective adsorbent to remove Remazol Brilliant Blue textile dye and it is a good alternative for treatment of textile liquid effluents.



1. Introduction

The scarcity of some natural resources, including water and feedstock, has been a major problem for textile industries. The search for alternative methods of their treatment and reuse has been growing, as it can reduce industrial costs and reduce hazardous impacts to the environment. The increasing consumption of industrial textile dyes has been responding for major environmental problems issued from industrial activities. Textile dyes are often complex organic molecules, which are usually difficult to be biologically broken down. They are to be attached to the fabric fiber to confer color to them. If these more commonly organic compounds are discharged into water bodies, they may mean real sources of pollution. Due to their recalcitrant nature, they impart long term color to the aqueous industrial

effluent and reduce the penetration of sunlight, which compromises the aquatic life^{1,2}.

The textile industries face enormous difficulty related with the great consumption of water to accomplish several chemical processes, including those of dyeing and rinsing the fabrics. The treatment of effluents in these processes implies three main stages: primary, secondary and tertiary. In the primary treatment, the larger particles in suspension are removed by decantation. In the secondary, microorganisms are used to remove suspended particles and biodegradable matter and, finally, in the tertiary treatment, dissolved solids and residual color and odor are removed by means electrochemical process, membranes technologies, ion exchange and other technologies³. However, since the primary and secondary treatments are not efficient enough to separate very small particles, the treated fluid still leaves with staining. The steps of the textile

processing are high costly and are not efficient enough to degrade the dye molecules. Thus, new technologies have been developed in an attempt to solve the problem of the residual staining in such effluents, even after conventional cleaning treatment.

Adsorption is putatively one of the most prospective way to treat effluents and consists of the physical or chemical interaction between the surface of a porous solid and molecules components from the fluid phase^{4, 5}. The adsorption process is mainly governed by the adsorbent properties (surface area, pore size, density, surface functional groups and hydrophobicity) of the solid material and by the adsorbate (polarity, molecule size, solubility and acidity or basicity) in the fluid, but also by some process conditions such as system temperature, the nature of the solvent and the pH of the medium⁵.

The solid adsorbent materials are characterized by their porous structure, which determines their high surface area. The larger the surface, the greater the adsorption efficiency^{6, 7}. Activated charcoal has been the most widely used adsorbent, regarding its high internal surface area and microporous structure, which render its high degree of surface reactivity⁸. Although, activated charcoal is very efficient and has many technological advantages, its use is high costly, mainly taking into account that it needs to be chemically treated to get it suitably functional. As an alternative way of minimizing process costs, agriculture crop staying or agro-industrial rejects, such as waste generated from pressing oilseed for oil extraction, sugarcane bagasse, among others have been evaluated as adsorbent for aqueous effluent due to their availability and low cost^{6, 9-13}.

The Remazol Brilliant Blue R (RBBR) dye is in the class of anthraquinone synthetic dyes and it is one of the most important dyes in the textile industry, which has been also used as a general compound model in essays of degradation studies. It is an anthracene-derived compound, highly toxic due to its polycyclic aromatic hydrocarbons (PAH), which are very difficult to be biologically metabolized^{14, 15}. The [Figure 1](#) shows the chemical structure of RBBR dye.



Figure 1. Chemical structure of Remazol Brilliant Blue R dye¹⁶.

The macaúba palm (*Acrocomia aculeata*) is a tree that can be found in several edaphoclimatic conditions of Brazil, with some predominance the cerrado biome, in Minas Gerais. The fruit is composed of the bark, the pulp, the seed (kernel) and the endocarp. Two types of oil, pulp oil and kernel oil can be extracted from macaúba fruits. It is estimated an average productivity of approximately 5 t ha⁻¹ of pulp oil along with 1.4 t ha⁻¹ of kernel oil for a density of 200 plants ha⁻¹¹⁷. High productivity, low production cost and good oil characteristics make it an attractive raw material for biodiesel production, generating a large amount of fruit cake from the oil press-extraction (macaúba cake)¹⁸.

In this context, this research had as objective to evaluate the residue generated in the extraction of the oil of the macaúba (*Acrocomia aculeata*) as adsorbent for the removal of the Remazol Brilliant Blue R (RBBR) dye in a simulated solution.

2. Materials and methods

2.1 Preparation and characterization of the oil extraction residue

The cake generated press-extracting the kernel oil of the macaúba (the macaúba cake, MC) used as adsorbent in these essays was provided by the Cooperativa de Agricultores Familiares e Agroextrativistas Grande Sertão Ltda, located in Montes Claros, Minas Gerais, Brazil. Initially, the cake material was washed, dried and sieved on a set of Bertel sieves; the fraction of particles larger than 212 μm and smaller than 300 μm was separated.

The zero-charge potential (pHpzc) of the MC was determined in duplicate by adding 50 mg of the adsorbent material to 12.5 mL of the KCl solution (0.1 mol L⁻¹). The pH was then varied from 1 to 14, adjusted with dilute HCl (0.1 mol L⁻¹) or NaOH (0.1 mol L⁻¹) solution, under constant stirring was for 24 h, at 25 °C. After 24 h, the final pH at equilibrium

was determined with a bench pHmeter. The zero-load potential of each sample was estimated by the method obtained in the range of constant pH (buffer effect).

2.2 Batch adsorption essays

The tests to check for the influence of the RBBR adsorbate concentration on the adsorption process with the macaúba cake were carried out with solutions of the dye in different concentrations (5, 10, 20, 30, 40, 50 mg L⁻¹) in a fixed mass of the adsorbent. The samples were placed on an orbital shaker for 24 h under 100 rpm. The equilibrium concentrations of the samples were measured using a UV-visible spectrophotometer. The experiment was done at constant temperature (25 °C).

The data for kinetic study of the adsorption process were collected at constant temperature with fixed mass of adsorbent and dye solution. The samples were collected at different contact times (5 to 1440 min) between the adsorbent and the adsorbate; the concentrations of RBBR were monitored with a UV visible spectrophotometer.

3. Results and discussion

3.1 Characterization of the adsorbent

The pH_{pzc} is one of the factors that most influence the adsorption process. The pH_{pzc} of the adsorbent material was approximately 5.70, as shown in Figure 2.

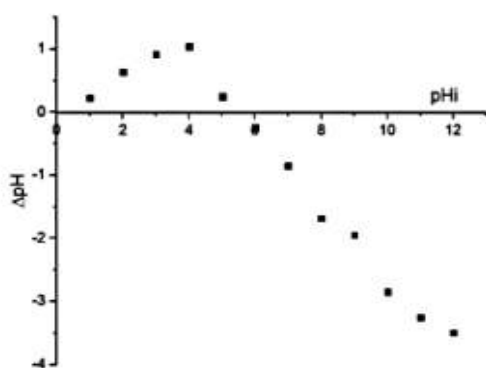


Figure 2. Point of zero charge (pH_{pzc}) for the macaúba kernel cake.

This result indicates that the surface charges of the adsorbent become more positive as the pH decreases: below 5.70, the adsorbent presents a positive surface charge, favoring the adsorption of anionic species. The RBBR dye presents three sulfonated groups that give them an anionic character, possibly in the

adsorption process interaction between the dye anion groups and protonated groups of the adsorbent surface, which may explain the high efficiency on removing the dye at pH below 5.7. The maximum initial pH of the solution employed in the present study was 5.0.

3.2 Adsorption isotherms

The adsorption capacity of the MC was determined the equation 1,

$$q_e = \frac{C_0 - C_e}{M} V \quad (1)$$

where, q_e is the dye concentration adsorbed onto the cake material (mg g⁻¹); C_0 is initial concentration of the textile dye in the liquid phase (mg L⁻¹); C_e is equilibrium concentration of the textile dye in the liquid phase (mg L⁻¹); M is the mass of the cake and V is the volume of solution (L)¹⁹.

The adsorption isotherm for textile dye onto the macaúba cake is shown in Figure 3. The curve describes the distribution of the dye molecules between the liquid and solid phases when the adsorption process reached the steady state. At equilibrium, the amount of the adsorbed dye was approximately 98 %.

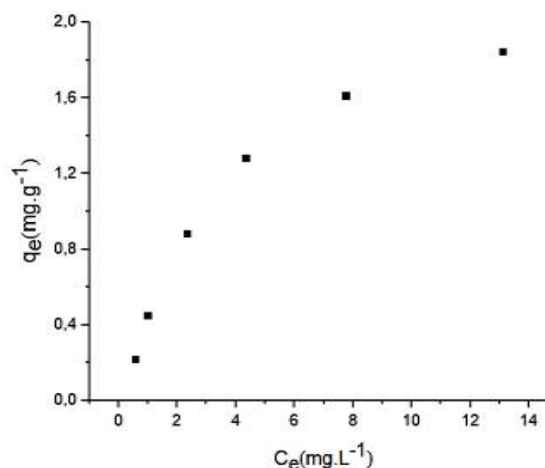


Figure 3. Adsorption isotherm for Remazol Brilliant Blue R on macaúba kernel cake

Two adsorption isotherm models, Langmuir and Freundlich, were used in this study to evaluate the equilibrium data. The applicability of the equation that best fitted the isotherm describing the adsorption process was indicated by the regression coefficient (R²) criterion. The Equation 2 corresponds to the

Langmuir model. In the equation, q_e is the adsorbate concentration at equilibrium in adsorbent (mg g^{-1}); k_a is Langmuir constant (L mg^{-1}); q_m is the adsorbate concentration when the monolayer is formed on the adsorbent (mg g^{-1}) surface and C_e is adsorbate concentration at equilibrium in solution (mg L^{-1})^{8, 20}.

$$q_e = \frac{q_m k_a C_e}{1 + k_a C_e} \quad (2)$$

The Langmuir isotherm is one of the most used equations for the representation of adsorption processes. This model assumes that there is a given number of sites with equivalent energy and the adsorbed molecules do not interact with one another. Although the adsorption process occurs in a

monolayer, each site contains only one adsorbed molecule.

The empirical model proposed by Freundlich presumes non-ideal systems, heterogeneous surfaces and multilayer adsorption. The Freundlich isotherm is described by equation 3,

$$q_e = K_f C_e^n \quad (3)$$

where K_f is the sorption capacity and n is the sorption intensity. Results from linear regression analysis of adsorption isotherms are shown in Table 1. The choice of the isotherm model was based on the highest R^2 value.

Table 1. Parameters of the Langmuir and Freundlich isotherms models for the adsorption of the RBBR dye on macaúba cake

Model	Isotherm equation	Parameters	Determination coefficient for the linear regression
Langmuir	$q_e = \frac{q_m k_a C_e}{1 + k_a C_e}$	$k_a = 2.985$ $q_m = 1.523$	0.983
Freundlich	$q_e = K_f C_e^n$	$K_f = 0.721$ $1/n = 3.798$	0.965

These coefficients provide values for q_m (mg g^{-1}), which indicates the maximum adsorption capacity of the MC, and k_a (adsorption constant), which is related to adsorption energy. The essential characteristic of the Langmuir isotherm can be expressed in terms of a dimensionless equilibrium parameter (R_L), given by equation 4, where R_L is the magnitude that determines the viability of the adsorption process.

$$R_L = \frac{1}{1 + k_a C_0} \quad (4)$$

Values of $R_L = 1$ indicate a linear adsorption process of Langmuir, $R_L > 1$ and $R_L < 1$ refer to unfavorable and favorable adsorption, respectively, whereas the adsorption would be

irreversible for $R_L = 0$. From this study, the found value of $R_L = 0.870$, indicating a favorable adsorption²¹.

The $1/n$ parameter of the Freundlich equation ranged from 0 to 1; it is a measure of the adsorption intensity or of the surface heterogeneity, becoming more heterogeneous as the value approaches zero. The found value of $1/n$ from this study indicates that the adsorption process of the dye on the MC was not heterogeneous, consistently with the result obtained for the Langmuir model.

4. Conclusions

The adsorption of the Remazol Brilliant Blue R dye, in this solution model of an industrial dye aqueous effluent, onto the surface of particles from the macaúba kernel cake was investigated in a

batch arrangement. The charge zero point (PZC) is a convenient reference for predicting the charge-dependent behavior of adsorbents and their suspensions.

It was found that the Langmuir Isotherm provides the best fit to the experimental data. The value of the dimensionless parameter was evaluated as $RL = 0.870$, indicating that the adsorption of RBBR on MC is a spontaneous favorable process. The adsorption isotherm for the adsorption of RBBR in MC can be well modeled by the Langmuir isotherm, with a linear regression determination coefficient of approximately $R^2 = 0.98$. It can be concluded that the macaúba kernel cake has homogeneous surface energy and can be a good alternative for the cleaning treatment of textile effluents.

5. References

- [1] Wong, Y. C., Szeto, Y. S., Cheung, W. H., McKay, G., Adsorption of acid dyes on chitosan - equilibrium isotherm analyses, *Process Biochem.* 39(6) (2004) 695-704. [https://doi.org/10.1016/S0032-9592\(03\)00152-3](https://doi.org/10.1016/S0032-9592(03)00152-3).
- [2] Araújo, F. V. F., Yokoyama, L., Teixeira, L. A. C., Color removal in reactive dye solutions by UV/H₂O₂ oxidation, *Quim. Nova* 29 (1) (2006) 11-14. <https://doi.org/10.1590/S0100-40422006000100003>.
- [3] Ghaly, A. E., Ananthashankar, R., Alhattab, M., Ramakrishnan, V. V., Production, Characterization and treatment of textile effluents: A Critical Review, *J. Chem. Eng. Process Technol.* 5 (182) (2014) 5-18. <https://doi.org/10.4172/2157-7048.1000182>.
- [4] Gupta, V.K., Application of low-cost adsorbents for dye removal - A review. *J. Environ. Manage.*, 90 (2009) 2313-2342. <https://doi.org/10.1016/j.jenvman.2008.11.017>.
- [5] Crittenden, B.; Thomaz, W. J.; Adsorption Technology and Design, Butterworth-Heinemann: Oxford, 1998.
- [6] Oliveira, L. S., Franca, A. S., Low-cost adsorbents from agri-food wastes, In: *Food Sci. Technol. New Res.* Greco, L. V. and Bruno, M. N., New Publishers: New York, USA, 2008, Ch. 3.
- [7] Rouquerol, J., Rouquerol, F., Llewellyn, P., Maurin, G., Sing, K. S.W., *Adsorption by Powders and Porous Solids: Principles, Methodology and Applications*, Oxford, 2nd ed., 2014, Ch.1.
- [8] Bansal, R. C., Goyal, M., *Activated Carbon Adsorption*, CRC Press: Boca Raton, 1st ed., 2005, Ch.1.
- [9] Franca, A. S., Oliveira, L. S., Oliveira, V. F., Alves, C.O., Potential use of *Crambe abyssinica* press cake as an adsorbent: batch and continuous studies, *Environ. Eng. Manage. J.*, 13 (12) (2014) 3025-3036 <http://omicron.ch.tuiasi.ro/EEMJ>.
- [10] Bhatnagar, A., Kaczala, F., Hogland, W., Marques, M., Paraskeva, C. A., Papadakis, V. G., Sillanpää, M., Valorization of solid waste products from olive oil industry as potential adsorbents for water pollution control--a review, *Environ. Sci. Pollut. Res.* 21 (1) (2014) 268-98. <https://doi.org/10.1007/s11356-013-2135-6>.
- [11] Nascimento, G. E., Duarte, M. M. M. B., Campos, N. F., Rocha, O. R. S., Silva, V. L., Adsorption of azo dyes using peanut hull and orange peel: a comparative study, *Environ. Technol.* 35 (9-12) (2014) 1436-1453. <https://doi.org/10.1080/09593330.2013.870234>.
- [12] Nascimento, G. E., Duarte, M. M. M. B., Campos, N. F., Barbosa, C. M. B. M., Silva, V. L., Adsorption of the reactive gray BF-2R dye on orange peel: kinetics and equilibrium studies, *Desalin. Water Treat.* (52) (5-9) (2014) 1578-1588. <https://doi.org/10.1080/19443994.2013.788457>.
- [13] Oliveira, R. S., Borges, M. F., Vieira, A. T., Henrique, M. A., Ribeiro, E. A. M., Bezerra, F. A., Portela, F. M., Pereira, N. R., Assunção, R. M. N., Ruggiero, R., Adsorção de contaminantes do biodiesel por fibras de bagaço modificadas na superfície, *Quim. Nova* (41) (2) (2017) 121-128. <https://doi.org/10.21577/0100-4042.20170164>.
- [14] Machado, K. M. G., Matheus, D. R., Biodegradation of remazol brilliant blue R by ligninolytic enzymatic complex produced by *Pleurotus ostreatus*, *Braz. J. Microbiol.* (37) (4) (2006) 468-473. <https://doi.org/10.1590/S1517-83822006000400013>.

[15] Hadibarata, T., Kristanti, R. A., Effect of environmental factors in the decolorization of remazol brilliant blue R by Polyporus sp. S133, J. Chil. Chem. Soc. (57) (2) (2012) 1095-1098. <https://doi.org/10.4067/S0717-97072012000200007>.

[16] Ahmad, M. A., Alrozi, R., Optimization of preparation conditions for mangosteen peel-based activated carbons for the removal of Remazol Brilliant Blue R using response surface methodology, Chem. Eng. Sci. (165) (3) (2010) 883-889. <https://doi.org/10.1016/j.cej.2010.10.049>.

[17] Clement, C.R., Pérez, E. L., Leeuwen, J. V., O potencial das palmeiras tropicais no Brasil: acertos e fracassos das últimas décadas. Agrociências, Montevideu, (9) (1-2) (2005) 67-71.

[18] Mota, C. S., Corrêa, T. R., Grossi, J. A. S., Castricini, A., Ribeirão, A. S., Exploração sustentável da macaúba para produção de biodiesel: colheita, pós-colheita e qualidade dos frutos. Informe Agropecuário: Belo Horizonte (32), 2011. Available from: <http://www.informeagropecuario.com.br/produtos.php?produto=129>.

[19] Itodo, A. U., Usman, A., Akinrinmade, G., Itodo, H. U., Ugboaja, V. C., Performance assessment of received and formulated carbon animalis: a comparative adsorption isotherm test, J. Environ. Prot. (3) (3) (2012) 288-295. <https://doi.org/10.4236/jep.2012.33036>.

[20] Demir, H., Top, A., Balköse, D., Ülkü, S., Dye adsorption behavior of Luffa cylindrica fibers. J. Hazard. Mater. (153) (1-2) (2008) 389-942. <https://doi.org/10.1016/j.jhazmat.2007.08.070>.

[21] Dada, A. O., Olalekan, A. P., Olatunya, A. M., Dada, O., Langmuir, Freundlich, Temkin and Dubinin-Radushkevich Isotherms studies of equilibrium sorption of Zn²⁺ onto phosphoric acid modified rice husk, J. Appl. Chem. (3) (1) (2012) 38-45. <https://doi.org/10.9790/5736-0313845>.

Complexations of Divalent Metallic Ions with Fulvic Acids

Denise de Oliveira Vaz¹⁺, Andreia Neves Fernandes², Bruno Szpoganicz¹

¹ Federal University of Santa Catarina (UFSC), University Campus Reitor João David Ferreira Lima, Florianópolis, Santa Catarina, Brazil

² Federal University of Rio Grande do Sul (UFRGS), 9500 Bento Gonçalves Av, Porto Alegre, Rio Grande do Sul, Brazil

+ Corresponding author: Denise de Oliveira Vaz, e-mail address: denisevaz.business@gmail.com

ARTICLE INFO

Article history:

Received: September 4, 2017

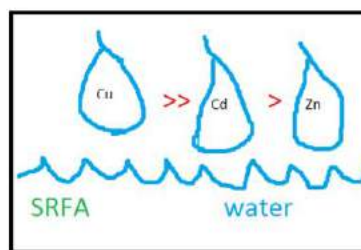
Accepted: May 23, 2018

Published: May 29, 2018

Keywords:

1. fulvic acids
2. SRFA
3. copper
4. cadmium
5. zinc

ABSTRACT: In this work, the interactions of the functional groups of fulvic acids with copper, cadmium and zinc bivalent ions was investigated by potentiometry. The BEST7 software was employed to investigate the interactions of the functional groups. The software SPE and SPEPLOT were used to generate and to plot the species diagrams. It was used the Suwannee River fulvic acid (SRFA) of the IHSS (International Humic Substances Society) to illustrate the process. The values of the proton dissociation and complexation constants with the divalent ions for each functional group were calculated and their values were very close to those previously published. The functional group present in the highest quantity in the complexes was catechol, and it is complexed with all the divalent ions, although with Cu(II). According to the results obtained by potentiometry, the reactivity series for the divalent ions and the SRFA is: Cu(II) >> Cd(II) > Zn(II). Thus, the method employed could be useful to estimate the role of fulvic acids in the transport of metals in the aquatic environments.



The potentiometric results allow to indicate the following reactivity order of the divalent ions with the SRFA (Suwannee River fulvic acids): Cu(II) >> Cd(II) > Zn(II).

1. Introduction

The study of the complexation of potential toxic metals at natural systems by substances as fulvic acids, which are in fresh-waters, for example, is important because these reactions can determine the metal speciation and bioavailability of the metal species. The metal speciation also can determine the mobility of trace metals in the ecosystems^{1, 2}. Free metal ions are more toxic to aquatic biota than metal ions bound to organic molecules like the fulvic acids³. The zinc, for example, is one of the essential metals for the cycle of life of the organisms, but it can be harmful when its concentrations overpass the limits required for a healthy nutrition⁴. Heavy metals, as zinc, have the ability to accumulate in living tissues throughout the food chain. Fish can become the main form of

population transfer to these elements, since they are capable of bioaccumulation and bioconcentration⁵. Copper and cadmium appear in the ecosystems as contaminants independent of their concentration or oxidation number. Cadmium, copper and zinc are prevalent in nature due to their high industrial use, and they can affect growth of plants, according their metal concentration. Their bioavailability is influenced by physical factors such as temperature, phase association, adsorption and sequestration. These metallic elements are considered systemic toxicants that are known to induce multiple organ damage, even at lower levels of exposure. Being classified as human carcinogens according to the U.S. Environmental Protection Agency⁶⁻¹¹. One of the best manners to study the metals interactions with fulvic acids is the using of analyses techniques in solution, as potentiometric titration, because it

can reproduce as closer as possible what occurs in the nature systems. In this work, to elucidate the titration curves of the fulvic acids and zinc (II), cadmium (II) and copper (II) ion complexation it was used the BEST7 software and the software SPE and SPEPLOT.

2. Experimental setup

All the reagents were analytical grade and were used without purification. It was used the SRFA (Suwannee River Fulvic Acid, IR101F) purchased from the IHSS. The solutions of SRFA (80.00 mg L⁻¹) were prepared in the titration cell, dissolving the quantity of SRFA in water, adding 8.00 mL of 0.01 mol L⁻¹ HCl and completing the volume with double distilled water to 50.00 mL. The stock solutions of 0.01 mol L⁻¹ CuCl₂.2H₂O, CdCl₂.H₂O and Zn(NO₃)₂.6H₂O (Vetec Química Fina Ltda.) were standardized by titration with EDTA (Merck), 1.0x10⁻²mol L⁻¹ using murexide as indicator and buffer solution pH=8. The titration agent was carbonate-free solution of 0.100 mol L⁻¹ KOH. The titrations were carried out in a thermostated bath

(25.00 ± 0.05 °C) sealed cell, in an inert atmosphere (argon gas). The experiments started in pH 3.0 (triplicates). The pH values of titrations were read using a pHmeter (Corning 350). It was used the BEST7 software to resolve the equilibrium data because it was developed to can be useful to refine the stability constants from potentiometric data of any kind of system with any number of interactions components. To generate the species diagrams it was used the SPE software and to plot them it was used the SPEPLOT software

3. Results and discussion

In the previous paper¹², it was determined the quantities of the functional groups of the SRFA. In this paper and using those values, it was determined by potentiometry titrations the complexations with divalent metallic ions. In the [Table 1](#), is presented the values of the complexation constants of the ions Cu(II), Zn(II) and Cd(II) to the functional groups of the SRFA.

Table 1. Equilibrium constants (log K) to the ions Cu(II), Cd(II) and Zn(II) and to the ligands phenol (A), benzoic (B), catechol (C), phthalic (D) and salicylic (E) of the SRFA

Species	A (log K)	B (log K)	C (log K)	D (log K)	E (log K)
Cu(II)					
[CuL]/[Cu].[L]	7.62 ± 0.07 (*)	(-) (1.60 ± 0.01)	13.42 ± 0.05 (13.00 ± 0.06)	(-) (3.22 ± 0.03)	11.13 ± 0.02 (10.62 ± 0.02)
[CuL ₂]/[Cu].[L ²]	(-)	(-)	25.39 ± 0.08 (24.90 ± 0.10)	(-) (5.46 ± 0.04)	18.95 ± 0.05 (18.45 ± 0.01)
Cd(II)					
[CdL]/[Cd].[L]	(-)	(-) (1.40 ± 0.01)	8.81 ± 0.03 (8.20 ± 0.01)	2.60 ± 0.05 (2.50 ± 0.01)	(-)
[CdOHL].[H]/[CdL]	(-)	(-)	0.28 ± 0.02 (*)	(-)	(-)
[CdL ₂]/[Cd].[L ²]	(-)	(-)	16.78 ± 0.03 (*)	(-)	(-)
Zn(II)					
[ZnL]/[Zn].[L]	(-)	(-) (0.90 ± 0.02)	10.05 ± 0.02 (9.90 ± 0.01)	(-)	(-)
[ZnOHL].[H]/[ZnL]	(-)	(-)	0.48 ± 0.09 (*)	(-)	(-)
[ZnL ₂]/[Zn].[L ²]	(-)	(-)	17.91 ± 0.09 (17.40 ± 0.30)	(-)	(-)

Where L (represents = A, B, C, D and E). The values of the literature are listed between parenthesis^{13,14}.

Note: The symbol (-) represents that the respective values were not observed experimentally and (*) are the values not published.

The values of the complexation constants to the

Cu(II) and the values of the literature were similar⁷.

⁸ although the values of the log K to the salicylate groups are slightly higher when are connected to the structure of the fulvic acids. It can be the factor on why the experimental values are higher than the values of the salicylic acid groups (simple substance). At this way, some differences are previewed due to the fact of the SRFA is a mixture so complex. The phenolic ligands are important as constituents of the complexes humic substances, on which are the main ligands, getting responsible in the transport and taking part in the transport and accumulation of the nutrients. Describe that in humic substances can exist functional groups as salicylate and the strong acidity of the salicylic groups can be due by the formation of structures of five member with intermolecular hydrogen bonds between the phenolic groups and the anion carboxylate. Evidences of this would be the fact that log K of the ML species (salicylate) diminishes 1.5 units and the log K of the ML₂ species (salicylic) increases 3 units, increasing the ionization of the first proton and weakening the acidity of the second proton. Steric effects are significant in the increase of the influence of the hydrogen linkages in the SRFA percentage. In Figure 1 is presented the graphic of distribution percentage of species of the SRFA complexed with Cu(II) versus p[H].

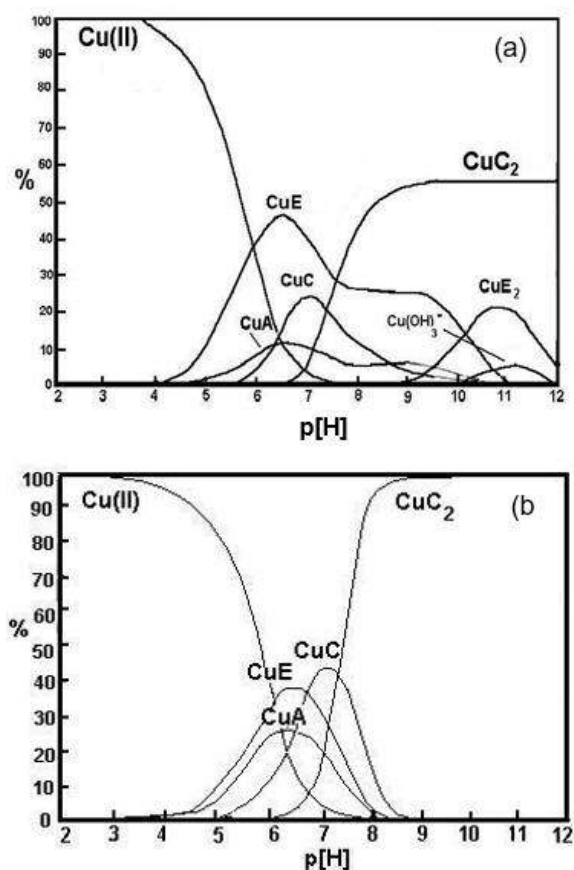


Figure 1. The percentage of species of SRFA with the Cu (II) versus p[H] in $V_{\text{sol CuCl}_2} = 2$ (a) and in $V_{\text{sol CuCl}_2} = 0.5$ mL, where: phenol groups (A); benzoic groups (B); catechol groups (C); phthalic groups (D) and salicylic groups (E). (Conditions: $\mu = 0.100$ mol L⁻¹ KCl; T = 25° C; $C_{\text{SRFA}} = 93$ mg L⁻¹; $C_{\text{sol CuCl}_2} = 10^{-2}$ mol L⁻¹).

In Figure 1, at p[H]= 4 its begins the complex CuE (Where: E = salicylic) reaching its maximum amount of 48 % at p[H]= 6.5. After appearing the CuA species (where: A = phenolic), at p[H]= 6.5 it has 11 %. The specie CuC (where: C = catechol) is at p[H] = 5.5 with the maximum of concentration of 22 % at p[H]= 7.0. The specie CuC₂ begins at p[H] 6.6 ranging the maximum of 58 % at p[H]= 9. The specie CuE₂ begins at p[H] = 9.0 and is on the top of 20 % at p[H]= 10.8. At p[H] 10 begins the hydroxide species with Cu(II). In Figure 1 (b) it is possible to observe the complexation with Cu(II) begin at p[H] 4, beginning the CuE and CuA species reaching their maximum at p[H] = 6.5 (38 %) and p[H] = 6.2 (25 %). The specie CuC begins its formation at p[H] = 5, reaching its maximum at p[H] = 7.0 (43 %). The specie CuC₂ begins at p[H] = 6.0 reaching the maximum at p[H] = 8 (98 %).

In Figure 2, it can be observed 4 complexes for the Zn(II) and the functional groups of SRFA. At $p[H] = 4$ appears the ZnD species (22 % at $p[H] = 6.5$), at $p[H] = 6.8$ is formed the ZnC species (75 % at $p[H] = 8.5$). At $p[H] 7.8$ the hydroxy species ZnOHC (maxim 33 % at $p[H] = 10$). The ZnC₂ species is formed after $p[H] = 8$ (maximum 60 % at $p[H] = 10.5$).

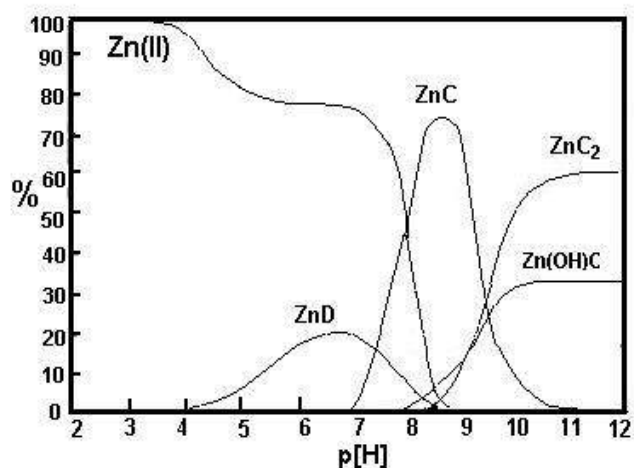


Figure 2. Percentage of SRFA species with Zn(II) versus $p[H]$, where the ligands are represented by phenol (A), benzoic (B), catechol (C), phthalic (D) and salicylic (E). (Conditions: $\mu = 0.100 \text{ mol L}^{-1} \text{ KCl}$; $T = 25 \text{ }^\circ\text{C}$; $C_{\text{SRFA}} = 93 \text{ mg L}^{-1}$, $C_{\text{sol Zn(NO}_3)_2} = 10^{-2} \text{ mol L}^{-1}$).

The Figure 3 shows the graphic of distribution of species of the fulvic acid complexed with the Cd(II) in percentage versus $p[H]$. The Cd(II) presented a chemical behavior very similar to the Zn(II) forming the same type of forming. The species formed with the Cd(II) are the CdD (where: D = phthalic) reaching its maximum of 7 % at $p[H] = 7$; at $p[H] = 7.2$ is formed the CdC species (where: C = catechol), reaching its maximum 28 % at $p[H] = 8.8$; at $p[H] = 8$ it was formed the hydroxy species CdOHC, reaching its maximum of 80 % at $p[H] = 8.0$, over the $p[H] = 8.2$ it was formed the CdC₂ species reaching its maximum of 30 % at $p[H] = 10.9$. The catechol was the functional group more reactive with all the divalent ions studied, it has complexed with all the ions. At second place, it was the salicylic group complexed in great quantity with the ions Cu(II). According the results of this work, this is the series of reactivity to the bivalent ions and the SRFA: Cu (II) \gg Cd(II) $>$ Zn (II).

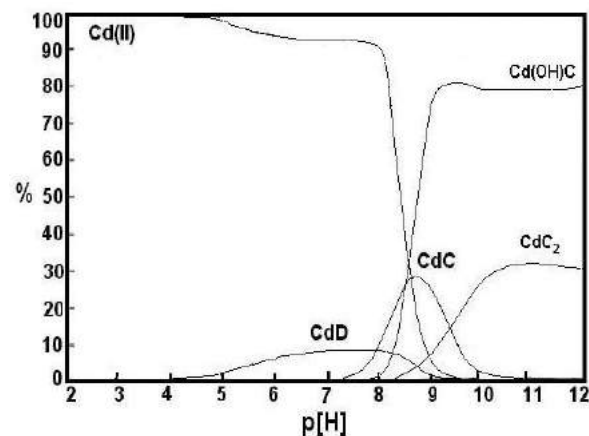


Figure 3. Percentage of species of the SRFA with Cd (II) versus $p[H]$. Where: phenol (A), benzoic (B), catechol (C), phthalic (D) and salicylic (E). (Conditions: $\mu = 0.100 \text{ mol L}^{-1} \text{ KCl}$; $T = 25 \text{ }^\circ\text{C}$; $C_{\text{SRFA}} = 93 \text{ mg L}^{-1}$; $C_{\text{sol CdCl}_2} = 10^{-2} \text{ mol L}^{-1}$).

4. Conclusions

The values of the proton dissociation and complexation constants with the divalent ions for each functional group were calculated and their values were very close to those of the literature. The functional group present in the highest quantity in the complexes was catechol, and it complexed with all the divalent ions, although to a greater extent with Cu(II). According to the results obtained by potentiometry, the reactivity series for the divalent ions and the SRFA is: Cu(II) \gg Cd(II) $>$ Zn(II).

5. Acknowledgments

Thanks to CNPq (Conselho Nacional de Desenvolvimento Científico e Tecnológico) and FUNCITEC (Foundation of Science and Technology).

6. References

- [1] Ephraim, J. H. Heterogeneity as a concept in the interpretation of metal ion binding by humic substances. The binding of zinc by aquatic fulvic acid. *Analytica Chimica Acta* 267 (1) (1992) 39-45. [https://doi.org/10.1016/0003-2670\(92\)85004-P](https://doi.org/10.1016/0003-2670(92)85004-P)
- [2] Bacstrom, M, Dario, M, Karlsson, S, Allard, B. Effects of a fulvic acid on the adsorption of mercury and cadmium on goethite. *Science of the total Environment* 364 (1-3) (2003) 257-268.

[https://doi.org/10.1016/S0048-9697\(02\)00573-9](https://doi.org/10.1016/S0048-9697(02)00573-9).

[3] Ephraim J. H., Marinsky, J. A., Cramer, S. J. Complex-forming properties of natural organic acids: fulvic acids complexes with cobalt, zinc and europium. *Talanta* 36 (4) (1989) 439-443. [https://doi.org/10.1016/0039-9140\(89\)80225-5](https://doi.org/10.1016/0039-9140(89)80225-5).

[4] Toxicological Profile for Zinc. National Technical Information Service (NTIS), USA, 1989 142 p.

[5] Nantsis, E. A., Carper, W. R. Molecular Structure of divalent metal-ion-fulvic acids complexes. *Journal of Molecular Structure* 423 (3) (1998) 203-212. [https://doi.org/10.1016/S0166-1280\(97\)00125-5](https://doi.org/10.1016/S0166-1280(97)00125-5).

[6] Merabito, E., Radaelli, M., Corami, F., Turella, C., Toscano, G., Copodagliom G. Temporal evolution of cadmium, copper and lead concentration in the Venice lagoon. Water in relation with the speciation and dissolved/particulate partition. *Marine Pollution Bulletin* (in press). 129 (2) (2018) 884-892. <https://doi.org/10.1016/j.marpolbul.2017.10.043>.

[7] Wang, F., Xu, S., Zhou, Y., Wang, R., Zhang., Trace elements exposure of whooper swans (*Cygnus cygnus*) wintering in a marine lagoon (Swan lake), northern China. *Marine Pollution Bulletin*, 119, (2) (2017) 60-67. <https://doi.org/10.1016/j.marpolbul.2017.03.063>.

[8] Hernández-Crespo, C., Martín, M. Determination of Background levels and pollution assessment for seven metals (Cd, Cu, Ni, Pb, Zn, Fe, Mn) in sediments of a Mediterranean coastal lagoon. *Catena*, 133 (2015) 206-214. <https://doi.org/10.1016/j.catena.2015.05.013>.

[9] Taria, J., Devenport, J., Townley, B., Dorador, C., Schneider, B., Tolorza, V., Von Turnpling W., Sources enrichment and redistribution of As, Cd, Cu, Li, Mo and Sb in the northern Atacama Region Chile: Implications for acid watersheds affected by mining. *Journal of Geochemical Exploration*, 185 (2018) 33-51. <https://doi.org/10.1016/j.gexplo.2017.10.021>.

[10] Sargentini Jr., E., Rocha, J. C., Rosa, A. H., Zara, L. F., dos Santos, A. Substâncias Húmicas Aquáticas: Fracionamento molecular e

caracterização de rearranjos internos após complexação com íons metálicos. *Química Nova*, 24, (3) (2001), 339-344. <https://doi.org/10.1590/S0100-40422001000300010>.

[11] Yan, M., Dryer, D., Karshin, G.V., Benedetti, M.F., In situ study of binding of copper by fulvic acid: comparison of differential absorbance data and model predictions. *Water Research*, 47, (2), (2013) 588-596. <https://doi.org/10.1016/j.watres.2012.10.020>.

[12] Vaz, D. O., Fernandes, A. N., Szpoganicz, B; Sierra, M. M. D. Potentiometric quantification and speciation of oxygenated groups in humic substances using Best7 software. *Eclét. Quím.* 35 (4) (2010) 147-152. <https://doi.org/10.1590/S0100-46702010000400019>.

[13] Martell, A. E., Smith, R. M. Critical Stability Constants. Plenum Press, Ed., New York, 1st ed. 1982, ch.4.

[14] Martell, A. E., Hancock, R. D. Metal Complexes in Aqueous Solutions, Plenum Publishing Corporation, New York, 1st ed. 1996, ch. 3.

Study of the thermal behavior in solid state of Mn(II)-Diclofenac Complex

Marcelo Kobelnik^{1+*}, Valdecir Ângelo Quarcioni², Adélia Emília de Almeida³, Clóvis Augusto Ribeiro⁴, Marisa Spirandeli Crespi^{4+*}

¹ Centro Universitário do Norte Paulista (UNORP), São José do Rio Preto, São Paulo, Brazil

² Instituto de Pesquisas Tecnológicas (IPT), São Paulo, São Paulo, Brazil

³ São Paulo State University (UNESP), School of Pharmaceutical Science, Araraquara, São Paulo, Brazil

⁴ São Paulo State University (UNESP), Institute of Chemistry, 55 Prof. Francisco Degni St, Araraquara, São Paulo, Brazil

* Corresponding authors: Marcelo Kobelnik, e-mail address: mkobelnik@gmail.com
Marisa Spirandeli Crespi, e-mail address: crespims@gmail.com

ARTICLE INFO

Article history:

Received: September 13, 2017

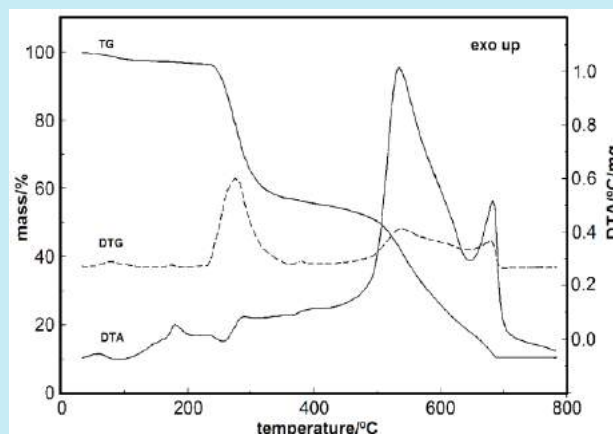
Accepted: April 9, 2018

Published: May 29, 2018

Keywords:

1. Mn(II)-diclofenac complex
2. thermal analysis
3. monotropic reaction
4. activation energy

ABSTRACT: The preparation, characterization and thermal behavior of Mn(II)-diclofenac solid-state complex was investigated by simultaneous TG/DTA and DTG curves, DSC, X-ray powder diffraction (XRD) and scanning electron microscopy (SEM) techniques. The thermal evaluation was carried out with sample masses of 2 and 5 mg, with the purpose of comparing the values of activation energy regarding dehydration, monotropic phase transition and thermal decomposition in both samples mass. The DSC curves were obtained in opened and with crimped lids crucibles of aluminum under oxygen purge gas and static air (without purge gas). The DTA and DSC curves show an exothermic peak between 150-180 °C depending on heating rate, which can be attributed to the monotropic non-reversible reaction. The activation energy (E_a /kJ mol⁻¹) to dehydration, the monotropic phase transition and the first thermal decomposition step were determined by Capela-Ribeiro nonlinear isoconversional method. The activation energy under oxygen dynamic purge gas shows lower values compared to those obtained under static air.



1. Introduction

The diclofenac (2-[2,6-dichlorophenylamino]phenylacetate) is a pharmaceutical drug that can be used as a chemical ligand and has the coordinating ability for complexing several metal ions due to its carboxyl group. The studies of the stable metal complex can be used for different purposes, such as the obtaining metallic oxides to advanced materials (ceramics, glasses, among others) or to obtain new properties of application in biological functions¹⁻⁴. Thus, the thermogravimetry is a valuable technique

for studying the thermal behavior of solid-state compounds of metal complexes, which are essential to synthesize complexes in the desired stoichiometry in several applications.

Recently, Kobelnik *et al.* reported the preparation and thermal characterization of a white powder of diclofenac-Sr and Ba compounds, which were evaluated by thermal analysis with two sample masses (2 and 5 mg). The activation energy of dehydration has the similar behavior, but the first and second thermal decomposition stages showed several values of activation energy⁵. Besides, compounds of aluminum and indium (III)⁶

and cobalt (II)⁷ ions were also evaluated by thermal analysis with the aim of obtaining the activation energy by thermal decomposition and phase transition, respectively. In these previous studies⁵⁻⁷, the activation energy was evaluated with several masses of sample and purge gases to comparison among them.

Thus, as an extension of that works⁵⁻⁷, the aim of the current work is the study of the thermal behavior and obtaining the kinetics parameters to dehydration, phase transition, and thermal decomposition of Mn (II)-diclofenac complex (Mn(Diclof)₂) in the solid-state. The investigations of the dehydration, the first thermal decomposition and a monotropic phase transition (exothermic reaction) of this complex were evaluated by thermogravimetry (TG), differential thermal analysis (DTA) and differential scanning calorimetry (DSC). In addition, to compare the thermal behavior obtained by TG and DSC curves, the analyses were carried out with two different sample sizes and under oxygen purge gas and static condition (without purge gas)^{4,5}. Nevertheless, the monotropic reaction stage (before and after this

reaction) was also evaluated by X-ray powder diffraction (XRD) and scanning electron microscopy (SEM). Moreover, the calorimetric evaluation of the complex by DSC curves was carried out under two main conditions: samples in opened and crimped aluminum crucibles to obtain a comparison between the values of activation energy.

1.1 Kinetic Parameters – Nonlinear isoconversional method

The kinetic parameters to the thermal decomposition step of the complex were estimated by Capela-Ribeiro⁸ nonlinear isoconversional method, using 4th order rotational approximation of the temperature integral⁹. For a given conversion α and a set of n experiments carried out at different heating rates β_i ($i = 1 \dots n$), the parameters activation energy, E , and the B term can be determined from Equation 1 minimizing the sum of squares to the plot of heating rate β to each α as function of the $z_i = 10^3/RT_i$ ($i = 1 \dots n$):

$$S(E, B) = \sum_{i=1}^n \left(\beta_i - \frac{\exp(B - Ez_i)}{z_i} \frac{E^3 z_i^3 + 14E^2 z_i^2 + 46E z_i + 24}{E^4 z_i^4 + 16E^3 z_i^3 + 72E^2 z_i^2 + 96E z_i + 24} \right)^2 \quad (1)$$

$$B = \ln \left(\frac{10^3 A}{Rg(\alpha)} \right) \quad (2)$$

where A is the pre-exponential factor, R is the gas constant, and $g(\alpha)$ represent the reaction mechanism.

2. Experimental

The experimental conditions to the preparation of Mn(Diclof)₂ complex is like that previously described⁵⁻⁷. A stoichiometric mixing of Mn(II) chloride and potassium diclofenac aqueous solutions was prepared with continuous stirring until total precipitation of the complex. The precipitate was filtered and washed with water up to the elimination of chloride ion. Then, the solid was dried at room temperature, macerated and stored in a desiccator over anhydrous calcium chloride up to constant mass.

The thermal analysis was performed by simultaneous TG-DTG and DTA using a TA Instruments 2960 SDT, in the 30-400 °C temperature range in open alumina reference and sample pans under a dynamic nitrogen purge gas

(flow rate: 100 mL min⁻¹), heating rates of 5, 10 and 20 °C min⁻¹ and sample masses of 2 and 5 mg. The stoichiometry evaluation of the complex was obtained by TG curve, using a sample of 7.516 mg in an α -Al₂O₃ crucible, with a heating rate of 20 °C min⁻¹ in synthetic air purge gas with a flow of 100 mL min⁻¹. The kinetic evaluation was carried out by Capela and Ribeiro method⁸, and the curves were obtained using heating rates of 5, 10 and 20 °C min⁻¹ and sample masses of around 2 and 5 mg, following the ICTAC Kinetics Committee recommendation¹⁰. The phase transition was evaluated by DSC curves in a equipment from TA Instruments, DSC 2910 model, between 40 and 200 °C, with heating rates of 5, 10 and 20 °C min⁻¹, aluminum crucible, either open or with crimped lids, in oxygen purge gas (50 mL min⁻¹) or static air.

The X-ray diffraction patterns (XRD) were performed in a Siemens D-500 X-ray diffractometer using $CuK\alpha$ radiation ($\lambda = 1.54056 \text{ \AA}$) and settings of 40 kV and 30 mA.

The morphology study of this complex was performed by SEM, using a JEOL Scanning Electron Microscope, model JSM-T-330A at an accelerating voltage of 20 kV. The sample was covered with a thin and uniform layer of gold, by sputtering, using a vacuum evaporator.

3. Results and discussion

3.1 Thermal behavior

Simultaneous TG/DTG-DTA curves of hydrated $Mn(Diclof)_2$ are shown in Figure 1. The TG curve of the complex shows that the first mass loss of 2.65 % between 30 and 118 °C, which can be attributed to the loss of one water molecule, corresponds to the broad endothermic event in DTA curve. The peak is seen in DTA curve between 155 and 182 °C, having a maximum at 172 °C, without corresponding mass loss in TG curve. Thus, the material was heated to a temperature immediately higher than the exothermic peak, rapidly cooled and then heated again to verify if this reaction is reversible or not, or if an oxidation reaction occurs. Based on the above information, the exothermic event was attributed to the monotropic phase transition. After heating up to 182 °C, this monotropic transition was evaluated by XRD (see below Figure 2C), where it is possible to observe the absence of diffraction lines, which can be attributed to a non-crystalline complex.

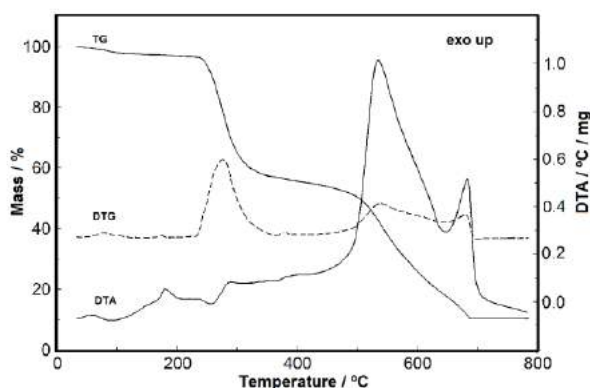


Figure 1. Simultaneous TG/DTG and DTA curves of $Mn(Diclof)_2 \cdot H_2O$ in synthetic air, sample mass of 7.516 mg, heating rate of 20 °C min^{-1} in $\alpha\text{-Al}_2O_3$ crucible.

Besides, Figure 1 shows that the complex has loss mass in three steps between 233 and 693 °C. The first step has a mass loss of 40.02 %, and it is remarkable the presence of a weak endothermic event at 258 °C. The presence of only one small endothermic event was attributed to the simultaneous reactions, which occur due to the thermal equilibrium between the exothermic and endothermic processes. The second and third steps of thermal decomposition occur between 355 and 693 °C, and the mass loss is 47.23 %. For this process, two exothermic peaks were observed in DTA curve. The analysis of the final residue, after a total mass loss, is in agreement with the formation of Mn_3O_4 , which was confirmed by XRD (residue of Mn_3O_4 from TG: 89.56 % (obtained); 89.67 % (calculated)).

The XRD powder patterns of the complex are shown in Figure 2 (A-C). These analyses reveal that this complex may exist in three conditions: hydrated (Fig. 2A), dehydrated (Fig 2B) and after the monotropic reaction (Fig. 2C). On the other hand, when this analysis was made under nitrogen purge gas after the temperature interval of 182 °C, (Figure 2 D) it was seen that under this condition the complex is also non-crystalline. SEM micrographs (Figure 3 A-C) show no significant difference in the morphology of the hydrated and dehydrated complex, and after the monotropic phase transition.

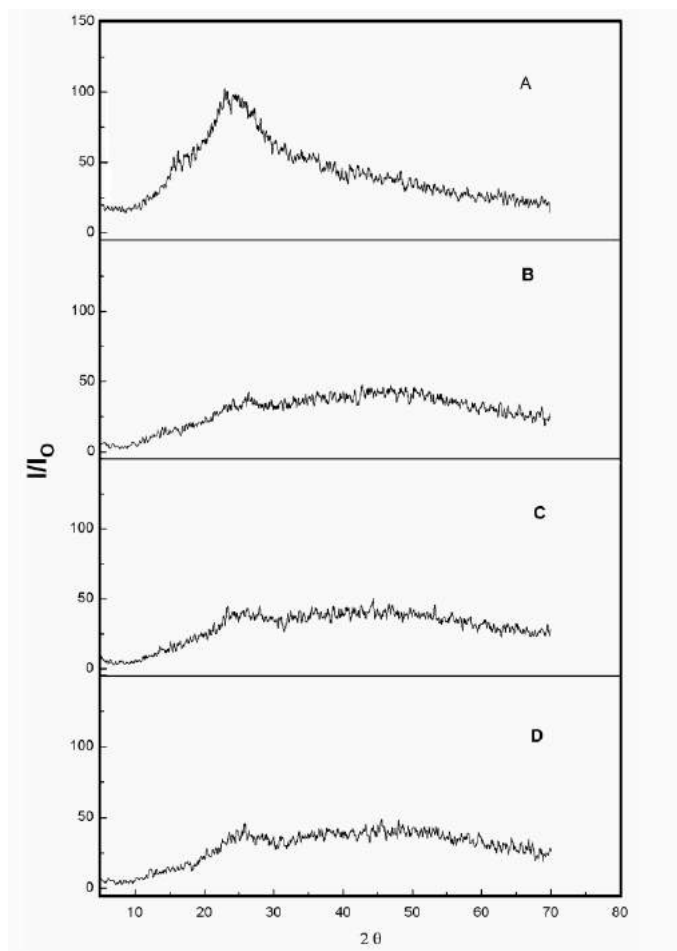


Figure 2. Characteristic parts of X-ray diffraction patterns before (A) and after (B) dehydration step and (C) after the monotropic phase transition. The Fig. 3D corresponding to analysis in nitrogen purge gas, after the monotropic phase transition.

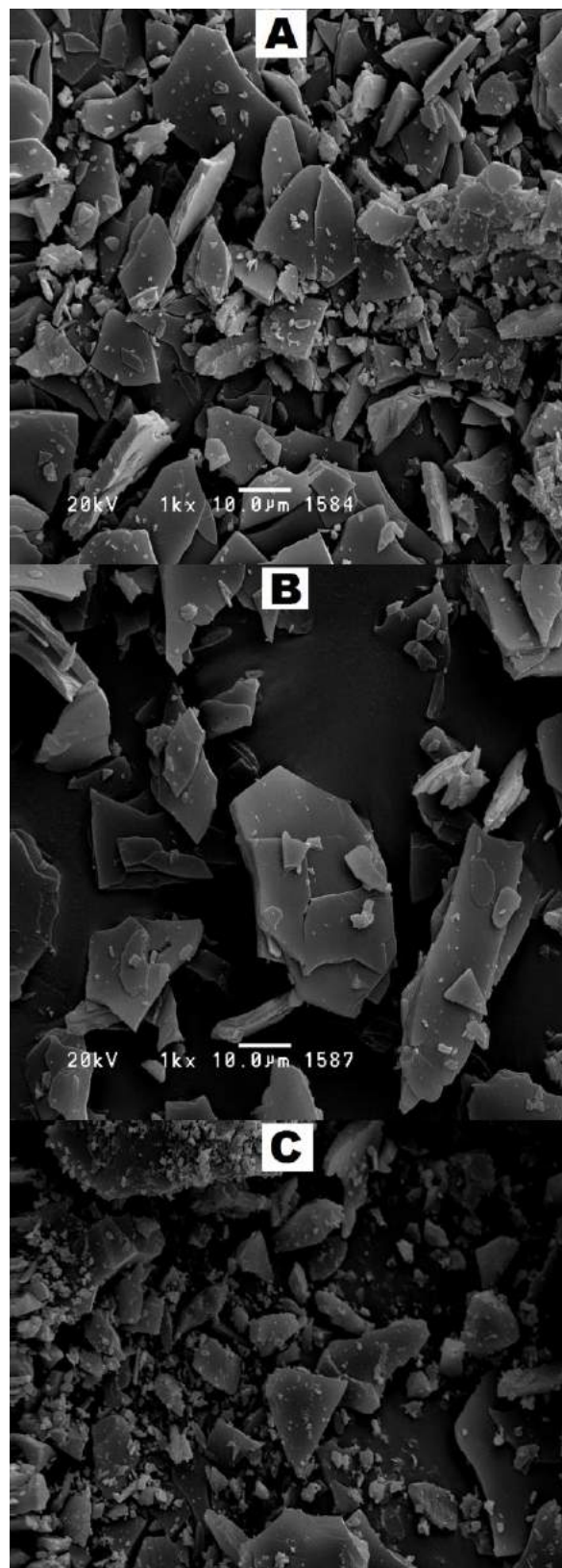


Figure 3. Scanning electron microscopy: (A) showing the $\text{Mn}(\text{Diclof})_2 \cdot \text{H}_2\text{O}$ complex; (B) showing the $\text{Mn}(\text{Diclof})_2$ complex after dehydration stage and (C) showing the $\text{Mn}(\text{Diclof})_2$ complex after the monotropic phase transition.

Figure 4 shows the TG/DTG curves for 2 mg of $\text{Mn}(\text{Dicl})_2 \cdot \text{H}_2\text{O}$ recorded in a nitrogen purge gas, which is an example of the set curves obtained to extract the kinetic parameters. The analyses with 5 mg of the complex were not included due to the significant similarity with the curves in Figure 1 (mass losses are the same: 2 mg = 78.01 % and 5 mg = 78.30 %). These curves show that the mass loss occurs in two steps, being: 1 – the first mass loss attributed to the dehydration in a single stage in the range from 30 to 110 °C and 2 – the thermal decomposition in the range between 190 and 290 °C.

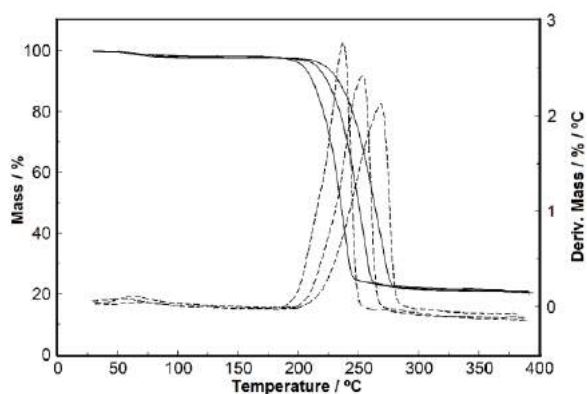


Figure 4. TG/DTG curves of $\text{Mn}(\text{Diclof})_2 \cdot \text{H}_2\text{O}$, sample mass around 2 mg, under nitrogen purge gas in α - Al_2O_3 crucible.

The DSC curves (Figures 5 and 6) show the monotropic phase transition in a static air and oxygen purge gas. Both open and crimped lids aluminum crucibles conditions show the same exothermic event between 140 and 180 °C, which is in agreement with DTA curve, as observed in Figure 1. Another aspect seen on these curves is the difference of displacement in monotropic phase transition peaks under an oxygen purge gas (Figure 5) when the mass of the sample was 5 mg. The peaks shift and became broader. However, under static condition (Figure 6), the peaks are very close to each other, for both masses of the sample, suggesting overlapping reactions. This fact shows that the alteration in the monotropic phase transition in this complex is due to the oxygen conductivity that is favored, while in static air, the reaction does not occur with the same velocity, leading to a broad peak.

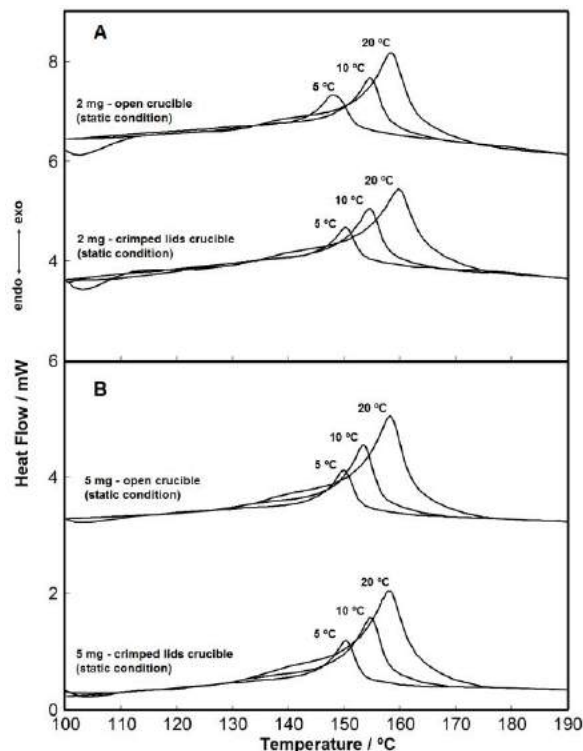


Figure 5. DSC curves in oxygen purge gas, sample mass around 2 mg (A) and 5 mg (B) in open and crimped lids aluminum crucibles.

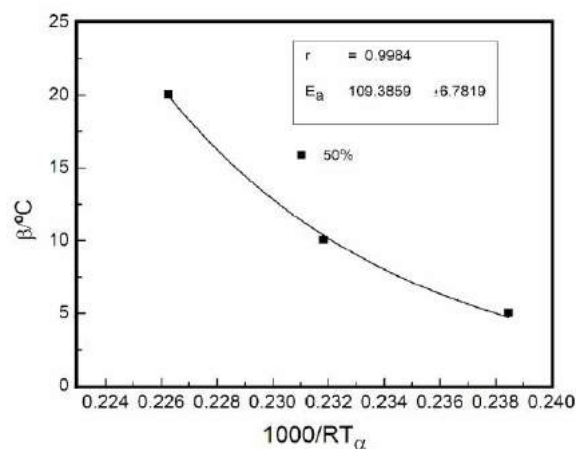


Figure 6. DSC curves in static condition (without purge gas), sample mass around 2 mg (A) and 5 mg (B) in open and crimped lids aluminum crucibles

3.2 Kinetic behavior

The kinetic evaluation of dehydration and thermal decomposition was carried out from three TG curves, with two masses and only in nitrogen purge gas. The kinetic evaluation was also performed by three DSC curves under oxygen purge gas and static condition (without purge gas)⁵⁻⁷.

Figure 7 shows the plot of the heating rate (β) as a function of the $1000/RT_{\alpha}$, obtained from decomposition stage with mass of 2 mg (TG curves), which allows determining the adjustment of activation energy (E_a) for each fixed value of α .

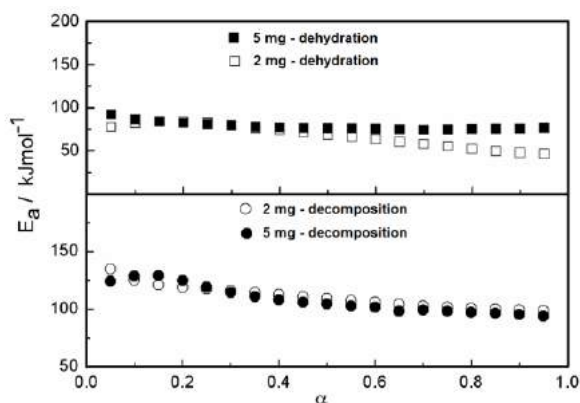


Figure 7. Diagram of β versus conversion degree (α - 50 %) in the decomposition step of 2 mg with the adjustment functions.

3.2.1 Dehydration and decomposition stages

The association between the activation energy (E_a) versus conversion degree (α) values from dehydration and decomposition stages are shown in Figure 8, and the values of activation energy are shown in Table 1.

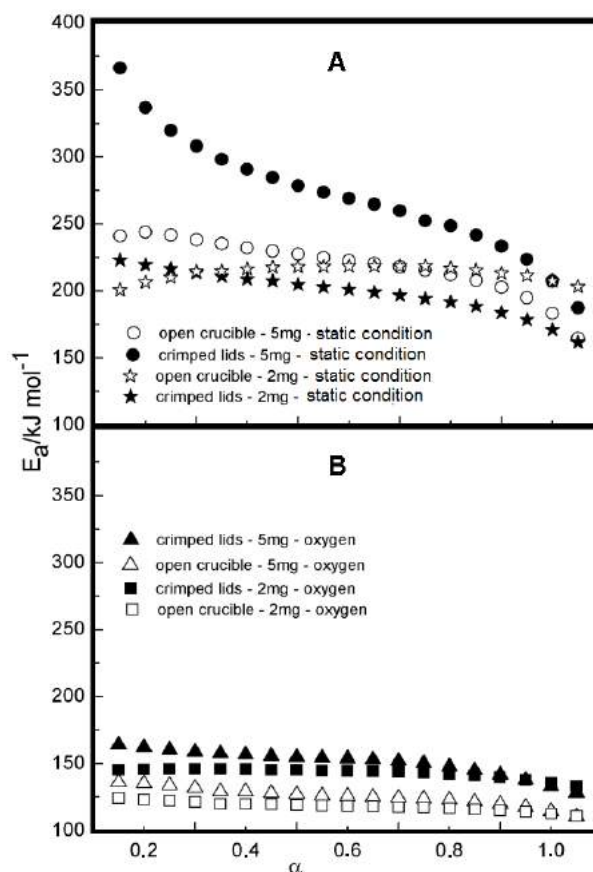


Figure 8. The calculated $E_a/\text{kJ mol}^{-1}$ as a function of α for the dehydration and decomposition processes.

Table 1. E_a (kJ mol^{-1}) and correlation coefficient (r) for the dehydration, thermal decomposition and monotropic phase transition

<i>sample mass</i>	$*E_a$	$*r$	<i>sample mass</i>	$*E_a$	$*r$
2 mg dehydration	67.2 ± 0.2	0.99127	2 mg Monotropic reaction (crimped lids) static condition	198.56 ± 0.08	0.99691
5 mg dehydration	77.29 ± 0.06	0.99525	5 mg Monotropic reaction (crimped lids) static condition	270.8 ± 0.2	0.99835
2 mg decomposition	110.7 ± 0.09	0.99810	2 mg Monotropic reaction (crimped lids) oxygen purge gas	142.91 ± 0.03	0.99995
5 mg decomposition	107.8 ± 0.1	0.99716	5 mg Monotropic reaction (crimped lids) oxygen purge gas	150.91 ± 0.06	0.99813

2 mg Monotropic reaction (open) static condition	213.56 ± 0.02	0.99150	2 mg Monotropic reaction (open) oxygen purge gas	118.21 ± 0.03	0.99964
5 mg Monotropic reaction (open) static condition	218.74 ± 0.09	0.99250	5 mg Monotropic reaction (open) oxygen purge gas	125.37 ± 0.05	0.99982

*Average

For the dehydration step, the samples showed a tendency to maintain the same behavior. In fact, as the water loss is relatively small, the adjustment of the temperatures of the TG curves gives very close results, and therefore, the activation energy values are similar. It occurs when the displacement of the TG or DTG curves is not observed with varying the temperature.

For the thermal decomposition process, the activation energy has a similar behavior for both masses used, but in this case, there was the displacement of the TG curves, which shows that the amount of mass used makes no difference in the kinetic behavior. Also, as observed in DTG curves (Figure 4), the thermal decomposition, for each heating rate, occurs in only one step, that is, without apparent overlapping reactions.

3.2.2 Monotropic phase transition step

The average activation energy values for the monotropic phase transition under static and oxygen purge gases are shown in Table 1. Figure 9 depicts the activation energy *versus* conversion degree (α).

As mentioned above about the behavior of DSC curves, the activation energy values under oxygen purge (Figure 9B) are smaller than in static condition (Figure 9A), but, show the same tendency in both conditions. This demonstrates that the kinetic reaction has the same behavior. In fact, the conductivity of the oxygen associate to the heat flow favors the reaction when compared to static air. This can be proved by the highest activation energy for this last condition using sample mass of 2 mg or 5mg, open or crimped lids aluminum crucible.

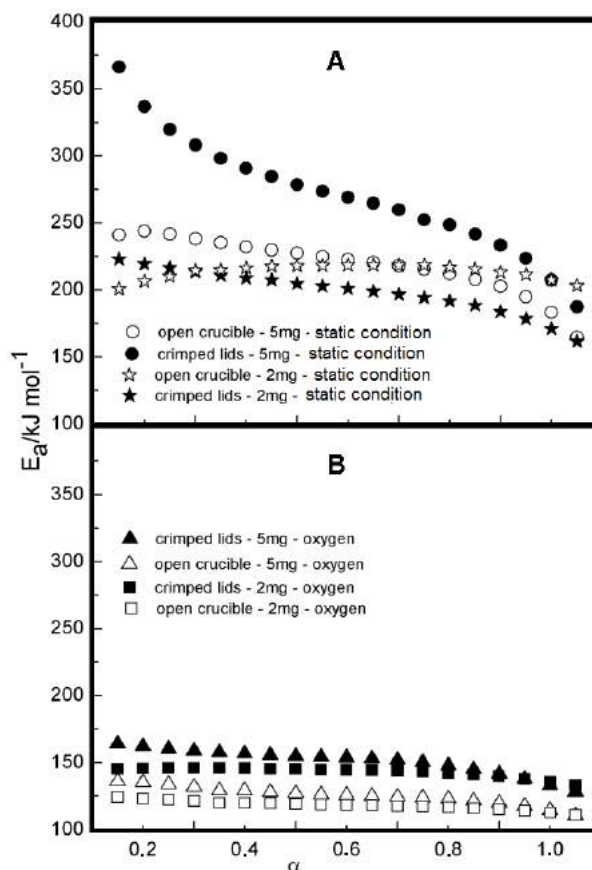


Figure 9, The calculated $E_a/\text{kJ mol}^{-1}$ under static condition (without purge gas) (A) and oxygen purge gas (B) as a function of α for the monotropic phase transition

4. Conclusions

The thermal behavior of Mn(II)-diclofenac complex was studied with two sample masses as well as it was established the stoichiometry of this complex as $\text{Mn}(\text{Diclof})_2 \cdot \text{H}_2\text{O}$. The thermal evaluation shows steps regarding dehydration, monotropic phase transition, and decomposition which could be evaluated from activation energy values. The results of activation energy for dehydration and decomposition steps showed that

both samples have similar behavior for the different sample masses used in the assays. The kinetic evaluation of monotropic phase transition showed that activation energy is dependent on the experimental conditions. The XRD patterns show the non-crystalline form and SEM micrograph indicate no significant change in the structure before thermal decomposition.

5. Acknowledgments

CAPES, IPT – Instituto de Pesquisas Tecnológicas do Estado de São Paulo by TG curves and we would like to thank the LME-IQ for the SEM facilities.

6. References

- [1] Issa, R. M., Gaber, M., Al-Wakiel, N. A., Fathalla, S. K., Synthesis, Spectral, Thermal and Biological Studies of Mn(II), Co(II), Ni(II) and Cu(II) Complexes with 1-(((5-Mercapto-1H-1,2,4-triazol-3-yl)imino)-methyl)naphthalene-2-ol, *Chin. J. Chem.* 30 (2012) 547-557. <https://doi.org/10.1002/cjoc.201280004>.
- [2] El-Ghamry, H. A., Sakai, K., Masaoka S, El-Baradie, K.Y., Issa, R. M., Preparation, Characterization, Biological Activity and 3D Molecular Modeling of Mn(II), Co(II), Ni(II), Cu(II), Pd(II) and Ru(III) Complexes of Some Sulfadrug Schiff Bases, *Chin. J. Chem.* 30 (2012) 881-890. <https://doi.org/10.1002/cjoc.201280024>.
- [3] Khalaji, A. D., Rad, S. M., Grivani, G., Rezaei, M., Gotoh, K., Ishida, H., Cobalt(III) Complex [CoL₃] Derived from an Asymmetric Bidentate Schiff Base Ligand L (L=(5-Bromo-2-hydroxybenzyl-2-furylmethyl)-imine): Synthesis, Characterization and Crystal Structure, *Chin. J. Chem.* 29 (2011) 1613-1622. <https://doi.org/10.1002/cjoc.201190241>.
- [4] Cong, C. J., Hong, J. H., Luo, S. T., Tao, H. B., Zhang, K. L., Kinetics of Thermal Decomposition of Zn_{1-x}Mn_xC₂O₄·2H₂O in Air, *Chin. J. Chem.* 24 (2006) 499-503. <https://doi.org/10.1002/cjoc.200690096>.
- [5] Kobelnik, M., Cassimiro, D. L., Dias, D. S., Ribeiro, C. A., Crespi, M. S., Thermal Behavior of Sr(II) and Ba(II)-Diclofenac Complexes in Solid State: Study of the Dehydration and Thermal Decomposition, *J. Chin. Chem.* 29 (2011) 2271-2277. <https://doi.org/10.1002/cjoc.201180391>.
- [6] Kobelnik, M., Cassimiro, D. L., Almeida, A. E., Ribeiro, C. A., Crespi, M. S., Study of the thermal behavior of Al(III) and In(III)-diclofenac complexes in solid state, *J. Therm. Anal. Cal.* 105 (2011) 415-419. <https://doi.org/10.1007/s10973-010-1266-y>.
- [7] Kobelnik, M., Ribeiro, C. A., Dias, D. S., Almeida, S., Crespi, M. S., Capela, J. M. V., Study of the thermal behavior of the transition phase of Co(II)-diclofenac compound by non-isothermal method, *J. Therm. Anal. Cal.* 105 (2011) 467-471. <https://doi.org/10.1007/s10973-010-1208-8>.
- [8] Cassimiro, D. L., Ribeiro, C. A., Capela, J. M. V., Crespi, M. S., Capela, M. V., Kinetic parameters for thermal decomposition of supramolecular polymers derived from flunixin-meglumine adducts, *J. Therm. Anal. Calorim.* 105 (2011) 405-410. <https://doi.org/10.1007/s10973-010-1116-y>.
- [9] Capela, J. M. V., Capela, M. V., Ribeiro, C. A., Rational approximations of the Arrhenius integral using Jacobi fractions and gaussian quadrature, *J. Mathem. Chem.* 45 (2009) 769-775. <https://doi.org/10.1007/s10910-008-9381-8>.
- [10] Vyazovkin, S., Chrissafis, K., Di Lorenzo, M. L., Koga, N., Pijolat, M., Roduitf, B., Sbirrazzuoli, N., Suñol, J. J., ICTAC Kinetics Committee recommendations for collecting experimental thermal analysis data for kinetic computations, *Therm. Acta.* 590 (2014) 1-23. <https://doi.org/10.1016/j.tca.2014.05.036>.